2012

Modification of Dynamic Modulus Predictive Models for Asphalt Mixtures Containing Recycled Asphalt Shingles

Jianhua Yu
Iowa State University

Modification of dynamic modulus predictive models for asphalt mixtures containing recycled asphalt shingles

by

Jianhua Yu

A thesis submitted to the graduate faculty

in partial fulfillment of the requirements for the degree of

MASTER OF SCIENCE

Major: Civil Engineering (Civil Engineering Materials)

Program of Study Committee:

R. Christopher Williams, Major Professor

Vernon R. Schaefer

W. Robert Stephenson

Iowa State University

Ames, Iowa

2012

TABLE OF CONTENTS

LIST OF TABLES

LIST OF FIGURES

ACKNOWLEDGEMENTS

I would like to express my gratitude to all those who helped me during the writing of this thesis.

My deepest gratitude goes first and foremost to my advisor Dr. Chris Williams for his support, guidance, and leadership throughout the course of my graduate studies and this research.

I gratefully acknowledge the help of Dr. Stephenson, who has offered me valuable suggestions in statistical analysis.

I would also like to thank Dr. Schaefer for his assistance in my academic studies and being part of my advisory committee.

I would additionally like to thank Debra Haugen and Andrew Cascione who provided valuable information to help me complete this research.

Last but not least, I would like to thank my family for their continuous support and encouragement. I own much to my parents who provided great support and understanding even though they were in a difficult time. This thesis would not have been possible without their helps.

ABSTRACT

Recycled asphalt shingles (RAS) have been used in road pavement construction for a number of years primarily on low volume roads. The use of RAS represents economic and environmental opportunities as it provides as good or better performance when processed and proportioned appropriately than commonly used asphalt mixtures. The primary components of RAS are asphalt, mineral filler, mineral granules, and felt. The effect of RAS fibers on an asphalt mixture's dynamic modulus, which is a key input in the Mechanistic-Empirical Pavement Design Guide (MEPDG) and one of the critical properties of asphalt mixtures affecting flexible pavement responses that are related to its performance, are still uncertain.

The National Pooled Fund Study #1208 conducted a series of researches to investigate various issues related to RAS utilization. Thirteen mix designs with RAS contents ranging from zero to six percent were developed and constructed in Indiana, Iowa, Minnesota, and Missouri. Field produced mixtures were procured and sent to Iowa State University Asphalt Lab for laboratory dynamic modulus tests. The testing results are used to evaluate two commonly used dynamic modulus predictive models, the Witczak and Hirsch models. Two versions of Witczak models, which were developed in 1999 and 2006, are evaluated in this research. It was found that the Witczak models were not very effective in estimating the modulus values of RAS mixtures and thus modifications were made to the models to account for the effects of RAS. The study did determine out that the commonly used dosage of RAS in asphalt mixtures does not affect the prediction accuracy of the Hirsch model, however updates were made to improve the Witczak model's accuracy.

CHAPTER 1: INTRODUCTION

BACKGROUND

Environmental and economic concerns are important components in decision making processes of infrastructure construction projects. With the fact that the global crude petroleum price has increased rapidly in the past decade, liquid asphalt price has grown dramatically and is more than $500/ton in 2010 [1]. As a product derived from petroleum distillation, asphalt is becoming less available and more expensive because the crude petroleum is being used to produce other products and restricted supply. Pavement engineers have been considering substitutions of virgin asphalt for the past few years. Recycling of wasted materials such as recycled asphalt pavement (RAP) and recycled asphalt shingles (RAS) provide possible solutions to address this issue. These recycled materials can be used in roadway construction in order to reduce the dependence on virgin asphalt binder.

RAS has been utilized in road paving practices for over 20 years. In the early 1990s, hot mix asphalt (HMA) pavements containing RAS were experimentally used in the State of Pennsylvania. A 0.93 mile four-lane highway was constructed with mix containing 5 percent RAS in July, 1991 which is the first road paved with RAS [2]. In the same year, the Minnesota Department of Transportation (Mn/DOT), the Minnesota Office of Environmental Assistance (OEA), and the University of Minnesota started a research project to investigate the effectiveness of pavements containing RAS and the influences of shingle products on mix properties. This study recommended a maximum RAS content of 5 percent to be used. This recommendation was legislated as a state specification in 1995[3]. Disney World in Orlando, Florida, built its parking lots with a high RAS content of 10 percent in the early 1990s. This pavement has performed very well for the past 20 years [4]. RAS can be recycled from either manufacturer's scrap or building reroofing process. Materials from manufacturer's scrap are known as pre-consumer shingles or manufacturer's shingles. Materials from reroofing projects are known as post-consumer or tear-off shingles. It is estimated that approximately 1 million tons of pre-consumer shingles and 10 million tons of post-consumer shingles are generated in the United States every year [5]. Most of them are deposited into landfills. Environmental issues related to this are considerable and become one of the motivations of utilization of recycled shingles in pavement construction. Some state agencies have allowed RAS to be used with certain maximum percentages in HMA.

Most states agencies limit the use of RAS to 5% by weight of the total aggregate. Figure 1 shows the states that currently allow the utilization of RAS in HMA. In a 2011 supplemental specification, the State of Ohio allows the use of either manufacturer's RAS or tear-off RAS depending on the particular pavement courses [6]. It should be noticed that the Ohio only allows the using of manufactured RAS in Figure 1.

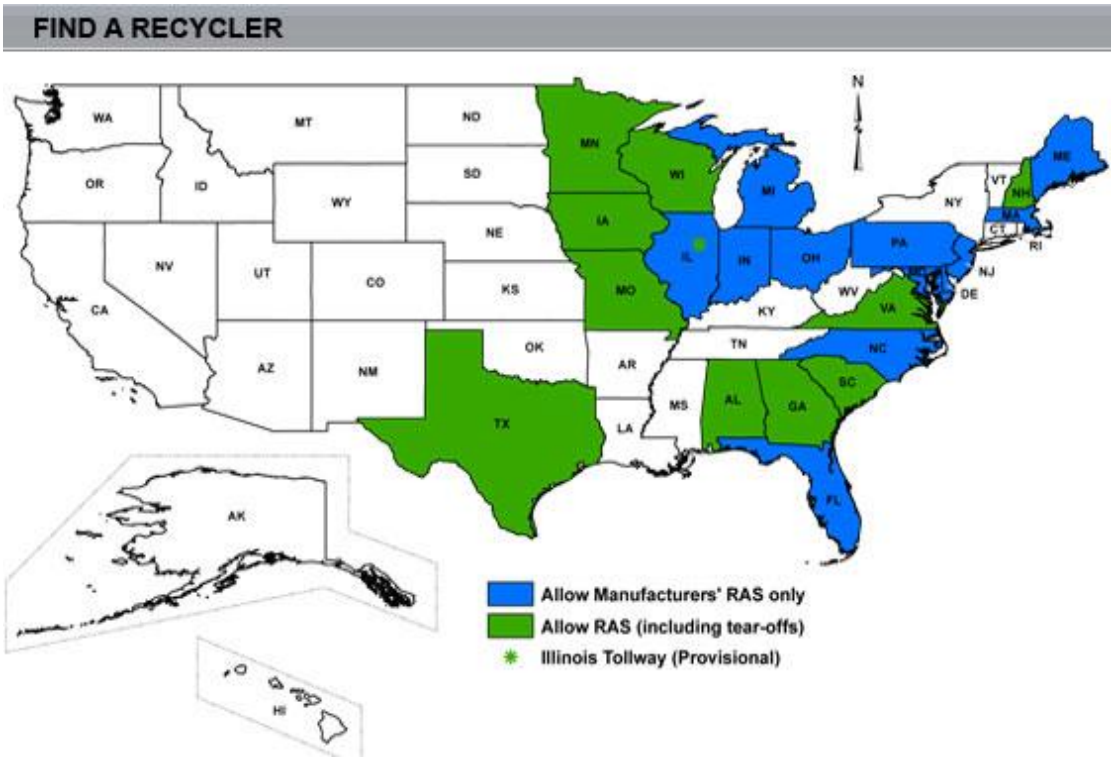

Figure 1: States in the United States Allowing Using of RAS [7]

Dynamic complex modulus (E^*) is a measure of the stiffness of viscoelastic materials. It is one of the most important HMA properties which are used to examine pavement responses such as stress, strain, and deflection in the Mechanistic-Empirical Pavement Design Guide (MEPDG). The MEPDG is a pavement design and performance predicting method developed by the National Cooperative Highway Research Program (NCHRP) in 2002 to address shortcomings in current pavement design methods [8]. The MEPDG uses mechanical principles to calculate aforementioned pavement responses. Empirical models are used to predict pavement performance from the pavement responses. There are many E* predictive models developed by various empirical and mechanical methods such as statistical regression, artificial neural networks, ultrasonic direct test method, and so on. The Witczak and Hirsch models are the most

well-known procedures among them. The Witczak Model is an empirical model developed by Matthew W. Witczak in 1972 [9]. Revisions were made to the model in 1995, 1999, and 2006. The model is based on a sigmoidal function which is used to describe the relationship between the dynamic modulus and loading rate. Aggregate gradation, volumetric properties of mixtures, and binder rheological properties are addressed in the Witczak Model. The Hirsch Model was developed by Y.J. Hirsch in the 1960s [10]. The Hirsch Model is a semi-empirical model based on the law of mixture. There are several versions of the Hirsch Model. Christensen, Pellinen, and Bonaquist conducted research in 2003 that evaluates various Hirsch models and recommends the most effective model to be used.

PROBLEM STATEMENT

The MEPDG was adopted as a pavement design guide by the American Association of State Highway and Transportation Officials (AASHTO) in April, 2011. With the promoted implementation of the MEPDG design procedures, pavement engineers' interest in a quick, easy, and accurate method of obtaining dynamic modulus value are increasing. Laboratory dynamic modulus testing is usually conducted to obtain the E* value directly from a subject mix. However, the testing requires a series of expensive sampling and testing equipment, experienced lab personnel, and a relative long waiting time before knowing the results. The E* predictive models were developed as an alternative method of obtaining the dynamic modulus values. The E* values can be easily calculated from other basic properties of aggregate, binder, and mixture without a specifically designed E* experiment. The predictive models do not require any lab equipment and the values can be estimated instantly. However, there are many factors that can affect the dynamic modulus of mixes and are not addressed in the E* predictive models. When these factors come into effect, the predicting accuracies of the models will decrease. RAS is one of the factors that are not addressed by the Witczak and Hirsch Model. The research is motivated by the needs of a reliable E* predictive method for mixes containing RAS.

OBJECTIVES

The demonstration projects for National Pooled Fund Study 1208 that were constructed in the Summers of 2008, 2009, and 2010 are contained in this thesis. The objective of the pooled fund study is investigating issues related to the use of RAS including effects on laboratory testing properties and field performance in different scenarios as well as issues in processing,

transportation, and storage of RAS. Mix designs for each demonstration project were developed individually for specific objectives. The Indiana demonstration project was developed to investigate different effects of RAS on HMA and warm mix asphalt using foaming technology. The demonstration project in Iowa was designed to study the influences of RAS content on performance. The Minnesota demonstration project was constructed for the purpose of comparing the effects of manufactured RAS and tear-off RAS. The Missouri DOT constructed the demonstration project to study the effects of RAS grind size. Various laboratory tests were performed to fulfill the objectives listed above. Some of the testing results are drawn to complete the following objectives for this research:

- Evaluate the predictive accuracies of the 1999 and 2006 Witczak Models, and the Hirsch Model;
- Identify factors that affect the predictive accuracies of the E* models;
- Examine if the E* predictive models need to be calibrated to account for the effects of RAS;
- Develop modified E* predictive models as needed; and
- Evaluate the effectiveness of the modified models.

METHODOLOGY

The mix designs were developed by SUPERPAVE design procedures. The testing materials were produced in the field and sampled randomly. Laboratory tests were conducted by following the corresponding ASTM and/or AASHTO standards. The dynamic modulus values were tested in the laboratory. The input parameters in the E* predictive models were collected from QA/QC reports, lab testing results, and mix designs. Statistical analyses including Analysis of Variance (ANOVA) and Student's t-test were performed to identify significant factors affecting the model accuracy and comparing multiple levels of significant factors. A non-linear regression approach based on the least square method was used to develop the modified models. The effectiveness of a model is evaluated by its goodness-of-fit and differences in master curves between the predicted E* values and the lab results.

ORGANIZATION

This thesis is divided into five chapters including the introduction (Chapter 1), literature review (Chapter 2), experimental plan (Chapter 3), evaluation and modification of the Witczak

and Hirsch Models (Chapter 4), and conclusions and recommendations (Chapter 5). Chapter 1 provides brief descriptions of the background, addressed issues, objectives, and methodology. Chapter 2 discusses previous studies that have been conducted on recycled asphalt shingles, dynamic modulus, and the Witczak and Hirsch E* predictive models. Chapter 3 outlines the experimental plan and testing procedures. Chapter 4 summarizes the results of evaluations for the original and modified E* predictive models as well as a detailed description of the modeling process. Chapter 5 states the conclusions of the study and provides recommendations for future research.

CHAPTER 2: LITERATURE REVIEW

ASPHALT SHINGLES

Asphalt shingles are the most widely used material for building roofs. Compared to other roofing materials, such as wood shakes, metal, concrete, or clay, asphalt shingles are less expensive and easier to install and replace. Asphalt shingles are typically classified into two types, organic and fiberglass, depending upon the materials used to produce the base felt. The base felts for organic asphalt shingles are made from cellulosic fibers from woods or paper wastes. The fiberglass shingles use fiberglass as the primary component of their base felts. The manufacturing processes for both organic and fiberglass shingles are very similar. Firstly, felts are saturated with liquid asphalt. Secondly, additional asphalt layers are attached to cover both sides of the felts in order to make them waterproof. Finally, shingles are surfaced with mineral granules. Powdered limestone is usually added to asphalts as mineral stabilizer. Fibers can be used as fibrous stabilizer in fiberglass asphalt shingles. The purposes of adding stabilizers to shingles are to improve their fire resistance and weatherability. The procedures for producing organic and fiberglass asphalt shingles are specified in ASTM D225 and ASTM D3462 [11]. Asphalts used in producing shingles are stiffer and more viscous than the virgin asphalts that are commonly used in road pavements. An "air-blown" process is applied to prepare the asphalts for shingles. Air is injected into oxidizer with petroleum residue which was preheated to 400 ℉ (204 ℃) at a constant rate of 0.008 to 0.026 m^3/sec/Mg. Oxygen reacts with asphalt molecules causing increase in the apparent molecular weight. The oxidization process increases the asphalt's softening point and viscosity while decreasing its penetration [12].

Shingles typically consist of asphalt binder, aggregate, and fibers. The proportion of each component varies with shingle type and manufacturer. The most valuable component of shingles is asphalt. In general, organic shingles have higher asphalt contents and lower fiber contents compared to fiberglass shingles. Post-consumer shingles from reroofing construction contain more asphalt than pre-consumer shingles, due to weathering caused loss of surface granules. The largest component of shingles is aggregate including the ceramic granules, headlap granules, backsurfacer sand, and the stabilizer. Aggregates contained in shingles are very fine aggregates that pass the No.12 (1.7mm) sieve [12]. The typical shingle compositions are summarized in

Table 1. The percentages in Table 1 are based on total weight of shingle products. The shingle aggregate compositions and particle sizes are presented in Table 2.

Table 1: Typical Shingle Composition [11]

Material	Organic Shingles	Fiberglass Shingles
Asphalt Binder	30-35%	15-20%
Aggregate	30-50%	30-50%
Fibers/Mineral Fines	15-35%	20-35%

Table 2: Shingle Aggregate Compositions and Size [11]

Component	Typical Quantity percent by weight of sample	Typical Size
Ceramic Granules	10-20%	passing No.12 retained No.40
Headlap Granules	15-25%	Same as above
Backsurfacer Sand	5-10%	passing No.40 retained No.140
Stabilizer	15-30%	90% passing No.100 70% passing No.200

Shingle Recycling

Roofing waste can contain 10 to 15% (by weight) extraneous matters other than asphalt shingles, such as metal flashing, wood sheathing, paper, and nails [13]. Shingle wastes from manufacturers are relatively pure, whereas, Tear-off shingles must be cleaned before further processing. Debris in tear-off shingles can be cleaned by manual or mechanical separations [14]. Asbestos containing materials (ACM) are strictly controlled due to the hazard to worker health. Federal law requires ACM in recycled materials do not exceed 1% by weight [15]. Both tear-off shingles and manufacturer's scrap have to be reduced into finer particles. Finer processed shingles are easier to transport and mix with asphalt mixtures. Georgia DOT requires all shingle scraps to pass the 12.5mm (1/2") sieve [16]. The Texas DOT requires 95% of shingle scraps to pass 1/2" sieve. In most current practices, shingles are reduced to less than 1/2". Processed asphalt shingles are recommended to use in a short range of time due to the storage and handling difficulties. Large clumps of asphalt can form and cause transportation and mixing problems, because shingle stockpiles can consolidate with time. Fine aggregate can be added to processed

shingles to alleviate the formation of asphalt clumps. This could reduce the asphalt content of processed shingles and has to be taken into account during mix design calculations [17].

Previous Researches and Practices of RAS Utilization

Early RAS research focused on studying pre-consumer asphalt shingles. Many state agencies historically allowed only pre-consumer shingles to be used. In recent years, the research focus has shifted to post-consumer asphalt shingles because of the increased pricing of asphalt. The combination of RAS and RAP were studied in several recent research projects.

Minnesota's Shingle Scrap Research [3]

A report prepared for the Minnesota Department of Transportation in October, 1996 studied the properties and performance of asphalt containing RAS pavements. In early the 1990s, three test sections were built on the Willard Munger recreational trail, Highway T.H.25 at south of Mayer and Highway 17 at Scott County respectively. Only pre-consumer RAS were studied in this research. Pavement conditions after 4 to 6 years from the completion of projects showed RAS content up to 7% by aggregate weight would not adversely impact pavement performance. Laboratory tests indicated the asphalt penetration at 77 ℉ of recovered binder containing RAS were less than those of binder without RAS. However, the stiffness increase of the asphalt binder due to RAS did not lead to significant low-temperature cracking problems. The Willard Munger recreational trail also included a test section containing recycled rubbers. A severe raveling issue was found for the rubber section.

Mn/DOT RAS/RAP Research [18]

A comprehensive research funded by the Minnesota Department of Transportation studied the effects of RAP and RAS on mixture lab testing results and field performance. Shingles studied in this research include both manufacturer's scrap and tear-off shingles. Mixture testing samples were made from lab produced mixes. Three or five percent RAS were added with 0%, 15%, 25%, and 30% RAP to make the mixtures for lab testing. Mixtures that contained RAP alone were also tested. Materials for binder testing were extracted from mixtures through a solvent centrifuge process described in ASTM D5404. Six field projects were observed to compare the pavement performance via resistance to different types of cracking and pavement permanent deformation. The following findings were found:

- The binder grading results showed both high and low temperature performance grades increased as the virgin to total binder ratio decreased. This correlation has R^2 value of 0.77 for the low temperature grade and 0.88 for the high temperature grade, respectively. Binders extracted from mixtures that contained tear-off shingles were found to be stiffer than binders from mixtures that contain manufacturer's scrap. The stiffness difference between tear-off shingles and manufacturer's scrap is larger for higher RAP contents.
- For 5% RAS content, the $|E^*|$ values for samples containing tear-off shingles are higher than those for samples containing manufacturer's scrap at the high frequency end of master curves. At the low frequency end, the differences between the two types of shingles are not obvious. For 3% RAS content, the difference between tear-off shingles and manufacturer's scrap is limited. Dynamic modulus test results also showed the virgin to total asphalt content–stiffness correlation was valid at a high temperature (100 ℉).
- Asphalt Pavement Analyzer (APA) results indicated that pavement with recycled materials tended to have less rutting,
- Moisture sensitivity test (Lottman) results indicated that RAS and RAP increased pavement moisture sensitivity which could potentially increase the risk of moisture damage cracking.
- Comparisons between laboratory and field produced mixtures showed that asphalt mixtures prepared in the lab exhibited a higher stiffness than those prepared in the field.
- Pavement condition survey results indicated that the pavement performance of mixes containing tear-off shingles and manufacturer's scrap contained pavement are very similar.

Laboratory Evaluation of Post-consumer RAS Contained HMA Mixture [19]

A conference paper prepared for the Association of Asphalt Paving Technologists (AAPT) 2011 annual meeting evaluated the influences of post-consumer RAS on various lab tests results. The binder and mixture materials were from an Illinois Tollway project on I-90 west of Chicago. The evaluated lab tests include DSR and bending beam rheometer (BBR) test for asphalt binders; as well as dynamic modulus, beam fatigue, and disc shaped compact tension (DCT) testing for

asphalt mixtures. In this project, RAS was used in combination with fractionated recycled asphalt pavement (FRAP). Eight mix designs with total recycled material content from 25% to 50% were developed. Mixes with 5% RAS were compared to the mixes with the same amount of recycled material but containing 0% RAS. Lab results indicated the RAS increases asphalt binder stiffness. The stiffening effect was significant when lower FRAP contents were used. Binder high temperature performance grades were increased by adding 5% RAS to mixtures with total recycled materials less than 40%.For recycled materials more than 40%, the stiffening effect of RAS is not obvious. Dynamic modulus test results showed the mixture high temperature $|E^*|$ values increased as additional FRAP was added. No significant improvements of $|E^*|$ values were observed for recycled material percentages higher than 40%.The paper also indicated that the utilization of RAS and FRAP in asphalt pavement did not caused more fatigue damage.

Oregon State University RAP/RAS Study [20]

Oregon State University conducted a research project to investigate the effects of various proportions of RAP and tear-off shingles on binder high and low temperature grades. The report was published in February, 2010. Seven mix designs were studied with 0% or 5% RAS and RAP percentages ranging from 0% to 50% by the weight of total mixture. The study determined that 5% RAS alone increased the recovered binder high and low temperature performance grades. Adding 10 to 30 percent RAP to mixes with 5% RAS could increase binder grades at both high and low temperatures. However, additional RAP above 30% did not cause further improvements of binder performance grades. The results agreed with the Cascione et al. study.

DYNAMIC MODULUS

Dynamic modulus, E*, is the absolute value of the complex dynamic modulus, which is the stress-to-strain ratio of linear viscoelastic materials under a continuous sinusoidal loading. It can be computed as the amplitude of the sinusoidal stress divided by the maximum recoverable strain:

$$|\mathbf{E}^*| = \frac{\boldsymbol{\sigma_0}}{\boldsymbol{\varepsilon_0}}$$

Equation 1

where $|E^*| =$ dynamic modulus,

σ_0 = maximum stress, and

ε_0 = maximum strain

When the strain is at a small level which is less than 100 micro-strain (με), the asphalt stress-strain relationship is considered linear viscoelastic [21]. For linear viscoelastic materials, material responses are time dependent. The corresponding strain occurs a period of time after a load is applied. The time lag is defined as the phase angle (Φ). For perfectly elastic materials, Φ equals to 0; and for perfect viscous materials, Φ equals to 1. The phase angle can be calculated by Equation 2 [22]:

$$\emptyset = \frac{\mathbf{t_i}}{\mathbf{t_p}} \times \mathbf{360}$$

Equation 2

where $\emptyset$ = phase angle,

t_i = lag time between stress and strain cycles, and

t_p = time of one strain cycle.

Figure 2 demonstrates this process. The term "perfectly elastic" means material strain reacts to stress instantaneously. In other words, the material achieves its maximum strain at exactly the same time that the maximum stress is applied. The term "perfectly viscous" means the maximum strain occurs at the same time the minimum stress is applied. For any given time, the material stress to strain ratio is the complex dynamic modulus. The complex dynamic modulus can be mathematically expressed by Equation 3 [23]:

$$\mathbf{E^*} = \frac{\boldsymbol{\sigma}}{\boldsymbol{\varepsilon}} = \frac{\boldsymbol{\sigma_0 \sin(\omega t)}}{\boldsymbol{\varepsilon_0 \sin(\omega t - \delta)}}$$

Equation 3

where the parameters are defined previously.

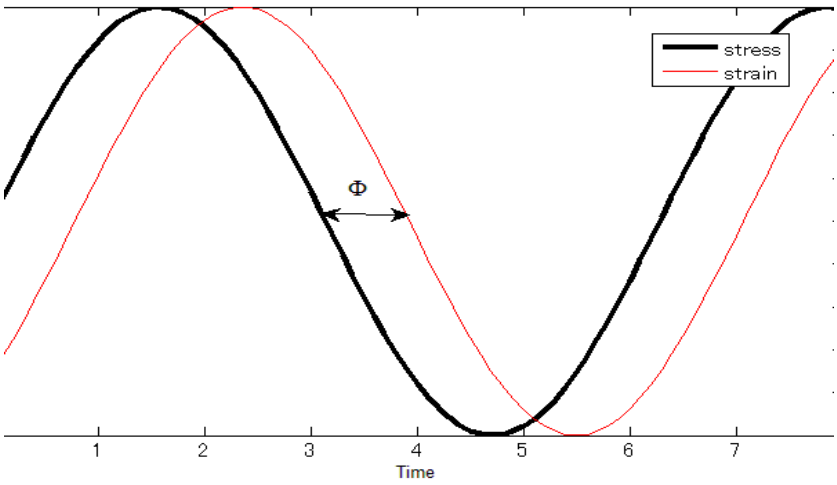

Figure 2: Stress and Strain of Typical Viscoelastic Material under Sinusoidal Loading

The dynamic modulus is a measure of relative stiffness for viscoelastic materials. Asphalt mixtures that have higher dynamic moduli tend to deform less under a traffic loading than mixtures with lower dynamic modulus. At high temperatures, less deformation is related to better resistance to rutting. At low temperatures, high dynamic modulus pavements achieve high internal stresses which could result in greater susceptibility to low-temperature cracking.

Dynamic Modulus Testing

Coffman and Pagen at Ohio State University developed the first dynamic modulus protocol in the 1960's [22]. It was accepted as an ASTM standard in 1979. The designation is D3496 in ASTM standards and TP62 in AASHTO specifications. The protocol came up with the idea of testing the dynamic modulus of viscoelastic materials from a triaxial test under a uniaxial sinusoidal stress. The stress could be either compressive or tensile; most dynamic tests were conducted with compressive stresses. Shear stress can also be used to determine the dynamic complex modulus for asphalt binders with a dynamic shear rheometer. The binder dynamic shear complex modulus is denoted as G^*; the testing procedures are specified in AASHTO D7175, *standard test method for determining the rheological properties of asphalt binder using a dynamic shear rheometer* [24]. The binder dynamic modulus is assumed to be 3 times of the G^* based on experiences [10]. For mixture dynamic modulus testing, AASHTO specification requires a servo-hydraulic testing machine to apply the sinusoidal loading. A Superpave

Gyratory Compactor (SGC) is used to compact $160mm \times 150mm$ (height by diameter) asphalt cylinder with air void content not exceeding $\pm 5\%$ from the specified target air void content. A Testing specimen is cored and cut to $150mm \times 100mm$ from the compacted asphalt specimen. Sample axial deformation is measured with linear variable differential transformers (LVDT). Samples are often tested at several temperatures. At each temperature, dynamic moduli are taken for multiple loading frequencies typically varying from 0.1Hz to 25Hz, in a strain controlled mode of loading. Loading is adjusted to obtain 50 to 150με.The permanent deformation of specimen is often controlled to less than 1500με [25]. The testing results are generally presented as master curves.

Dynamic Modulus Master Curve

Asphalt mixture dynamic modulus varies with temperature and loading frequency. The comparisons of testing results are complicated, especially when the testing temperatures are different. The dynamic modulus master curve provides a direct visual expression of dynamic modulus results. Comparisons between two sets of dynamic modulus results can be possible [26].The standard dynamic testing procedure elaborated by ASTM D3497 recommends using three temperatures (5, 25, and 40 ℃). At each temperature, $|E^*|$ values are tested at three frequencies (1, 4, 16Hz). In order to develop more precise master curve, five temperatures (-9, 4.4, 21.1, 37.8, and 54.4 ℃) with six frequencies (25, 10, 5, 1, 0.5, and 0.1Hz) at each temperature are usually used for dynamic modulus testing. According to the research conducted by Li and Williams [36], testing $|E^*|$ values at three temperatures (4.4, 21.1, and 37.8 ℃) did not change the shape of master curves constructed by data from the nine temperatures. In practice, engineers are interested in pavement properties in the worst scenarios. The lowest temperatures at most places of U.S. are far below the lab low temperature test. Master curve also provides estimations of dynamic moduli out of the lab testing range. The 2002 NCHRP pavement design guide uses asphalt dynamic moduli determined from master curves [27].

The$|E^*|$ master curve can be constructed at a reference temperature or frequency based on the time-temperature superposition principle. Asphalt exhibits higher E* values at low temperatures or high loading frequencies. Therefore, an E* value tested at a lower temperature could equal to an E* value tested at a higher temperature but at a lower frequency. Therefore, E* values tested at different temperatures and frequencies can be transferred to a single reference temperature or

frequency. Often times, dynamic modulus testing can be easily done at multiple frequencies. Changing the test temperature is usually time consuming and thus costly. As a result, researchers usually test dynamic modulus at few temperatures but many different frequencies. The transition from frequency to temperature is much easier than from temperature to frequency. A number that is used to equalize frequencies at different temperatures is called a shift factor, a(T). Equation 4 shows the mathematical definition of this shift factor:

$$\mathbf{f_r = \frac{f}{a(T)} \rightarrow \log(f_r) = \log(f) - \log(a(T))}$$

Equation 4

where f_r = reduced frequency (loading frequency at the reference temperature),

f = loading frequency, and

a(T) = shift factor.

The Shift factor is 1 at the reference temperature; and the log(a(T)) is therefore 0.The *"2002 Guide for the Design of New and Rehabilitated Pavement Structures"* uses a sigmoidal function shown below to construct a master curve fitting line [27]:

$$\mathbf{\log(|E^*|) = \delta + \frac{\alpha}{1 + e^{\beta + \gamma \log(t_r)}}}$$

Equation 5

where $|E^*|$ = dynamic modulus,

t_r = time for loading at the reference temperature (reduced time),

δ = minimum modulus value,

$\delta + \alpha$ = maximum modulus value, and

β, γ = parameters describing the shape of the sigmoidal function.

The parameters that are used to represent the master curve including $\alpha, \beta, \gamma,$ and a(T) can be solved by using Excel Solver Function to match the calculated E* values from the sigmoidal function with the lab tested E* values. Figure 3 illustrates the shifting of E* values and construction of master curve.

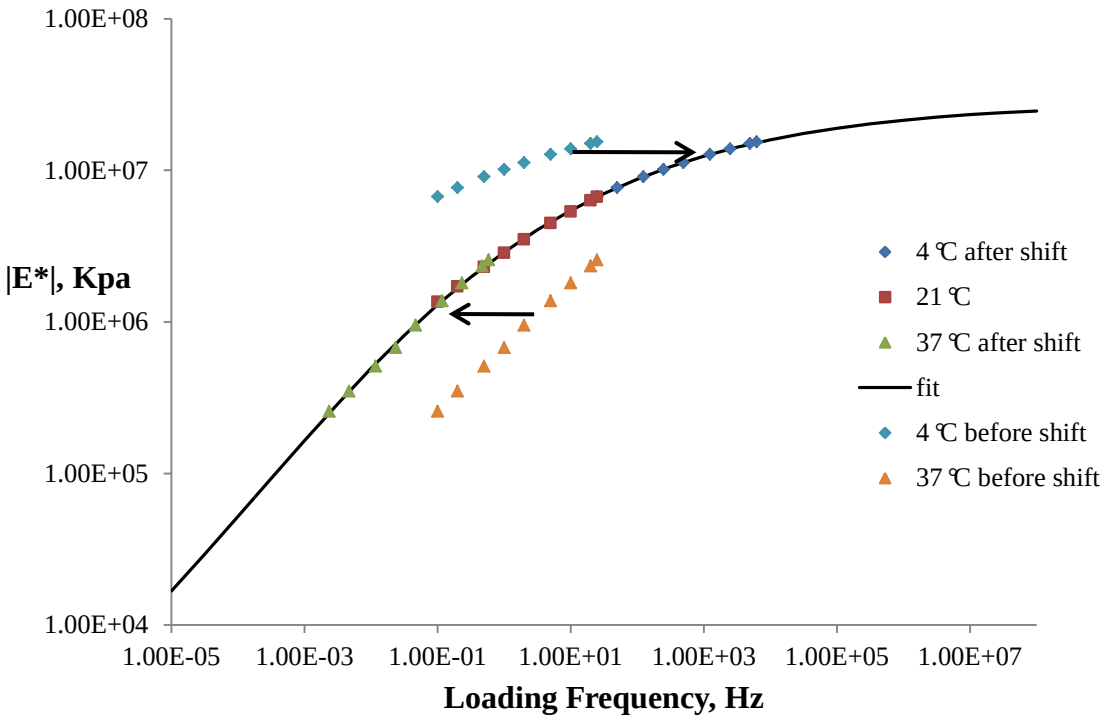

Figure 3: Master Curve Construction

Witczak E* Predictive Model

The early Witczak's dynamic modulus predictive model was developed in 1972. The model was based on non-linear polynomial regression of laboratory E* values. The early model was established from 29 mixtures with 87 total data points. Several revisions were made ensuring twenty years. The current MEPDG pavement design program uses the Witczak model developed in 1999 for E* estimation. The 1999 Witczak model is developed from 205 laboratory mixtures including 171 unmodified asphalt binders and 34 modified binders that produced 2750 data points. The newest Witczak model was published in 2006 including 7400 data points from 346 HMA mixtures [9].

The 1999 Witczak model is the most widely used version of Witczak model because of the application of the MEPDG program in pavement design. This model predicts E* values of HMA mixtures from 8 input parameters that characterize aggregate gradation, asphalt binder behavior, binder–aggregate interaction, and loading condition. An R^2 of 0.96 and Se/Sy of 0.24 were observed for this model on a logarithm scale. The model is shown in Equation 6 [23]:

$$\log|E^*| = 3.750063 + 0.02932\rho_{200} - 0.001767(\rho_{200})^2 - 0.002841\rho_4 - 0.058097V_a - 0.802208\left(\frac{V_{beff}}{V_{beff}+V_a}\right) + \frac{3.871977 - 0.0021\rho_4 + 0.003958\rho_{38} - 0.000017(\rho_{38})^2 + 0.00547\rho_{34}}{1 + e^{(-0.603313 - 0.31335\log(f) - 0.393532\log(\eta))}}$$

Equation 6

where $|E^*|$ = dynamic modulus (psi),

η = bitumen viscosity (10^6Poise),

f = loading frequency (Hz),

V_a = air void content (%),

V_{beff} = effective bitumen content(% by volume),

ρ_{34} = cumulative % retained on the 19-mm (3/4inch) sieve,

ρ_{38} = cumulative % retained on the 9.5-mm (3/8inch) sieve,

ρ_4 = cumulative % retained on the 4.75-mm (No.4) sieve, and

ρ_{200} = % passing the 0.075-mm (No.200) sieve.

Laboratory viscosity tests can only be done at high temperatures that allow asphalt binders to flow. Asphalt binders at low temperatures are difficult to test directly. The viscosity-temperature-susceptibility (VTS) method allows estimation of asphalt's viscosity at any temperature from lab tested viscosities at several temperatures from laboratory testing can be easily done. It should be noticed that this log-log to log linearity is only applicable for conventional type "S" asphalt cement. There are several ways to obtain the laboratory viscosities. Viscosities can be tested directly with the rotational viscometer by following *ASTM D2983*. The viscosities can be also estimated from binder penetration test results and dynamic shear rehometor (DSR) test results. The penetration–viscosity relation is expressed in Equation 7 [28]:

$$\log(\eta) = 10.5012 - 2.2501\log(Pen) + 0.00389\log(Pen)^2$$

Equation 7

where η = viscosity (Poise), and

Pen = penetration for 100 g, 5 seconds loading (0.1 mm).

The penetration viscosities were used prior to the DSR testing being available. This empirical equation is developed from regression of 17 test sections with 766 data points. The R^2 value is 0.377 in normal scale and 0.927 in logarithm scale [23]. The Equation 8 is commonly used now [9]:

$$\boldsymbol{\eta = \frac{|G^*|}{10}\left(\frac{1}{\sin\delta}\right)^{4.8628}}$$

Equation 8

where η = viscosity (Poise),

$|G^*|$ =asphalt binder shear modulus (Pa), and

δ = asphalt binder phase angle.

One problem that is brought up regarding the 1999 Witczak model is that the binder stiffness is characterized by viscosity which does not take into consideration of the effects of loading frequency. Frequency is treated as another independent input variable in the predictive equation. However, binder viscosity is frequency dependent. Changes in loading frequencies also induce viscosity changes of the binder. The scenario intimated by the 1999 Witczak model that binder viscosity can remain the same while loading frequency varies may never happen in reality. This contradiction was addressed and modified by the 2006 Witczak model which uses the dynamic shear complex modulus ($|G^*|$), and phase angle (δ), from DSR tests instead of viscosity to characterize binder stiffness. The G* values at each temperature and loading frequency and the corresponding δ values can be estimated by constructing a master curve based on asphalt binder DSR results. The 2006 Witczak predictive equation is expressed in Equation 9 [9]:

$$\begin{aligned}\boldsymbol{\log_{10}E^*} &= \boldsymbol{-0.349 + 0.754\left(|G_b^*|^{-0.0052}\right)} \\ &\times\left(\boldsymbol{6.65 - 0.032\rho_{200} + 0.0027\rho_{200}^2 + 0.011\rho_4 - 0.0001\rho_4^2}\right. \\ &\left.\boldsymbol{+ 0.006\rho_{38} - 0.00014\rho_{38}^2 - 0.08V_a - 1.06\left(\frac{V_{beff}}{V_a + V_{beff}}\right)}\right) \\ &+ \frac{\boldsymbol{2.56 + 0.03V_a + 0.71\left(\frac{V_{beff}}{V_a+V_{beff}}\right) + 0.012\rho_{38} - 0.0001\rho_{38}^2 - 0.01\rho_{34}}}{\boldsymbol{1 + e^{(-0.7814 - 0.5785\log|G_b^*| + 0.8834\log\delta_b)}}}\end{aligned}$$

Equation 9

where E^* = dynamic modulus (psi),

ρ_{200} = aggregates (by weight of the total aggregates) passing through no. 200 sieve (%),

ρ_4 = cumulative aggregates (by aggregates weight) retained on no. 4 sieve (%),

ρ_{38} = cumulative aggregates (by aggregates weight) retained on the 3/8" sieve (%),

ρ_{34} = cumulative aggregates (by aggregates weight) retained on the 3/4" sieve (%),

V_a = air voids (by volume of the mix) (%),

V_{beff} = effective binder content (by volume of the mix) (%),

$|G_b^*|$ = dynamic shear modulus of binder (psi), and

δ_b = phase angle of binder associated with $|G_b^*|$ (degree).

Hirsch E* Predictive Model

The Hirsch dynamic modulus predictive model is a semi-empirical method based on various modified law of mixtures developed by Y.J. Hirsch in the 1960s. There are two versions of the law of mixtures presented in Equations 10 and 11 [10]:

$$\mathbf{E_c = v_1 E_1 + v_2 E_2}$$

Equation 10

$$\mathbf{1/E^c = v_1/E_1 + v_2/E_2}$$

Equation 11

Where E_c is the composite material property, v_1 and v_2 are the volume fractions of component phase 1 and 2 of the composite material, respectively, and E_1 and E_2 are the material properties of component phase 1 and 2, respectively. The principle of the law is that a composite material property can be treated as a combination of the properties of its components. The influence of each component is proportional to its volume fraction. Phases of composite material can be arranged either in parallel, or series, or even a combination of both. The Hirsch model uses the combined arrangement of phases. The schematic expression of Hirsch model is shown in Figure 4 (a). Figure 4 also shows some important the variations of the Hirsch model.

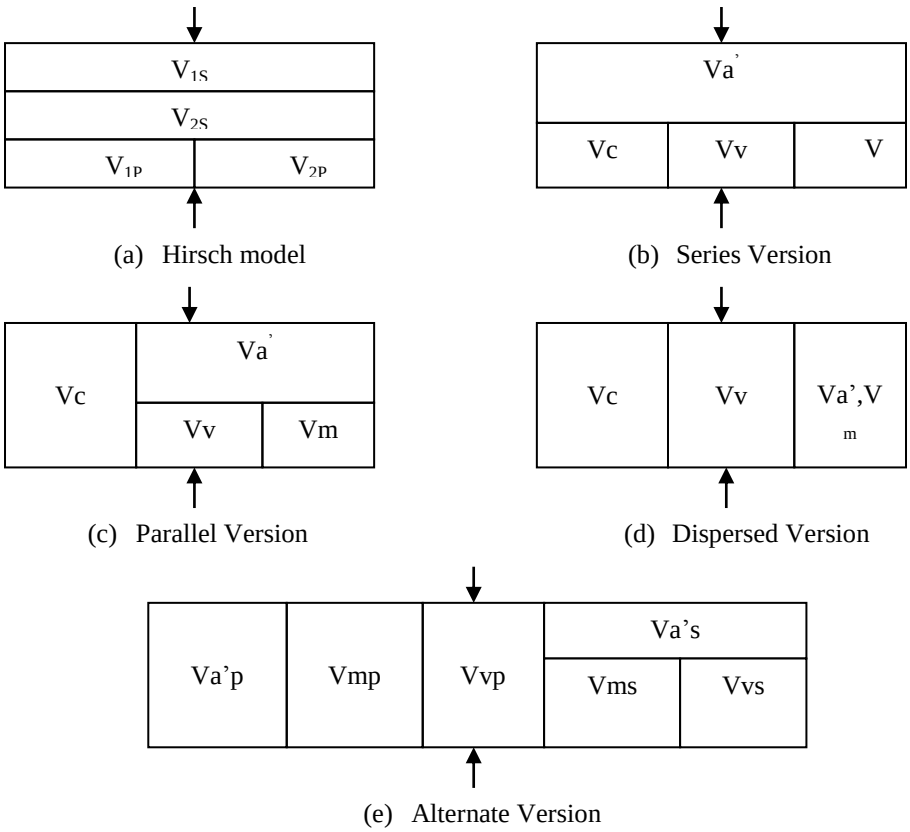

Figure 4: Schematic Representation of Hirsch Model and Four Modified Versions [10]

In Figure 4, Va' is the volume fraction of aggregate excluding the contact volume and mineral filler, Vc is the aggregate contact volume, Vv is the volume fraction of air voids, and Vm is the mastic volume. The subscripts "p" and "s" refer to the arrangement type "parallel" and "series", respectively. Christensen, Pellinen, and Bonaquist did evaluations on various versions of Hirsch model and found out the alternate version in Figure 4(e) was the most accurate model. The alternate version of Hirsch model can be mathematically represented as Equation 12 [10]:

$$\mathbf{Ec = Pc(Va'Ea + VmEm) + (1 - Pc)}\left[\frac{\mathbf{Va'}}{\mathbf{Ea}} + \frac{\mathbf{(Vm + Vv)^2}}{\mathbf{VmEm}}\right]^{\mathbf{-1}}$$

Equation 12

where Ec = modulus of asphalt mixture,

Ea = aggregate modulus,

Em = mastic modulus, and

Pc = aggregate contact volume fraction.

Other parameters are as defined before. The aggregate contact volume can be calculated by Equation 13 [10]:

$$\mathbf{Pc} = \frac{(\mathbf{P_0} + \frac{\mathbf{VFM \times Em}}{\mathbf{VMA'}})^{\mathbf{P_1}}}{\mathbf{P_2} + (\frac{\mathbf{VFM \times Em}}{\mathbf{VMA'}})^{\mathbf{P_1}}}$$

Equation 13

where VMA'= voids in the mineral aggregate,

VFM = voids filled with mastic, and

P_0, P_1, and P_2= empirically determined constants

Several Hirsch model equations were constructed and evaluated by Christensen and his colleagues. The final model for predicting mixture dynamic modulus is presented by the following functions [10]:

$$|\mathbf{E^*}|_{\mathbf{mix}} = \mathbf{Pc} \times \left[\mathbf{4200000} \times \left(\mathbf{1} - \frac{\mathbf{VMA}}{\mathbf{100}}\right) + \mathbf{3} \times |\mathbf{G^*}|_{\mathbf{binder}} \left(\frac{\mathbf{VFA \times VMA}}{\mathbf{10000}}\right)\right] + (\mathbf{1} - \mathbf{Pc}) \times \left[\frac{\mathbf{1} - \frac{\mathbf{VMA}}{\mathbf{100}}}{\mathbf{4200000}} + \frac{\mathbf{VMA}}{\mathbf{3 \times VFA \times |G^*|_{binder}}}\right]^{\mathbf{-1}}$$

Equation 14

$$\mathbf{Pc} = \frac{(\mathbf{20} + \frac{\mathbf{VFA \times 3 \times |G^*|_{binder}}}{\mathbf{VMA}})^{\mathbf{0.58}}}{\mathbf{650} + (\frac{\mathbf{VFA \times 3 \times |G^*|_{binder}}}{\mathbf{VMA}})^{\mathbf{0.58}}}$$

Equation 15

where parameters are defined previously.

In Equation 14, the term VFA which is the volume of voids filled by asphalt is equivalent to VFM in Equation 15. The dynamic modulus of the asphalt binder is considered 3 times binder shear modulus ($|G^*|_{binder}$). The aggregate modulus is estimated as 4,200,000 psi with standard error of 6.5%. The unit of predicted mixture dynamic modulus ($|E^*|_{mix}$) is pounds per square inch.

Previous Evaluation of the Witczak and Hirsch E* Predictive Models

This section contains the main findings of several studies on accuracies of the Witczak and Hirsch dynamic modulus predictive models. Many researchers have compared the efficiencies of Witczak and Hirsch models. Pavement projects studied cover the majority of the United States climate regions. An overseas project from Argentina is also included.

University of Minnesota Study [29]

Clyne, Li, Marasteanu, and Skok from the University of Minnesota tested the dynamic complex modulus and phase angle of asphalt mixtures from Mn/ROAD test cells. Mixtures from cells 33, 34, and 35 at Mn/ROAD used the same mix design with different types of asphalt. Sample cylinders for cells 33, 34, and 35 were made by field produced loose mixes. Cores were taken at cell 21 which was paved 6 years before the other cells and therefore loose mix was not available. This project also included two polymer modified asphalts. Table 3 summarizes the source material properties and Table 4 summarizes the mixture gradations.

Table 3: Material Properties [29]

Cell	21	33	34	35
Binder Type	120/150	PG 58-28	PG 58-34	PG 58-40
Polymer Modified?	No	No	Yes	Yes
Sample Type	Core	Loose Mix	Loose Mix	Loose Mix
Paving Date	07-1993	08-1999	08-1999	08-1999

Table 4: Mixture Gradation [29]

		Percent Passing			
Sieve Size, mm	**Sieve Size, in.**	**Cell 21**	**Cell 33**	**Cell 34**	**Cell 35**
19	3/4	100	100	100	100
16	5/8	99			
12.5	1/2	96	94	94	94
9.0	3/8	88	86	86	86
4.75	#4	70	66	66	66
2.36	#8		54	54	54
2.0	#10	58			
1.0	#20	44			
0.45	#40	26			
0.25	#80	9			
0.0075	#200	4.3	4.7	4.7	4.7

Figure 5 through Figure 8 show master curves constructed based on the laboratory dynamic modulus results and the 1995 and 2000 Witczak's predictive models.

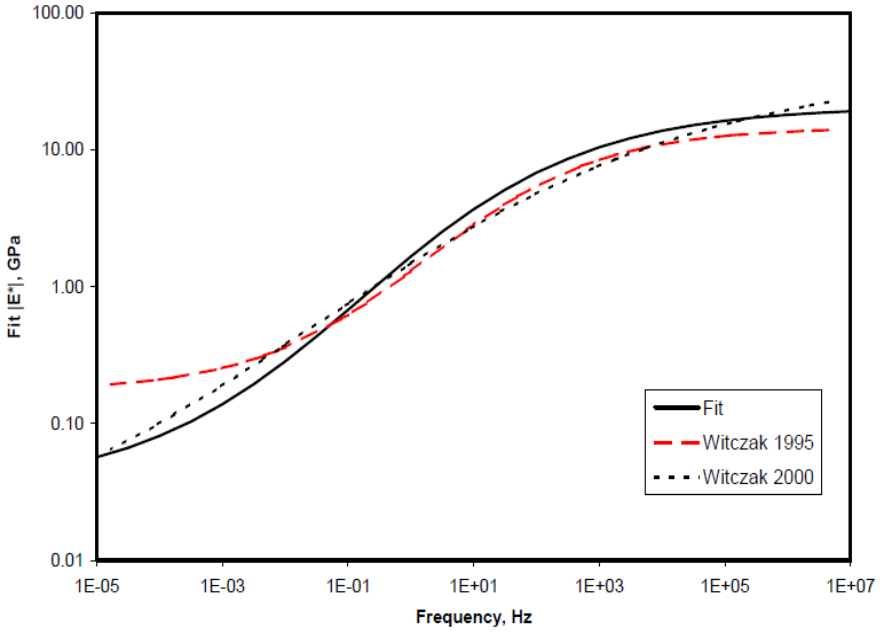

Figure 5: Master Curve Comparison for Cell 21 [29]

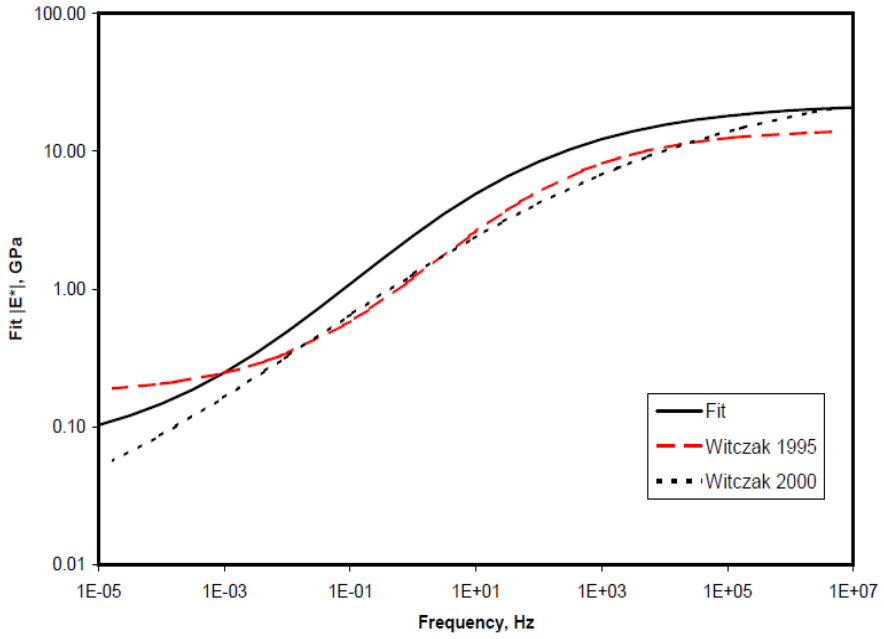

Figure 6: Master Curve Comparison for Cell 33 [29]

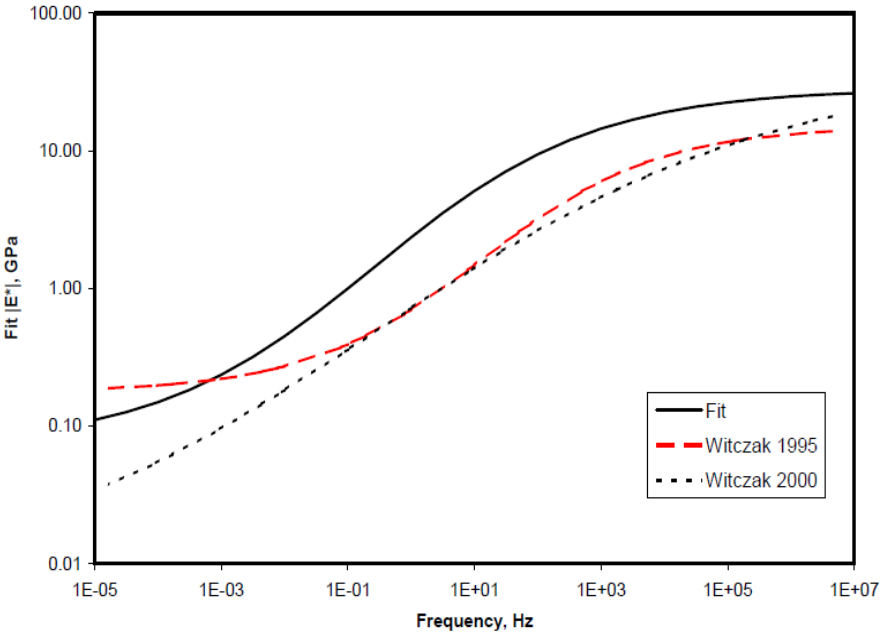

Figure 7: Master Curve Comparison for Cell 34 [29]

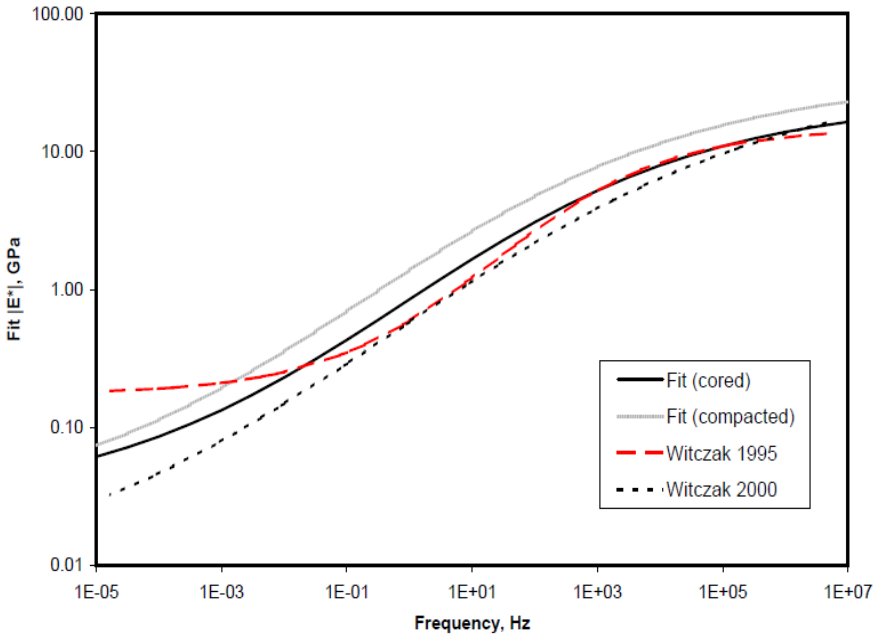

Figure 8: Master Curve Comparison for Cell 35 [29]

The master curve comparisons show that the Witczak model made relatively accurate predictions at intermediate and low temperatures for cells 21 and 35. At the high temperature range, the Witczak model did not fit the lab data. For mixtures from cells 33 and 34, the Witczak predictive model is poor to fit the lab results. The 2000 Witczak model tends to predict lower dynamic modulus values at high temperatures than those tested.

North Carolina State University Study [30]

This research performed by Y. Richard Kim et al. [30] studied dynamic complex modulus of mixtures made from materials that were commonly used in North Carolina. The study includes 42 different mix designs with two types of asphalt binder. The laboratory results were compared with the 2000 Witczak predictions as well as the Hirsch predictions. In the final report, accuracy of the predictive model is quantified by the percent of error which is the difference between lab result and model prediction divided by the lab result. Figure 9 and Figure 10 show the results of comparisons.

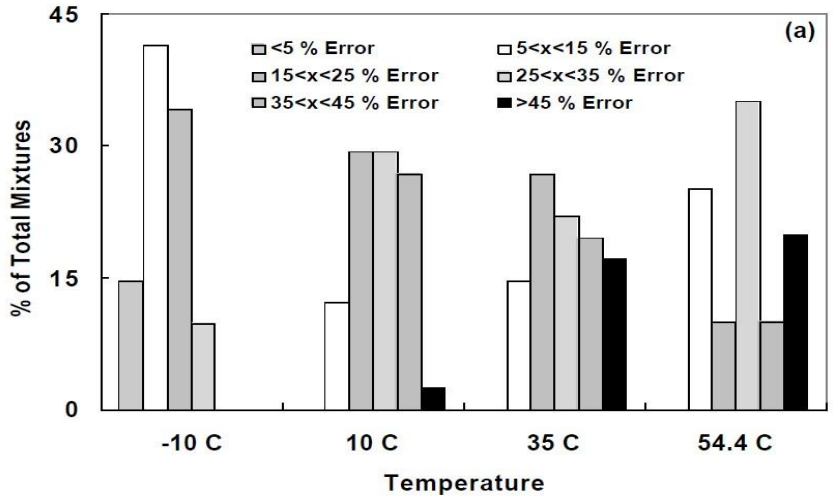

Figure 9: Summary of Percent Error in Dynamic Moduli for Witczak's Prediction [30]

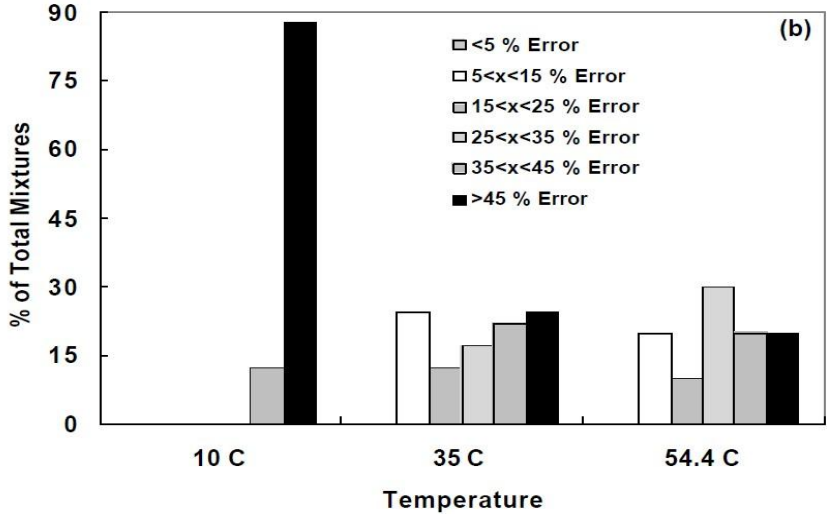

Figure 10: Summary of Percent Error in Dynamic Moduli for Hirsch's Prediction [30]

The results indicate that the Witczak model fits lab observations better at lower temperatures than high temperatures. Similar model efficiencies were found at 35 ℃ and 54.4 ℃. However, the Hirsch model showed very low accuracy of prediction at 10 ℃. The authors explained this as a result of extrapolating binder viscosities at 10 ℃ instead of testing directly.

Christensen, Pellinen and Bonaquist [10]

This study evaluated three different versions of the Hirsch model using 206 data points collected from the Federal Highway Administration's Accelerated Loading Facility (ALF) project, the Mn/Road project, and the WesTrack project. The three Hirsch models included the "simple version", the "mastic version" which accounts for the mineral filler's effects on mixture

stiffness, and the "transition zone version" which is modified for the effects of film thickness. The authors found out that a R-square value of 0.968 were observed for all three of the models. Taking into account for the effects of mineral filler and film thickness did not improve the model efficiency. In addition, a comparison between the Hirsch model and Witczak models were also made. The comparison result is shown in Figure 11.

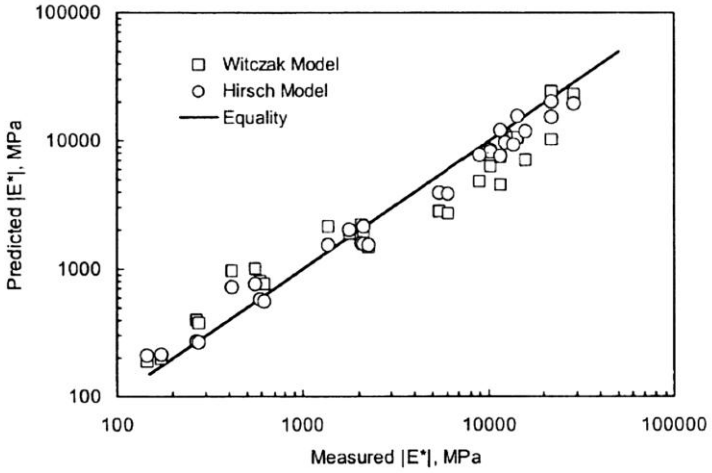

Figure 11: Predicted and Measured E* Values [10]

Figure 11 indicates the accuracies of Witczak and Hirsch models are on similar scales. At low temperatures, the Hirsch model tends to be more effective.

University of Florida Study [31]

The study is focusing on the efficiency of Witczak model (1999) on predicting the dynamic modulus of Florida mixtures. Twenty eight commonly used mixtures in the state of Florida were studied. Three methods were used to obtain binder viscosities including: 1. directly test asphalt viscosities with Brookfield viscometer; 2. calculate viscosities by shear modulus and phase angle values from DSR test; 3. use empirical A and VTS parameters recommended by Witczak and Fonseca for mix/laydown condition. The results are shown in Figure 12 through Figure 14 respectively.

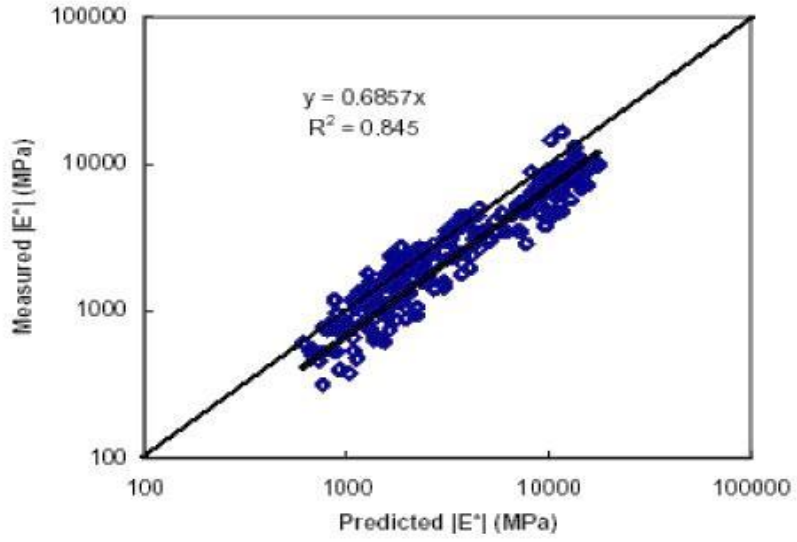

Figure 12: Witczak Model Accuracy (RTFO Condition, Viscosity from RV Test) [31]

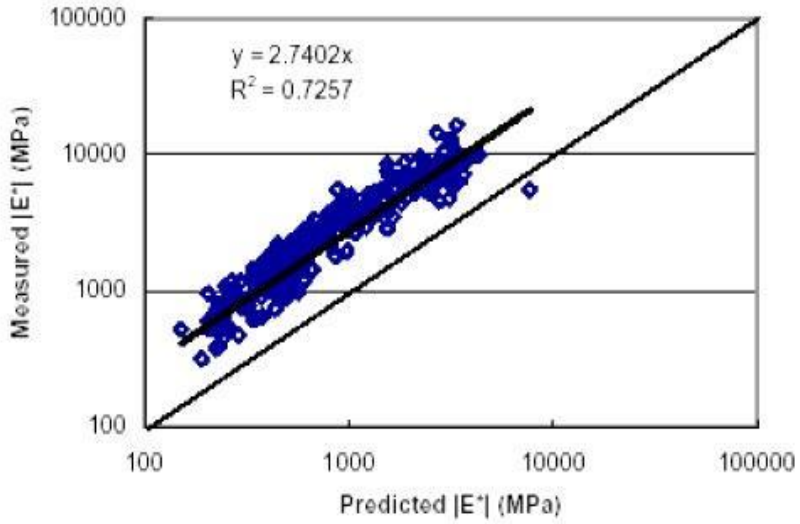

Figure 13: Witczak Model Accuracy (RTFO Condition, Viscosity from DSR Test) [31]

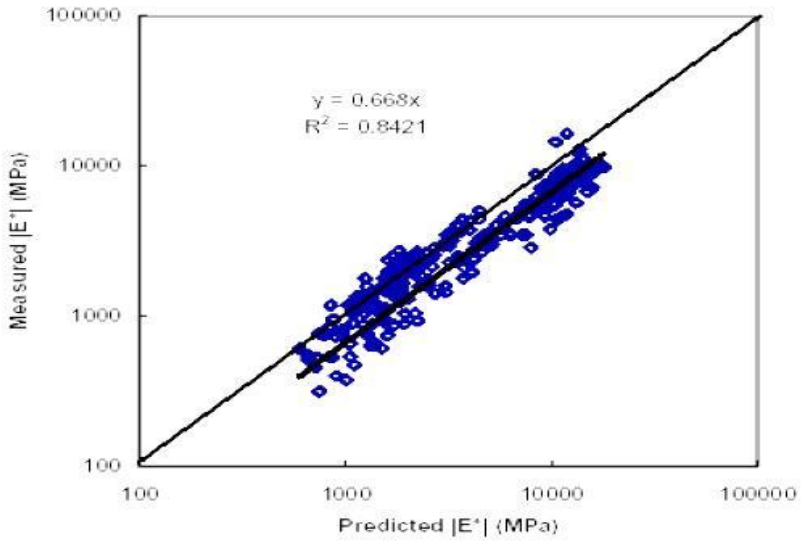

Figure 14: Witczak Model Accuracy (Mix/Laydown condition) [31]

The results indicate the Witczak model well simulates the trend of dynamic modulus values. The best fitting lines parallelly deviate from the lines of equality. By applying a multiplier or shift factor for each method, the Witczak model showed high accuracy on predicting dynamic modulus values for Florida mixtures. It should be noticed that using DSR test results to estimate a binder's viscosity results in lower predicted dynamic modulus values.

Argentina Study [32]

Materials studied in this research contain both lab produced mixtures and field cores. Field cores were taken from 17 sections around Rosario in the Littoral region of Argentina containing 42 types of mixtures. Eight laboratory mixtures were designed and compacted to sample cylinders using Marshall Procedures. Lab data were used to evaluate the 2000 Witczak model, the Hirsch clarify model, and the Heukelomp and Klomp equation developed in 1964. Figure 15 through Figure 18 show the dynamic modulus values predicted by the Witczak and Hirsch models versus laboratory results on log-log scale for lab produced mixtures and field mixes, respectively.

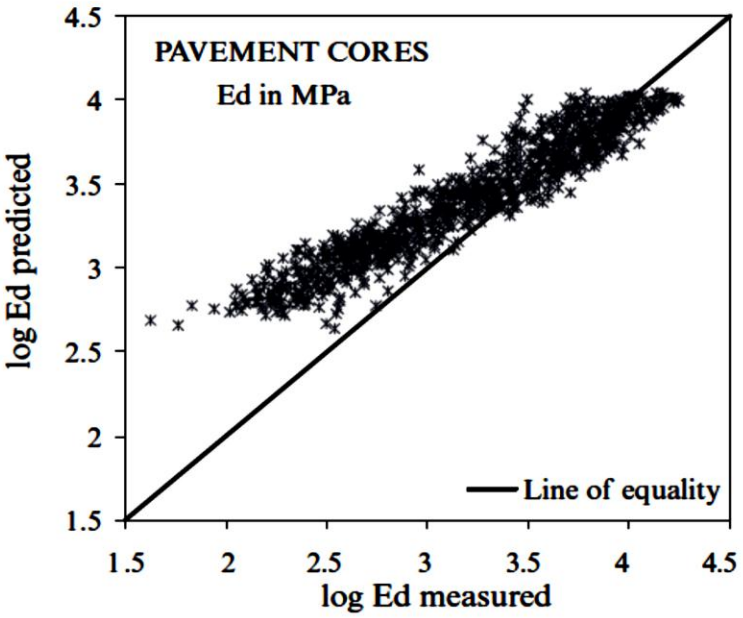

Figure 15: Comparison of Values Using the Witczak Predictive Equation [32]

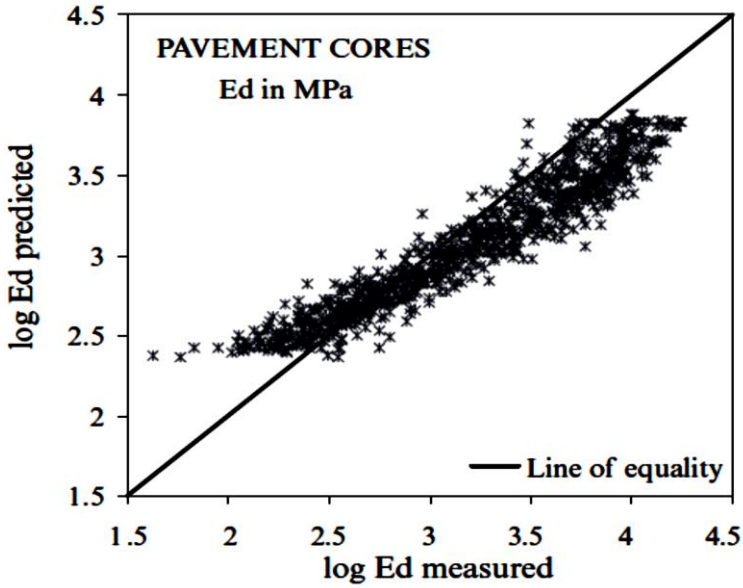

Figure 16: Comparison of Values Using the Hirsch Model [32]

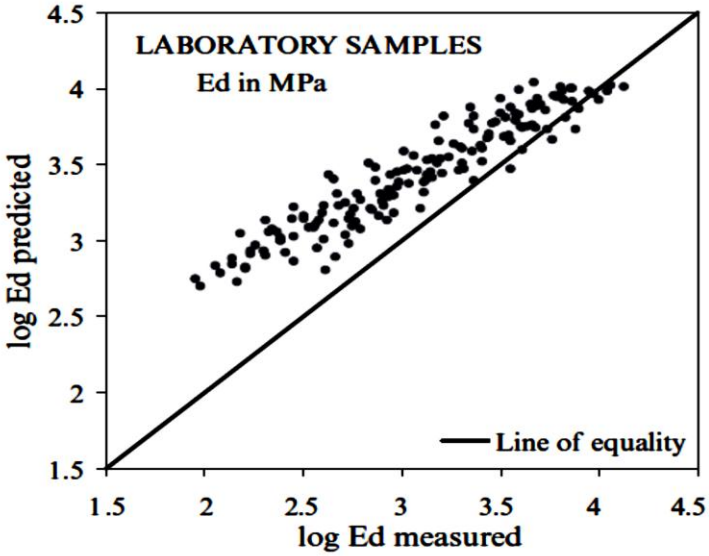

Figure 17: Comparison of Values Using the Witczak Predictive Equation [32]

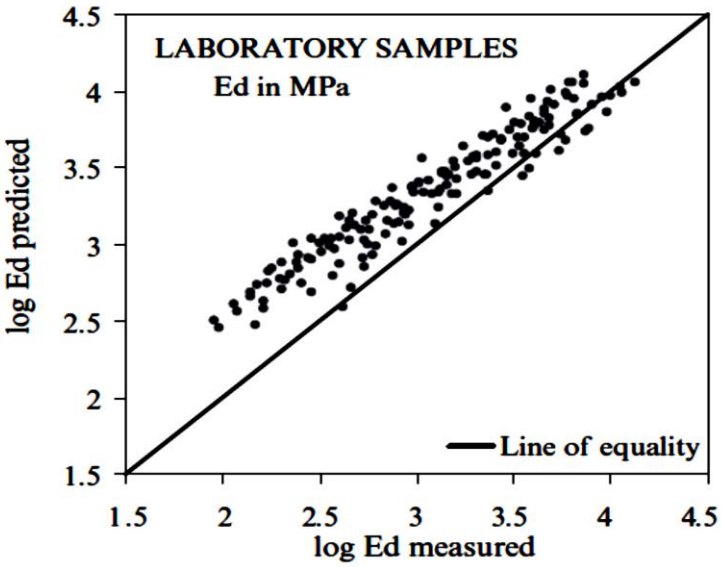

Figure 18: Comparison of Values Using the Hirsch Model [32]

The results indicate that the Witczak and Hirsch models have the similar accuracy predicting dynamic moduli of Argentina mixtures. Both of the models have good prediction at lower temperatures. At high temperatures, the predicted E* values tend to be larger than the measured values.

Effects of Fibers on Asphalt Concrete Mixture Dynamic Modulus

This section summarizes the findings of two research projects: Serfass and Samanos' study [33], and a Wuhan University of Technology study [34]. Four types of manufactured fibers were studied by Serfass and Samanos, and three types of manufactured fibers were studied by the Wuhan University of Technology. The conclusions of two studies are agreed showing that different fibers have notable strengthening effects on mixture dynamic modulus values.

Serfass and Samanos Study [33]

The comprehensive study performed various laboratory tests on mastics, mortars, and asphalt concretes. Two types of mixtures were tested: thin course mixes, and porous mixes. Static and dynamic moduli tests were performed only for the thin course mixes. Pavement conditions surveys were also conducted. Pavement skid resistance, sand patch depth, and cracking information were collected over more than ten years. The fibers studied included chrysotile, rock wool, glass wool, and cellulose. Some of the research conclusions were:

- Fibers could reduce the loss of binder in coating mastic, thus increasing a pavement's resistance to moisture, aging, and fatigue damage;
- Attention needs to be paid on rutting resistance for thin wearing courses; and
- The static and dynamic modulus values of fiber-modified asphalt mixtures are distinctly higher than mixtures that use the same binders but without fibers.

Wuhan University of Technology Study [34]

The three types of fibers used in this study were cellulose, polyester and mineral fibers. Unconfined dynamic modulus tests were performed at five temperatures from -10 ℃ to 54.4 ℃, and nine frequencies ranging from 0.1 Hz to 25 Hz. The results indicate adding fibers to asphalt mixtures can increase HMA dynamic modulus values. Lower phase angles at lower temperatures and higher phase angles at higher temperatures were observed for fiber-modified asphalt mixtures. Asphalt mixtures containing fibers tend to have lower loss modulus values at medium temperatures.

CHAPTER 3: EXPERIMENTAL PLAN AND TESTING METHODS

EXPERIMENTAL PLAN AND TESTING MATERIALS

Experimental materials were procured from the national pooled fund study #1208 testing sections. The national pooled fund study #1208 conducted a comprehensive research on application of RAS in asphalt pavement including the study of mixture and binder properties, issues in RAS processing and storage, and pavement field performance. Missouri is the lead state of the pooled fund study. Participating states include California, Colorado, Indiana, Iowa, Illinois, Minnesota, and Missouri. This research studied the materials produced for the Indiana, Iowa, Minnesota, and Missouri projects. For each state project, a control section that does not contain any shingles was constructed. Mixtures containing different types and percentages of RAS were produced as experimental sections. RAP was used with RAS in the Minnesota, Indiana, and Missouri sections. Iowa mixtures used RAS alone as the virgin asphalt replacement material. Minnesota testing sections used both tear-off and manufactured RAS. RAS used in other states are all tear-off RAS. The gradations of RAS in Missouri mixes are different; one is ground finer than the other. Only one type of RAS was used in Iowa and Indiana projects. Warm mix asphalt (foaming method) was studied in the Indiana project. Detailed material information for each state project is covered in this chapter.

Field produced loose mixtures and extracted binders were provided to the Iowa State University (ISU) Asphalt Lab in Ames by the state agencies. Sample cylinders were compacted with Superpave procedures to test dynamic moduli. Five replications were prepared for each mix. Three replications were prepared for each extracted binder to test shear moduli and phase angles. One frequency sweep test was also conducted for each type of binder. A table of experimental plan is presented below in Table 5. Due to not enough material, three samples were made for the mix #11 instead of five samples which were prepared for other mixes.

Table 5: Experimental Plan

Project	Mix Number	Mix Description	Dynamic Modulus	DSR	DSR frequency sweep
Minnesota	1	5% Mfr. RAS[1]	xxxxx[2]	xxx	x
	2	5% Tear-off RAS	xxxxx	xxx	x
	3	Control Mix	xxxxx	xxx	x
Iowa	4	Control Mix	xxxxx	xxx	x
	5	4% RAS	xxxxx	xxx	x
	6	5% RAS	xxxxx	xxx	x
	7	6% RAS	xxxxx	xxx	x
Missouri	8	Control Mix	xxxxx	xxx	x
	9	5% Fine RAS	xxxxx	xxx	x
	10	5% Coarse RAS	xxxxx	xxx	x
Indiana	11	Control Mix	xxx	xxx	x
	12	3% RAS & HMA	xxxxx	xxx	x
	13	3% RAS & WMA	xxxxx	xxx	x

1: manufactured Recycled Asphalt Shingle

2: each "x" states for one experiment replication

Minnesota DOT Demonstration Project

The Minnesota demonstration project is located at the Mn/Road Cold Weather Road Research Facility in Albertville, Minnesota. The project is 3.5 miles long with 18 test sections on the passing and driving shoulders of westbound I-94 mainline. A plan view of test cells is shown in Figure 19. Mix laid down in Cell 20 contains 30% RAP and serves as the control section. Mixes of Cells 5, 6, 13, and 14 contain 5% manufactured RAS. Mixes of Cells 15 to 23 contain 5% tear-off RAS. Each cell is 500 feet long including a 50 feet transition area. All cells are 3 inches thick with a granular base, except for Cell 5 is paved on top of a HMA base. Construction of test sections was completed in September, 2008 [35].

The Minnesota demonstration project used a 12.5mm (1/2 inch) NMAS (nominal maximum aggregate size) aggregate gradation for all test mixes. The aggregate gradations are shown in Table 6 and Figure 20. The gradations of mixes containing 5% RAS are similar to each other. The control mix gradation contains more coarse aggregates than the mixes containing RAS. All

mixes used the same performance grade (PG) 58-22 virgin binder. The asphalt content is 17.1% for the manufactured RAS and 23% for the tear-off RAS. The RAP used in control section has an asphalt content of 6%. The total asphalt content for all mixes is 5%. The loose mixes received by ISU Asphalt Lab are from randomly chosen from Cells 5, 6, 15, 18, 19, and 22. Control mix from Cell 20 was also received and tested by the ISU Asphalt Lab.

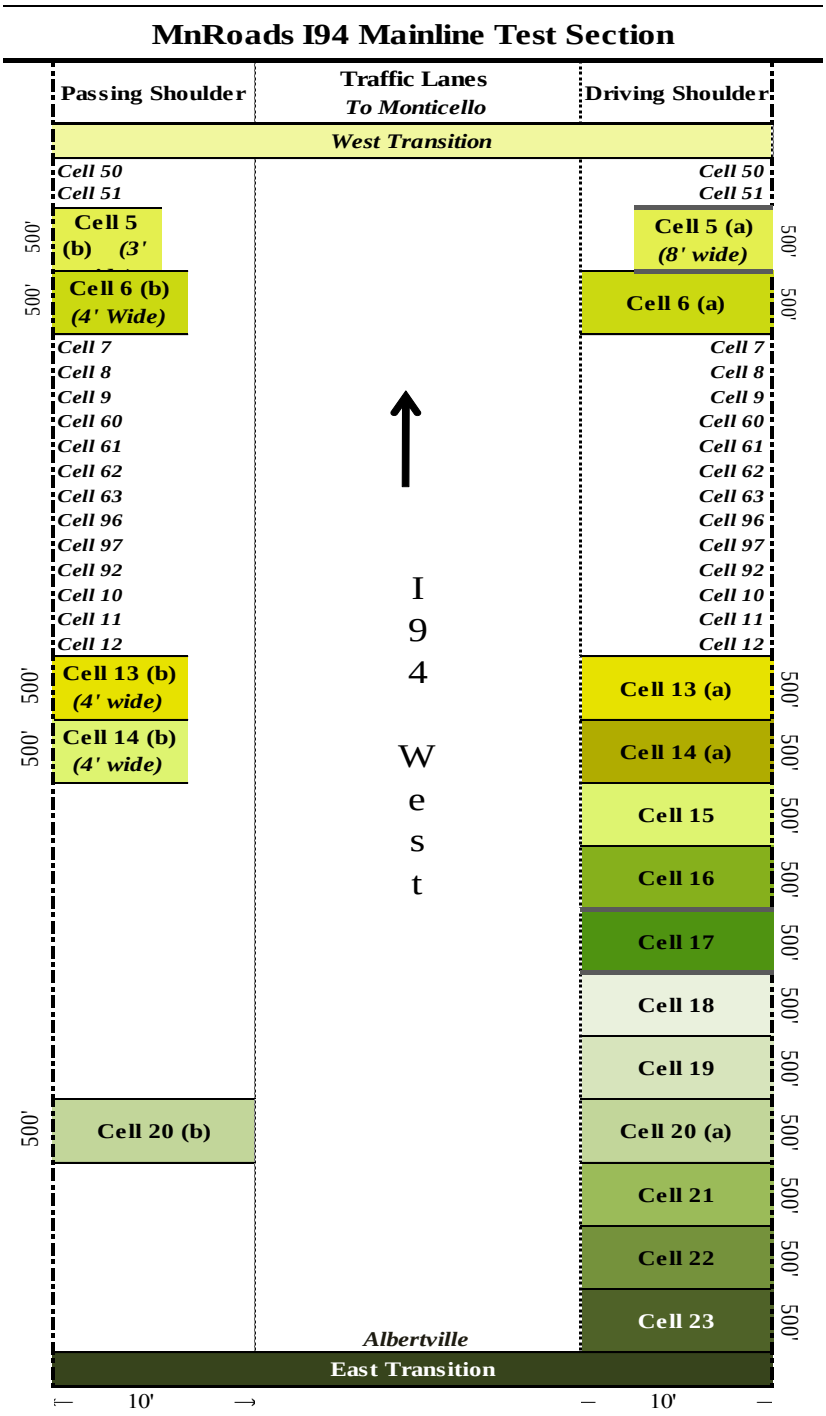

Figure 19: Plan View of MnROAD Test Cells [35]

Table 6: Minnesota Demonstration Project Sieve Analysis Results

SIEVE	%PASS		
	Control Mix	Mfr. RAS Mix	Tear-off RAS Mix
1"	100	100	100
3/4"	100	100	100
1/2"	95	91	86
3/8"	89	84	73
#4	66	58	39
#8	52	45	28
#10	48	43	26
#16	36	34	21
#30	23	22	14
#40	17	16	10
#50	12	10	7
#100	4	4	2
#200	1	1.3	1

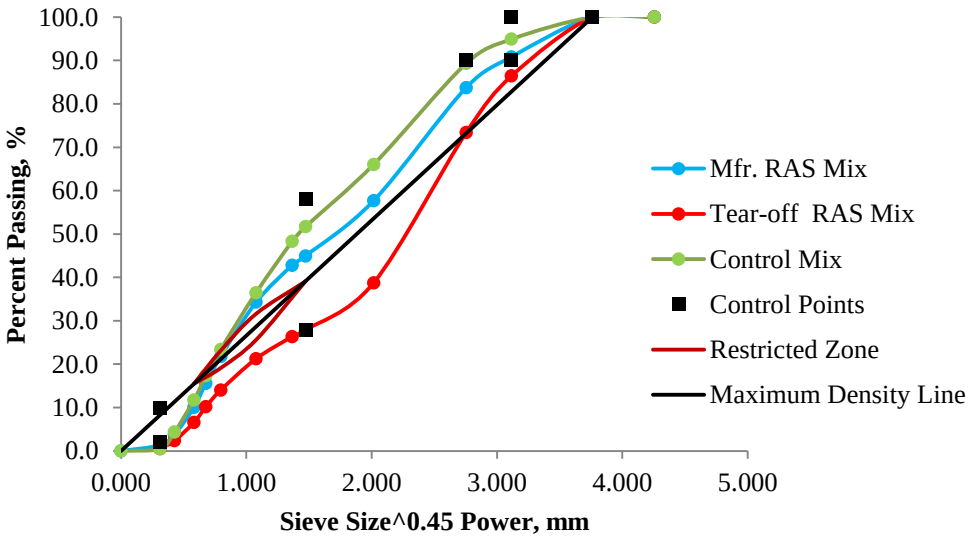

Figure 20: Aggregate Gradation Chart for Minnesota Demonstration Project Gradations

Iowa DOT Demonstration Project

The Iowa DOT demonstration project is located on Highway 10 west of Pavlina, Iowa. The project was constructed in June and July, 2010. The total project is 32.5 lane miles including four

test sections. Every test section has a 2 inch thick surface course underlying by a granular base. Figure 22 shows a plan view of the demonstration project sections. Four types of mixes were randomly assigned to the four test sections as shown in Figure 22.The mixes were designed with the same aggregate gradations and virgin binders, but different RAS contents ranging from 0% to 6%. The Iowa demonstration project used a 12.5mm NMAS for mix design and a PG64-22 binder for the virgin asphalt. The aggregate gradation is summarized in Table 7 and schematically presented in Figure 23. The total asphalt content is 5.5%, and the virgin binder content is varying with the amount of shingle in each mix. Figure 21 shows how much virgin binder is replaced by the asphalt in the recycled shingles. The figure indicates that adding 4% to 6% RAS to asphalt mix can reduce the use of virgin asphalt by 15% to 20%.

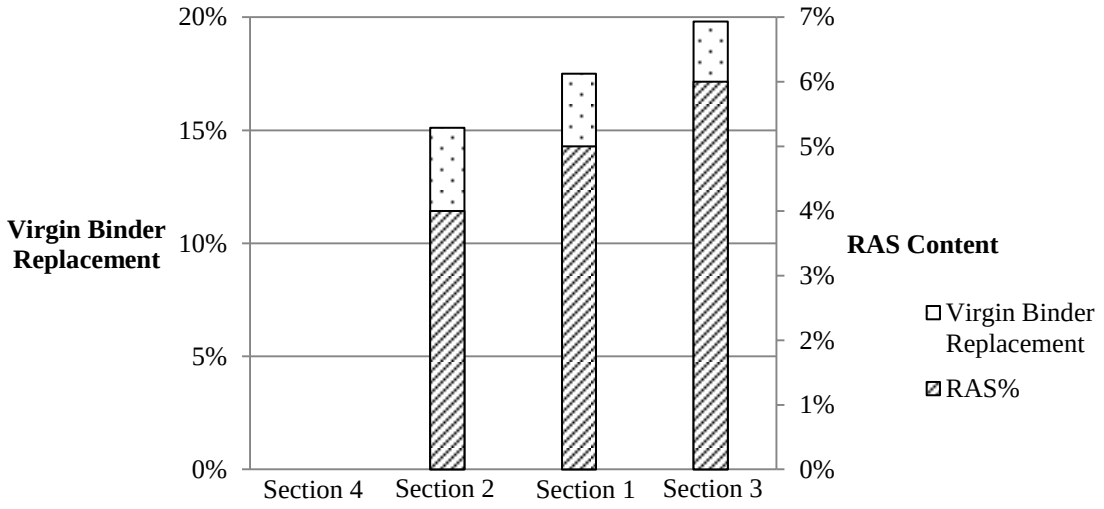

Figure 21: RAS Content and Virgin Binder Replacement for Iowa Test Sections

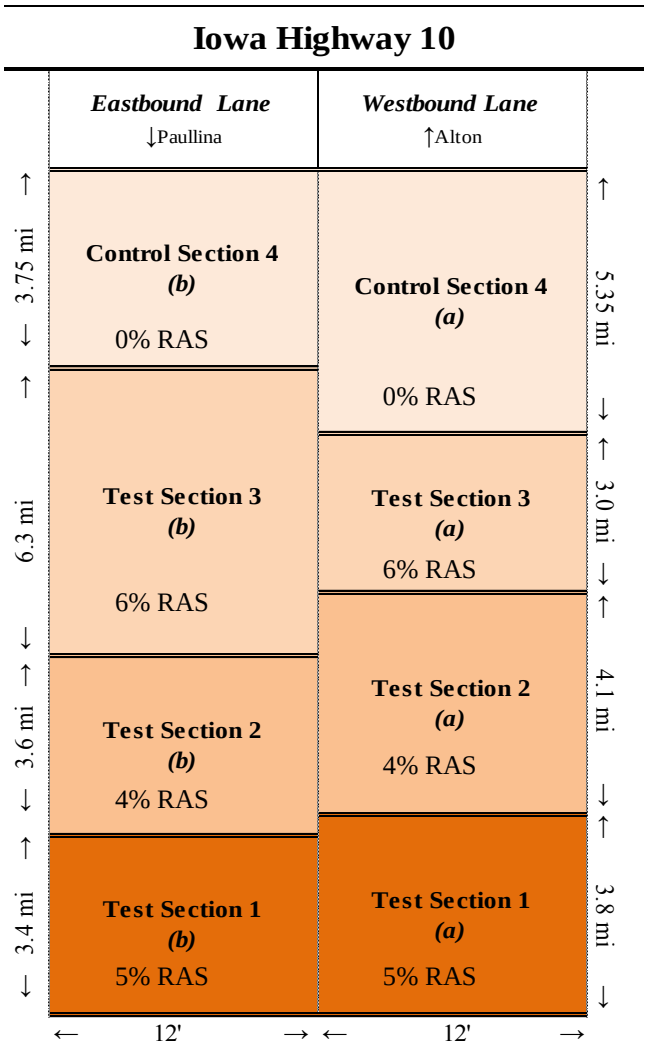

Figure 22: Plan View of Iowa Demonstration Project Test Sections [35]

Table 7: Iowa Demonstration Project Sieve Analysis Results

SIEVE	%PASS			
	0%RAS	4%RAS	5%RAS	6%RAS
1"	100	100	100	100
3/4"	100	100	100	100
1/2"	94	95	94	93
3/8"	84	85	87	84
#4	66	67	71	66
#8	46	45	48	44
#10	43	41	44	40
#16	34	31	33	30
#30	23	20	22	20
#40	17	15	16	14
#50	11	9	9	9
#100	3	3	3	3
#200	0.6	0	1	0.6

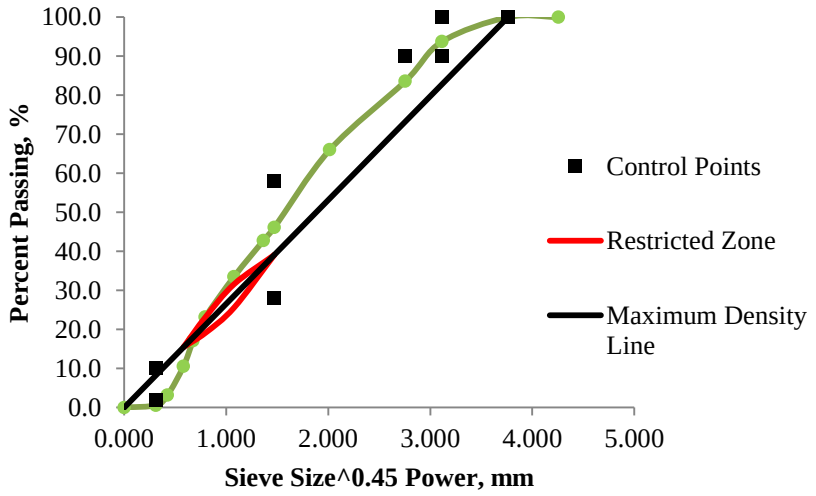

Figure 23: Aggregate Gradation Chart for Iowa Demonstration Project

Missouri DOT Demonstration Project

The Missouri DOT constructed the demonstration project for the pooled fund study in May and June, 2010. The 8.8 mile project is located on US Route 65 south of Springfield, Missouri. The total project is 17.6 lane miles with a 3.75 inches surface layer underlying by a concrete pavement. This demonstration project was developed to study the influences of RAS grind size

on pavement performance and the economic feasibility of incorporating ground tire rubber (GTR) and asphalt mixes containing RAS and RAP. Three test sections were paved as shown in Figure 24. A PG 64-22 asphalt was selected as the virgin binder. The virgin binder was modified with GTR and a vestenamer polymer to achieve a 70-22 performance grade. The control section contains 15% RAP and 0% RAS. Test section 2 contains 5% fine ground RAS which 100% of RAS particles pass the 3/4 inch sieve and 95% particles pass the #4 sieve. Test section 3 contains 5% coarse ground RAS which 100% RAS particles pass 1/2 inch sieve. Both test sections 2 and 3 contain 10% RAP so that all mixes have 15% recycled materials. The same aggregate gradations were designed for the three test sections. Figure 25 shows the designed aggregate gradation. The sieve analysis results are summarized in Table 8. The design asphalt content was 5.3%. Test sections containing 5% RAS used 3.7 virgin binders content to achieve the design binder content.

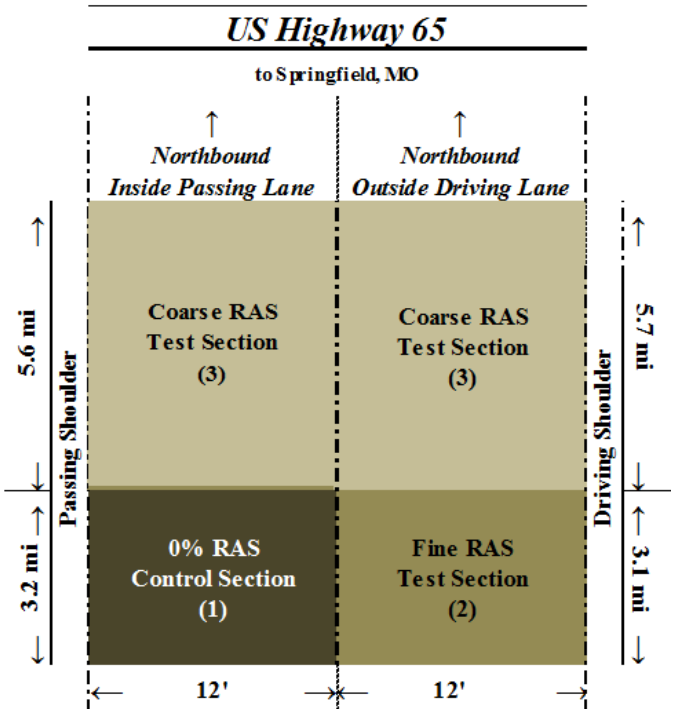

Figure 24: Plan View of Missouri Demonstration Project Test Sections [35]

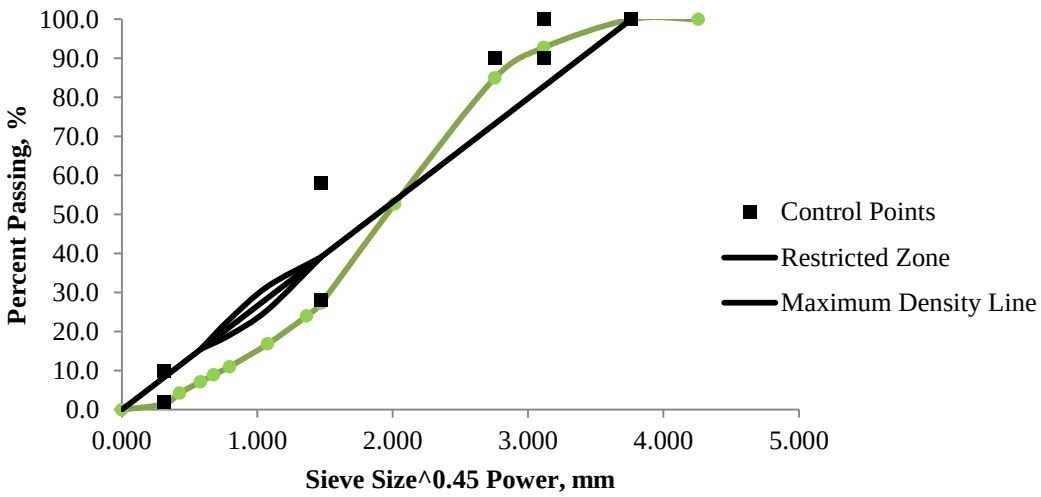

Figure 25: Aggregate Gradation 0.45 Power Chart for Missouri Demonstration Project

Table 8: Missouri Demonstration Project Sieve Analysis Results

SIEVE	%PASS		
	Control Mix	5% Fine RAS	5% Coarse RAS
1"	100.0	100.0	100.0
3/4"	100.0	99.2	100.0
1/2"	92.8	94.1	94.2
3/8"	85.0	85.7	85.6
#4	52.7	49.1	51.4
#8	27.3	26.0	26.7
#10	24.0	23.3	23.6
#16	16.8	17.0	16.4
#30	11.0	11.6	10.8
#40	8.9	9.5	8.9
#50	7.2	7.8	7.3
#100	4.2	4.5	4.4
#200	1.5	1.3	1.3

Indiana DOT Demonstration Project

The Indiana DOT demonstration project was completed in July, 2009. The project is located on U.S. Route 6 east of Nappance, Indiana. The overall construction is 13.6 lane miles. A 1.5 inch surface layer was placed on top of a previously existing asphalt surface with an underlying

concrete pavement. The demonstration project was developed to evaluate the performance of incorporation of RAS and warm mix asphalt in asphalt concrete pavements. Three test sections were constructed as shown in Figure 26. The control section used a hot mix asphalt containing 15% fractionated recycled asphalt pavement (FRAP). Test section 2 used the same hot mix asphalt with 3% RAS. A foaming method was applied to produce warm mix asphalt which is laid down in test section 3. The test section 3 also contains 3% RAS. The same aggregate gradation was designed for different test sections as shown in Figure 27. The sieve analysis results are summarized in Table 9. A PG 70-22 asphalt was selected as the virgin binder. The design binder content was 6.2%. Test sections containing 3% RAS used 5.4% virgin binder content to achieve the design total binder content.

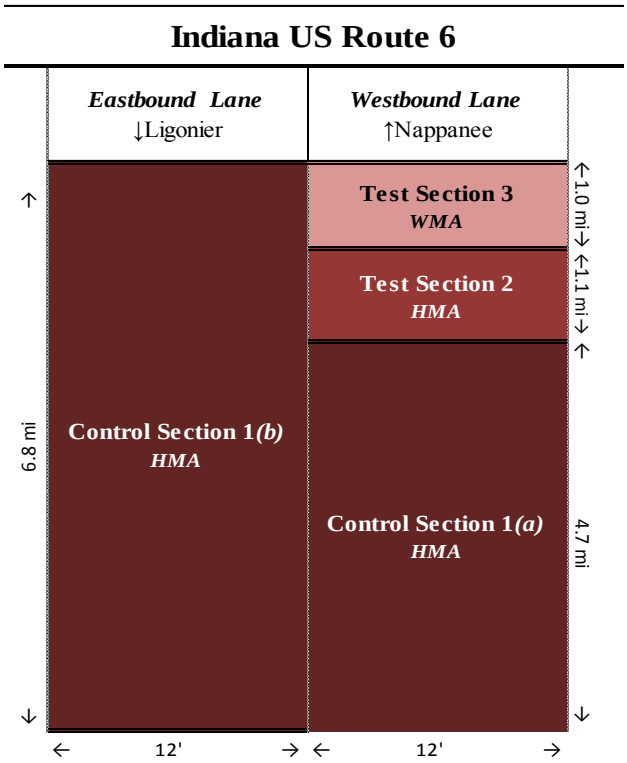

Figure 26: Plan View of Indiana Demonstration Project Test Sections [35]

Table 9: Indiana Demonstration Project Sieve Analysis Results

SIEVE	%PASS		
	Control Mix	3% RAS HMA	3% RAS WMA
1"	100.0	100.0	100.0
3/4"	100.0	100.0	100.0
1/2"	100.0	99.9	100.0
3/8"	96.6	94.6	96.0
#4	75.7	72.1	73.5
#8	53.7	50.1	51.5
#10	49.5	46.3	47.7
#16	35.8	33.6	34.3
#30	22.2	21.2	21.2
#40	16.1	15.9	15.7
#50	10.5	10.9	10.7
#100	3.8	4.4	4.2
#200	0.5	0.6	0.6

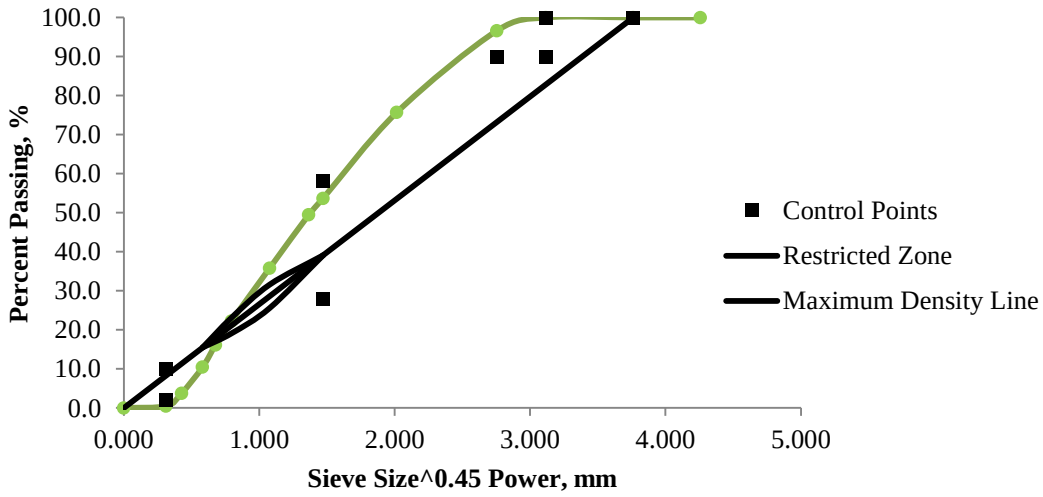

Figure 27: Aggregate Gradation 0.45 Power Chart for Indiana Demonstration Project

LABORATORY TESTING DESIGN

Dynamic Modulus Test

The dynamic modulus tests were performed with a universal testing machine (UTM) in a environmental chamber shown in Figure 28. The UTM has a hydraulically driven load frame which can provide a maximum load of 25kN (5620lbs) at various frequencies. The magnitude and frequency of applied load can be precisely controlled. The applied sinusoidal load was carefully selected to maintain a sample strain level of 85 to 110με to ensure a measurable strain and prevent excessive damage to sample. Excessive unrecoverable deformation can be achieved if the strain is too high. The testing was conducted following ASTM D3496. The standards requires 150mm × 100mm (height by diameter) asphalt cylinder cored from a 160mm × 150mm cylinder compacted by the Superpave Gyratory Compactor (SGC). Extra time and costs are needed to core an asphalt cylinder. According to Robinette and Williams' study (2006), the dynamic modulus test results of cored and directly compacted samples are not significantly different. More than 70 samples were made for this research including trial samples to determine the required mass for target air void and samples for testing dynamic modulus. In order to lower the cost and make the laboratory work more practical, the 150mm by 100mm cylinders in this research were compacted by the SGC with a special mold designed specifically for samples in this size. The sample strain was tested with three evenly spaced LVDTs attached on the side of the sample.

The statistical design of dynamic modulus experiment is split plot. Dynamic moduli were tested at 4 ℃, 21 ℃, and 37 ℃ and nine frequencies (0.1, 0.2, 0.5, 1, 2, 5, 10, 20, and 25Hz) at each temperature for each sample. Therefore, each sample was tested with 27 treatment combinations. The 13 types of mixtures form the whole plots. Mixture type is the whole plot factor. Five samples were made from each mixture to form the sub plots. The sub plot factor is the individual cylinder. Thus, the variability caused by mixture type and treatments can be determined. The variability between the five replications for each mixture can be also calculated and separated from the total error, increasing the chance to identify the significant differences between different types of mixtures.

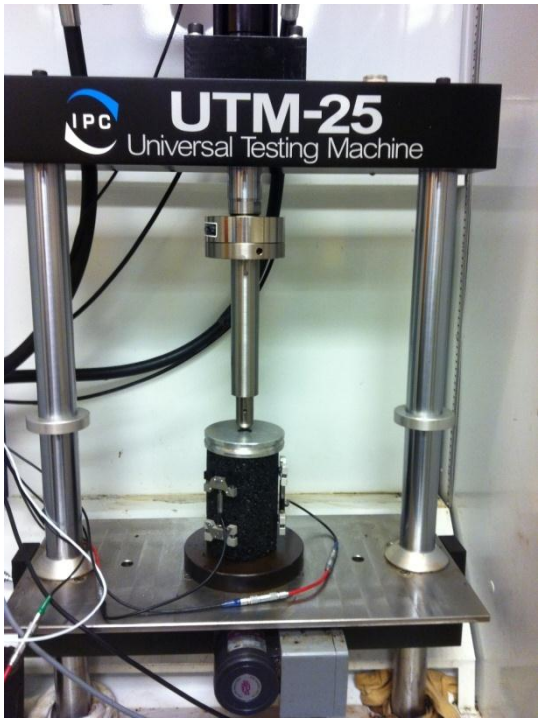

Figure 28: Universal Testing Machine and Environmental Chamber

Direct Shear Rehometer (DSR) Test

The DSR tests were conducted to model the asphalt rheological properties. Testing materials were extracted from field mixes of the pooled fund study demonstration projects by following AASHTO Designation TP2-94, *Standard Test Method for the Quantitative Extraction and Recovery of Asphalt Binder from Hot Mix Asphalt (HMA)*. The extraction method uses asphalt solvents blended with ethanol to separate the asphalt binder from aggregates. The commonly used asphalt solvents are n-Propyl Bromide, Trichloroethylene, and Toluene. Asphalt binder is recovered through a centrifuge. The extractions were performed by the Minnesota DOT. The referenced standard for DSR testing is ASTM D7175, *Standard Test Method for Determining the Rheological Properties of Asphalt Binder using a Dynamic Shear Rheometer*. Two DSR experiments were designed for different research interests elaborated in following paragraphs.

Binder High Temperature Grading

DSR tests were performed to determine asphalt binder high temperature grade by following the Superpave test specifications. Because the asphalt binders were extracted from field produced mixtures which were short-term aged, the grading procedures followed the Superpave grading method for rolling thin film oven (RTFO) aged asphalt material. DSR tests were

conducted with a dynamic shear rheometer shown in Figure 29. At least three temperatures were tested for each sample in order to grade the asphalt.

Figure 29: AR1500 Dynamic Shear Rheometer

Frequency Sweep

DSR frequency sweep tests were designed to construct master curves of binder complex shear modulus (G*) and phase angle (Φ). The master curves characterize binder rheological properties over a wide range of temperature or frequency. The master curves can be used to estimate binder G* and Φ values at any interested temperature and frequency. The G* and Φ for each binder were tested at seven temperatures and 15 frequencies [1] ranging from 0.1Hz to 50Hz for each temperature. The seven testing temperatures are 13, 21, 29, 37, 46, 58, and 70 ℃. Because the binders were tested over a large temperature range, different sample sizes were selected. The 25mm diameter samples were tested at 46, 58 and 70 ℃. The required stress to maintain a measurable strain level of a 25mm sample at low temperature exceeds the machine capacity. Therefore, the 8mm diameter sample size was selected to test the G* and Φ values at 13, 21, 29, and 37 ℃. The dynamic rheological properties were tested by measuring the required

[1] 15 frequencies: 0.1, 0.158, 0.251, 0.398, 0.631, 1, 1.585, 2.512, 3.981,6.31, 10, 15.849, 25.121, 39.809, and 50Hz.

shear stress to achieve a preset strain level. The strain level should be large enough so that it is measurable and also small enough so that the required stress does not exceed the capacity of the testing device or damage the sample. The controlled strain level for the 8mm sample is 0.1% and for the 25mm sample is 10%.

CHAPTER 4: EVALUATION AND MODIFICATION OF WITCZAK AND HIRSCH MODELS

Many previous studies, such as studies conducted by University of Minnesota [29], Christensen, Pellinen, and Bonaquist [10], North Carolina State University [30], University of Florida [31], and Marinez and Angelone [32] have shown that the Witczak and Hirsch models have reasonable accuracy to predict the dynamic modulus of HMA mixtures. The Witczak model uses four input parameters ($\rho_{3/8}$, $\rho_{3/4}$, ρ_4[2], and ρ_{200}[3]) to characterize aggregate gradation, two parameters (V_a[4] and V_{beff}[5]) to describe mixture volumetric property, and two parameters (frequency and viscosity, or shear modulus and phase angle[6]) to include the binder rheological behavior. In the Hirsch model, three input parameters including voids in mineral aggregate (VMA), voids filled by asphalt (VFA), and binder shear modulus are considered as the factors that are used to estimate a mixture dynamic modulus. The primary components of RAS include asphalt, granules (passing #12 screen), dust (passing #200 screen), and fibers. The asphalt in RAS is manufactured through an "air-blown" process and exposed to long-term weathering. Therefore, the asphalt usually has a higher stiffness than typical asphalt used in asphalt mixtures. The effects of shingles in HMA include a change in aggregate gradation and volumetric properties, an increase in binder viscosity and shear modulus, a decrease in binder's phase angle, and a stiffening effect introduced by fibers. The changes in gradation, volumetrics, and binder rheology can be explained by the original Witczak and Hirsch models. However, both models do not include the effects of fibers. In this chapter, two versions of the Witczak model (1999 and 2006 versions) and the latest Hirsch model are evaluated to determine the accuracy of predicting mixture dynamic modulus caused by the fibers in shingles. Modifications were made to account for this effect using the results of aforementioned tests in Chapter 3.

[2] $\rho_{3/8}$, $\rho_{3/4}$, ρ_4: cumulative percent of aggregate mass retaining on 3/8", 3/4", and U.S. #4 (4.75mm) sieves
[3] ρ_{200}: percent of aggregate mass passing U.S. #200 (0.075mm) sieve
[4] V_a is the air content of compacted mixture
[5] V_{beff} is the effective bitumen content by volume
[6] Frequency and viscosity are used in the 1999 Witczak Model, shear modulus and phase angle are used in the 1999 Witczak Model

ORIGINAL MODEL EVALUATION

A total number of 1701 dynamic modulus values were observed from 13 mixes to evaluate the 1999 Witczak Model. The comparisons between predicted and tested E* values on both normal and logarithm scales are plotted in Figure 30 and Figure 31, respectively. The plotted points lined up along the line of equality, except for the data of the Iowa mixes are above the line of equality. This indicates the 1999 Witczak Model tends to overestimate the E* of Iowa mixes. The overall linear trend line matches the line of equality showing a high prediction accuracy of the 1999 Witczak Model. On a normal scale, the overall variability becomes larger when the model is used to predict larger E* values which is referring to the scenario that the pavement is subjected to a lower temperature or higher loading rate. The model tends to overestimate the E* values of Iowa mixes and underestimate the Minnesota mixes. Each project has a distinct linear trend line. On the logarithm scale, the overall variability becomes smaller when the predicted E* values are larger. Compared to the overall variability, the variability within each project is small. The overall variability includes the variability between projects and the variability within each project. Variability in accuracies of predictions arises from differences in materials, asphalt plant operations, RAS contents, and sampling and testing errors. The effects of different RAS contents do not result in the variability between projects. The coefficient of determination, R^2, is 0.86 on a normal scale, and 0.87 on a logarithm scale. The standard error ratio, Se/Sy, is 0.37 for a normal and 0.36 for a logarithm scale. A commonly used criterion of measuring a model's goodness-of-fit is given in Table 10. According to the subjective criteria, the goodness-of-fit for the1999 Witczak Model is good.

Table 10: Subjective Classification of the Goodness-of-Fit Statistical Parameters [37]

Criteria	R2	Se/Sy
Excellent	>0.90	<0.350
Good	0.70 – 0.89	0.36 – 0.55
Fair	0.40 – 0.69	0.56 – 0.75
Poor	0.20 – 0.39	0.76 – 0.90
Very Poor	<0.19	>0.90

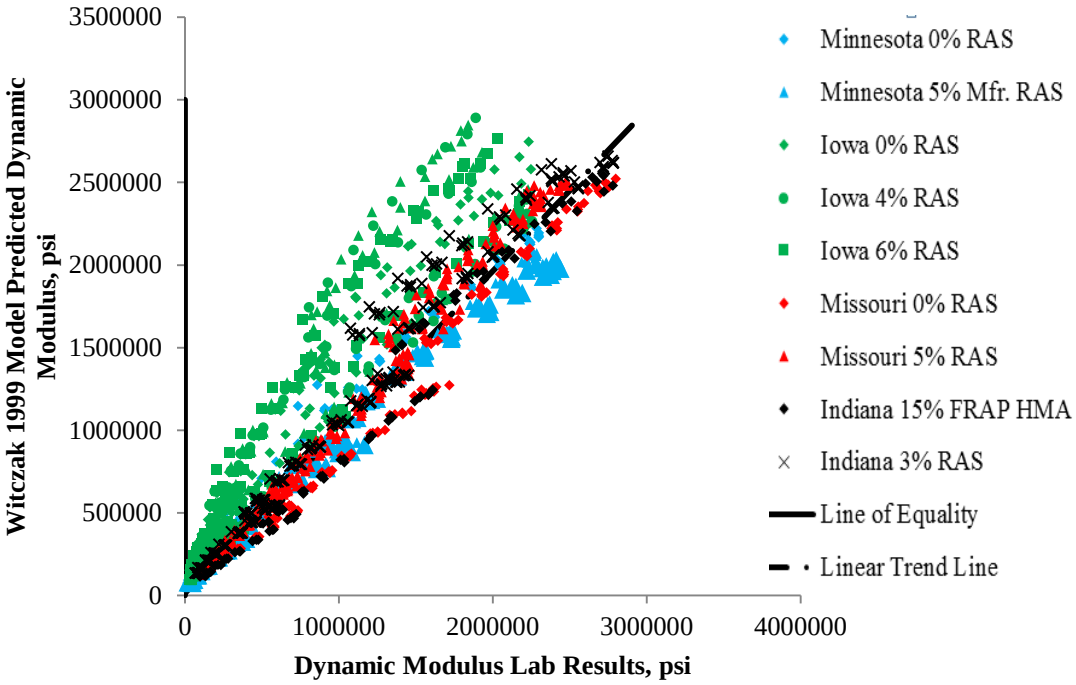

Figure 30: Lab Tested vs. Witczak Model (1999) Predicted E* Values on Normal Scale

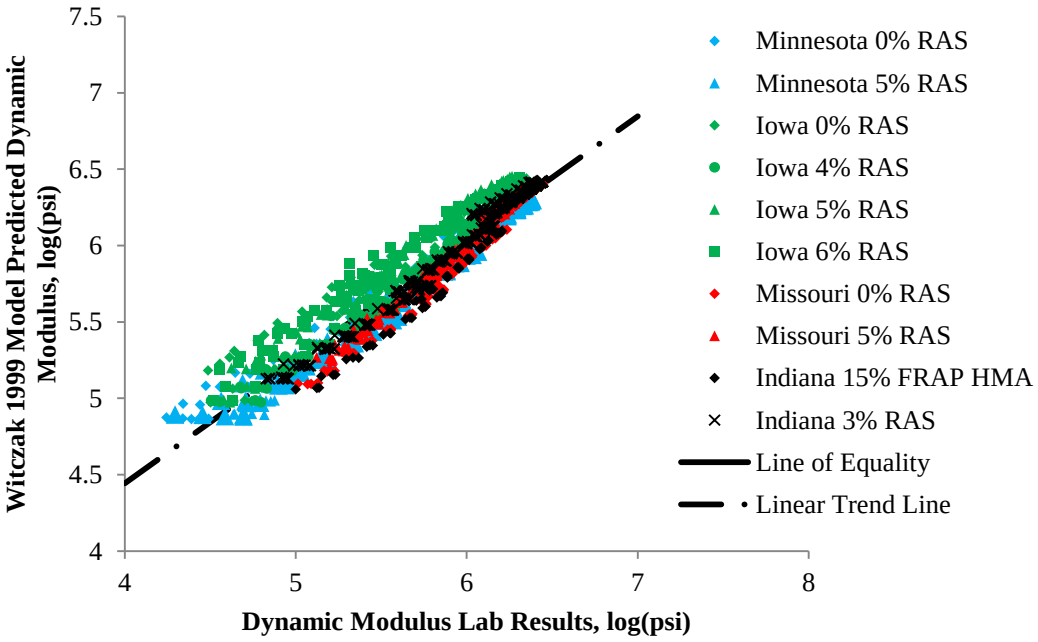

Figure 31: Lab Tested vs. Witczak Model (1999) Predicted E* Values on Logarithm Scale

Because of material shortages of the recovered asphalt binders from Minnesota tear-off RAS mix and Iowa 5% RAS mix, the G* values and phase angles were not able to be tested for Mixes

#2 and #6. Therefore, 1431 dynamic modulus values from lab tests were observed to evaluate the 2006 Witczak Model. The comparisons between predicted and tested E* values on both the normal and logarithm scales are plotted in Figure 32 and Figure 33, respectively. The linear trend lines in both Figure 32 and Figure 33 are above the line of equality. This indicates the 2006 Witczak Model tends to overestimate the E* values in general. Compared to the 1999 Witczak Model, the trend for each project is not that obvious. However, the linear trend line for each project is still distinct. This indicates a large portion of overall variability is caused by the differences between projects. On the normal scale, the overall variability becomes larger when the model is trying to predict larger E* values. However, on the logarithm scale, the overall variability becomes smaller when the predicted E* values are larger. The variability within each project is smaller than the overall variability. The 2006 Model has a R^2 value of 0.44 and Se/Sy of 0.75 on logarithm scale. The prediction accuracy of the 2006 Witczak Model is fair.

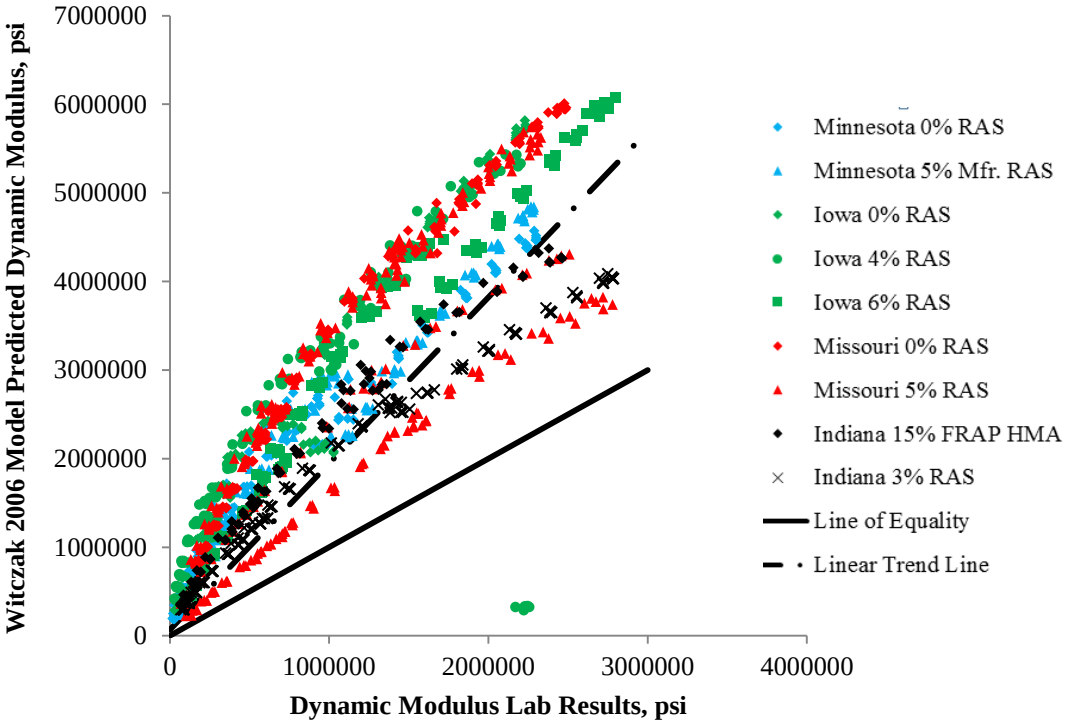

Figure 32: Lab Tested vs. Witczak Model (2006) Predicted E* Values on Normal Scale

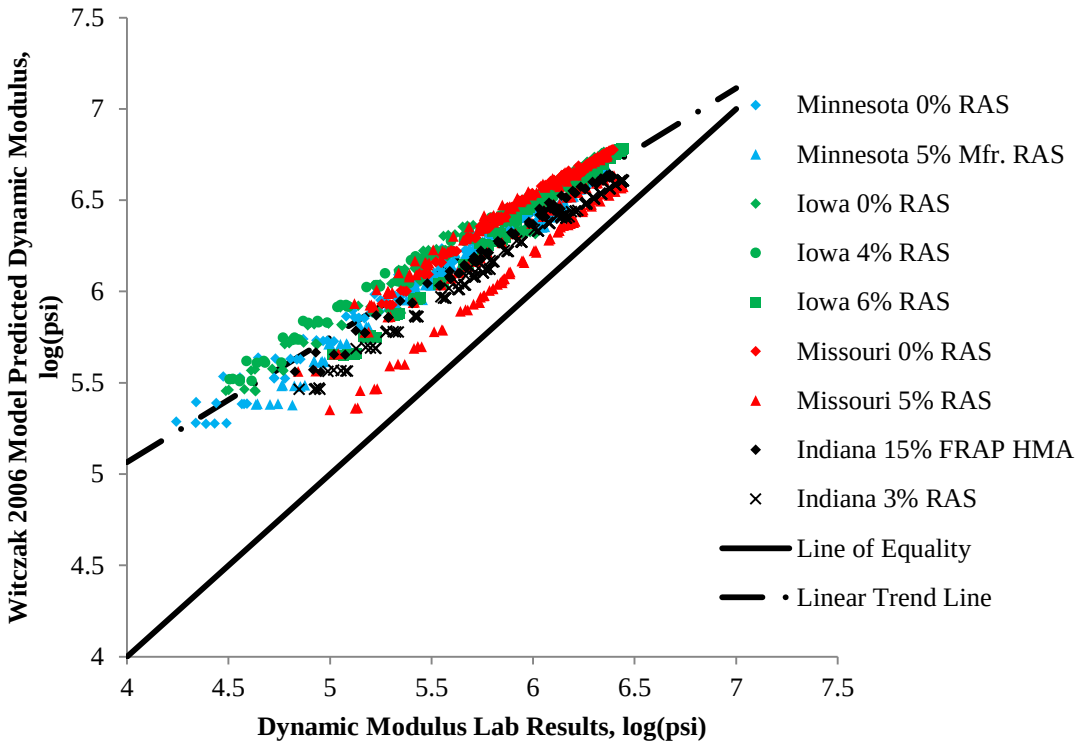

Figure 33: Lab Tested vs. Witczak Model (2006) Predicted E* Values on Logarithm Scale

The evaluation of the Hirsch model includes 1431 dynamic modulus values. The comparison between predicted and tested E* values are plotted in Figure 34 and Figure 35 on normal and logarithm scales, respectively. On both figures, the linear trend line is very close to the line of equality indicating the Hirsch model has a high level of accuracy for dynamic moduli of asphalt mixtures. There is not distinct trend for each project. Different projects have similar variability. Figure 34 shows the Hirsch model tends to overestimate the E* values for Iowa mixes, and underestimate the Minnesota mixes. However, the differences between prediction accuracies of different projects are very small. This indicates that the differences between projects do not contribute too much variability to the total error. The R^2 values of the Hirsch model on normal and logarithm scales are 0.90 and 0.83, respectively. The corresponding Se/Sy values for the normal and logarithm scales are 0.31 and 0.41 respectively. Therefore, according to Table 10, the goodness-of-fit of Hirsch model is excellent on a normal scale, and good on a logarithm scale.

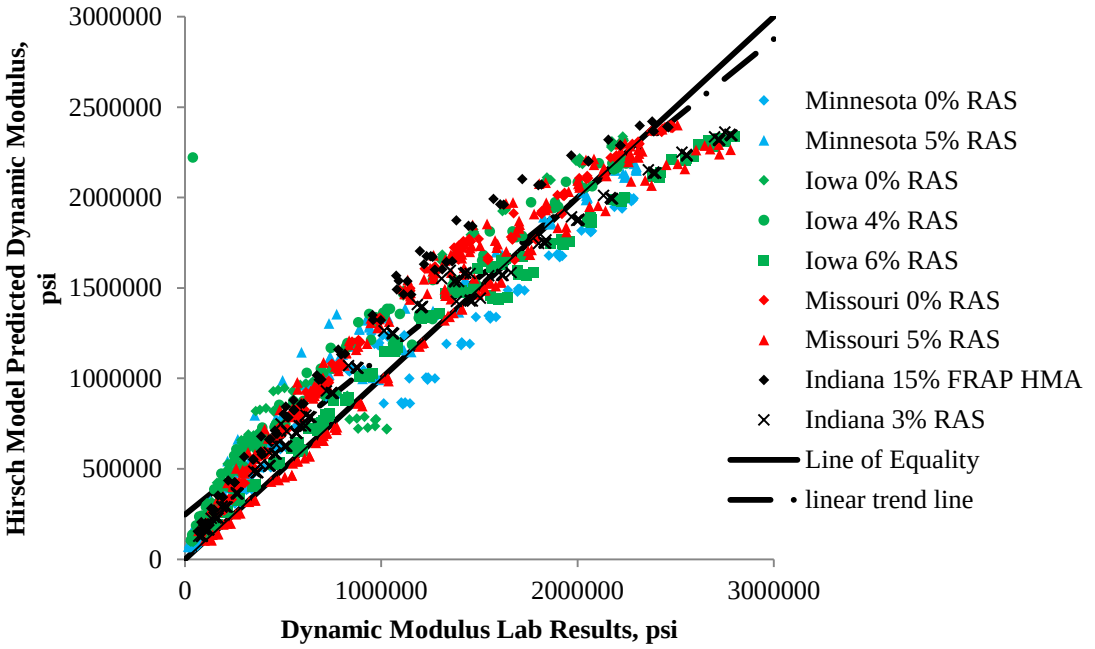

Figure 34: Lab Tested vs. Hirsch Model Predicted E* Values on Normal Scale

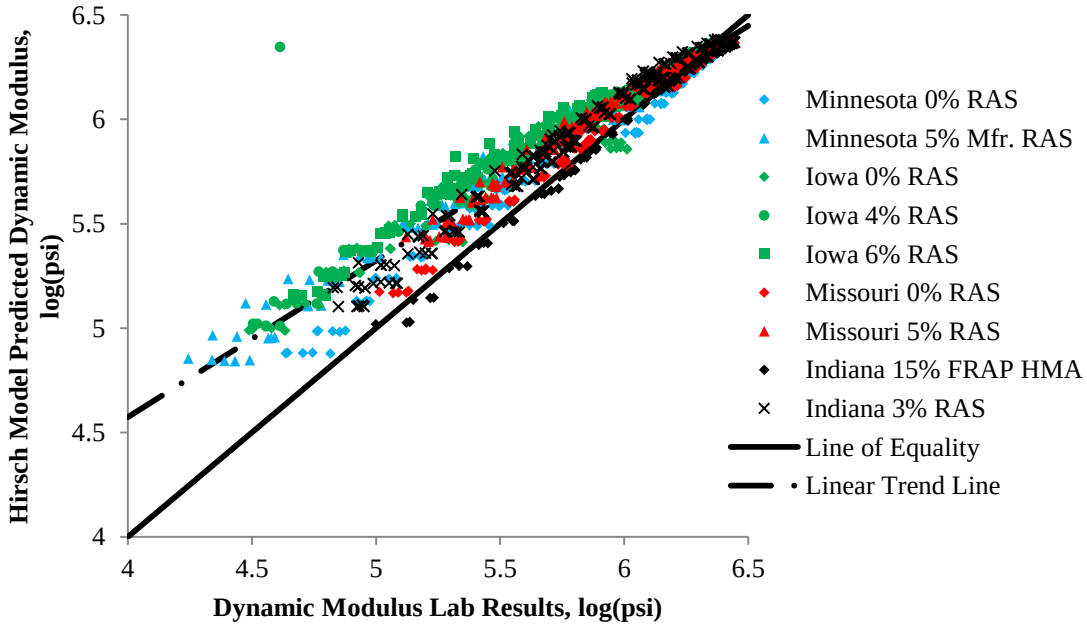

Figure 35: Lab Tested vs. Hirsch Model Predicted E* Values on Logarithm Scale

Evaluations of the three E* predictive models show that the 1999 Witczak Model has the highest prediction accuracy, and the prediction accuracy of the 2006 Witczak Model is the

lowest. The three models tend to overestimate mixture dynamic moduli in general. The accuracies of both Witczak models are dependent upon different projects. The differences between projects do not have significant impact on prediction accuracies of the Hirsch model. On the tested vs. predicted E* figures (Figure 30 through Figure 35), the mixes containing 0%, 3%, 4%, 5%, and 6% RAS are denoted by rhombus, cross, circle, triangle, and rectangle symbols, respectively. For each project, the plotted points with the same denotation are concentrated with a distinct trend line. This indicates the differences between RAS contents have impacts on the prediction accuracies of the three models. Analysis of Variance (ANOVA) tables with the ratio of model predicted E* to lab tested E* as the response are given in Table 11 through Table 13for the 1999 Witczak, 2006 Witczak, and Hirsch models, respectively. Three main factors are RAS content, treatment type, and project. The results show that RAS content in each model has a p-value less than 0.0001. It indicates the RAS content is a significant factor that can affect the value of model predicted E* divided by the lab tested E* values which is referring to the prediction accuracy of a predictive model. A prediction accuracy value of 1 indicates the predicted value is exactly the same as the actual value. The prediction accuracy decreases as this number deviates from 1.

Table 11: ANOVA Table for Witczak 1999 Model

Source	Degree of Freedom	Sum of Squares	F Ratio	Prob>F
RAS%	4	119	393	<.0001
Treatment	26	120	46	<.0001
Project	3	42	104	<.0001

Table 12: ANOVA Table for Witczak 2006 Model

Source	Degree of Freedom	Sum of Squares	F Ratio	Prob>F
RAS%	4	390	183	<.0001
Treatment	26	1775	86	<.0001
Project	3	110	38	<.0001

Table 13: ANOVA Table for Hirsch Model

Source	Degree of Freedom	Sum of Squares	F Ratio	Prob>F
Project	3	37.12814	6.0789	0.0004
Treatment	29	165.25453	2.7990	<.0001
RAS%	4	22.96658	2.8202	0.0240

Student's t-tests results were conducted to determine whether or not two levels with a set of mixtures for each state are statistically different. The t-test results are summarized in Table 15. The results show that every project has different prediction accuracy for the 2006 Witczak Model. For the 1999 Witczak Model, only the prediction accuracies for Missouri and Indiana projects do not have significant differences. However, four out of six comparisons in the Hirsch Model prediction accuracies of different projects do not have significant differences. This indicates that the Witczak models are more sensitive to different material types and manufacturing processes. The average prediction accuracy of the Witczak models for mixes containing 6% RAS is lower than mixes containing 0% RAS. Significant differences are also detected between 0% and 6% RAS contents. The average prediction accuracies for mixes containing 4% and 5% RAS are lower than that of mixes containing 0% RAS. Significant differences between 0% and 4% RAS, and 0% and 5% RAS are detected for the 1999 Witczak Model. This indicates that adding shingles to HMA decreases the prediction accuracy of the Witczak models. The 1999 Witczak Model is more sensitive to RAS content. This research involves only 13 mixes with 5 RAS contents. However, more research work is needed to verify this statement. Some of the Hirsch predictions show significantly different accuracies. However, there is not an obvious trend in the mean accuracies. The Hirsch prediction accuracy for 0% RAS is not significantly different from that of 5% and 6% RAS contents. The effects of shingles on the prediction accuracy of Hirsch Model cannot be identified. A larger database with more levels of RAS contents is needed to evaluate the shingle effects on the Hirsch Model accuracy.

Table 14: Mean of Model Prediction Accuracy

Model	Level	Mean
1999 Witczak	0%	1.21216
	3%	1.14153
	4%	1.43447
	5%	1.27868
	6%	2.15744
2006 Witczak	0%	3.36279
	3%	2.45701
	4%	4.5773
	5%	3.38944
	6%	5.2273
Hirsch	0%	1.31907
	3%	1.685497
	4%	1.31907
	5%	1.223297
	6%	1.525975

Table 15: Student-t Test Results for Model Prediction Accuracy

Model	Project Comparison		RAS% Comparison	
	Comparison	Significant Difference	Comparison	Significant Difference
Witczak 1999	MN vs. IA	Yes	0% vs. 3%	Yes
	MN vs. MO	Yes	0% vs. 4%	Yes
	MN vs. IN	Yes	0% vs. 5%	Yes
	IA vs. MO	Yes	0% vs. 6%	Yes
	IA vs. IN	Yes	3% vs. 4%	Yes
	MO vs. IN	No	3% vs. 5%	Yes
			3% vs. 6%	Yes
			4% vs. 5%	Yes
			4% vs. 6%	Yes
			5% vs. 6%	Yes
Witczak 2006	MN vs. IA	Yes	0% vs. 3%	Yes
	MN vs. MO	Yes	0% vs. 4%	No
	MN vs. IN	Yes	0% vs. 5%	No
	IA vs. MO	Yes	0% vs. 6%	Yes
	IA vs. IN	Yes	3% vs. 4%	Yes
	MO vs. IN	Yes	3% vs. 5%	Yes
			3% vs. 6%	No
			4% vs. 5%	Yes
			4% vs. 6%	Yes
			5% vs. 6%	No

Table 15: Student-t Test Results for Model Prediction Accuracy (Continued)

Hirsch	MN vs. IA	No	0% vs. 3%	Yes
	MN vs. MO	Yes	0% vs. 4%	Yes
	MN vs. IN	Yes	0% vs. 5%	No
	IA vs. MO	Yes	0% vs. 6%	No
	IA vs. IN	Yes	3% vs. 4%	No
	MO vs. IN	No	3% vs. 5%	Yes
			3% vs. 6%	No
			4% vs. 5%	Yes
			4% vs. 6%	No
			5% vs. 6%	No

MODELING METHDOLOGY

The philosophy of modifying the E* predictive models for shingle effects is identifying the prediction accuracy variability caused by differences of RAS contents. The prediction accuracy for each pair of predicted and tested E* values can be measured by their difference (e.g. predicted E* - tested E*) or ratio (e.g. predicted E*/ tested E*). The prediction accuracies are affected by errors in measuring the true dynamic moduli of HMA mixtures, and inaccuracies of the predicted E* values. The E* measurement errors can be caused by systematic errors which are due to the inaccuracies of testing apparatuses, and variability in sampling and testing procedures. The inaccuracies of the predicted E* result from incorrect values of input parameters and the inaccuracies of the models themselves. The three E* predictive models have 12 different input parameters characterizing aggregate gradation, binder rheology, and mixture volumetric properties. The parameters for aggregate gradation and mixture volumetrics were calculated or directly observed from testing results. The parameters to describe binder rheology were obtained from asphalt rheological models. Errors in lab testing and models can result in inaccurate input parameter values, too. The models themselves can be inaccurate because of incorrect assumptions that are made to construct the model, missing factors that have effects on the prediction results, and limitations of databases that were used to develop the models. The Witczak models assume the relation between E* and loading frequency is depicted by a sigmoid function. The Hirsch Model is based on the assumption that the law of mixture can be applied to HMA. In the Hirsch Model, the dynamic modulus of an asphalt binder is assumed to be three times the binder shear modulus. Although these assumptions provide high accuracy for simulations, errors of the simulations still exist. Missing effective factors include RAS content,

aggregate stiffness, and other factors that have effects on the E* values. The coefficients of a model are determined by regression of lab tested E* values. The size and diversity of a database can affect a model's applicability. The objective of this chapter is to determine the effects of different RAS contents on the model prediction accuracies. Three steps were taken to approach this objective: firstly, determine the input parameters; secondly, calibrate the predictive models using E* of the control mixes to eliminate the project variability in prediction accuracies; and thirdly, modify the predictive models with RAS content as a factor if possible.

Model Input Parameters

At the beginning of this Chapter, the 12 input parameters related to aggregate gradation, volumetrics, and binder rheology are introduced. The 12 input parameters include cumulative aggregate percentage retained on #4 (ρ_4), 3/8" (ρ_{38}), and 3/4" (ρ_{34}) sieves, fine content (ρ_{200}), voids in mineral aggregate (VMA), voids filled by asphalt (VFA), effective binder volume content (V_{beff}), air voids (V_a), dynamic shear modulus of binder (G*), phase angle of binder (δ), loading frequency (f), and binder viscosity (η). The aggregate gradation parameters, ρ_4, ρ_{38}, ρ_{34}, and ρ_{200}, are obtained from the sieve analysis tests for quality assurance and quality control (QA/QC). The results of the sieve analysis tests are provided in the experimental plan in Chapter 2. The mixture volumetric parameters, VMA, VFA, V_a, and V_{beff}, are calculated from the specific gravities of aggregate (G_{sb}), asphalt binder (G_b), mixture (G_{mm}), and compacted sample cylinder (G_{mb}). The G_{sb} and G_{mm} values for each type of mix are procured from the mix design of each project. The specific gravity of asphalt binder is estimated from the pooled fund study literature to be 1.038 for all types of binder in this research. Cylinder bulk specific gravity values were observed from lab tests following the standard test procedures specified in AASHTO T166. The volumetric properties are summarized in Table 16. The binder rheological properties are predicted by the viscosity-temperature susceptibility (A-VTS) method and the master curves for binder shear modulus and phase angle.

Table 16: Volumetric Properties of Compacted Sample Cylinder

Sample Number	Project	Mix Description	Gsb	Gmb	Gmm	Va	VMA	VFA	Vbeff
1	MN	5% Mfr. RAS	2.697	2.348	2.527	7.1	17.2	58.8	10.1
2	MN	5% Mfr. RAS	2.697	2.342	2.527	7.3	17.4	58.1	10.1
3	MN	5% Mfr. RAS	2.697	2.346	2.527	7.2	17.3	58.3	10.1
4	MN	5% Mfr. RAS	2.697	2.348	2.527	7.1	17.2	58.7	10.1
5	MN	5% Mfr. RAS	2.697	2.345	2.527	7.2	17.3	58.4	10.1
6	MN	5% Tear-off RAS	2.697	2.378	2.547	6.7	16.3	59.0	9.6
7	MN	5% Tear-off RAS	2.697	2.379	2.547	6.6	16.3	59.4	9.7
8	MN	5% Tear-off RAS	2.697	2.369	2.547	7.0	16.6	57.9	9.6
9	MN	5% Tear-off RAS	2.697	2.374	2.547	6.8	16.5	58.7	9.7
10	MN	5% Tear-off RAS	2.697	2.366	2.547	7.1	16.7	57.6	9.6
11	MN	30% RAP	2.697	2.355	2.527	6.8	17.1	60.3	10.3
12	MN	30% RAP	2.697	2.359	2.527	6.6	17.0	61.1	10.4
13	MN	30% RAP	2.697	2.352	2.527	6.9	17.2	60.0	10.3
14	MN	30% RAP	2.697	2.350	2.527	7.0	17.3	59.6	10.3
15	MN	30% RAP	2.697	2.349	2.527	7.1	17.4	59.1	10.3
16	IA	0% RAS	2.617	2.275	2.443	6.9	17.8	61.3	10.9
17	IA	0% RAS	2.617	2.270	2.443	7.1	18.0	60.7	10.9
18	IA	0% RAS	2.617	2.279	2.443	6.7	17.7	62.2	11.0
19	IA	0% RAS	2.617	2.273	2.443	7.0	17.9	60.9	10.9
20	IA	0% RAS	2.617	2.271	2.443	7.0	18.0	61.1	11.0
21	IA	4% RAS	2.617	2.298	2.464	6.7	17.0	60.6	10.3
22	IA	4% RAS	2.617	2.289	2.464	7.1	17.3	59.1	10.2
23	IA	4% RAS	2.617	2.298	2.464	6.7	17.0	60.6	10.3
24	IA	4% RAS	2.617	2.288	2.464	7.1	17.4	59.2	10.3
25	IA	4% RAS	2.617	2.291	2.464	7.0	17.3	59.5	10.3
26	IA	5% RAS	2.617	2.293	2.460	6.8	17.2	60.5	10.4
27	IA	5% RAS	2.617	2.283	2.460	7.2	17.6	59.0	10.4
28	IA	5% RAS	2.617	2.280	2.460	7.3	17.7	58.7	10.4
29	IA	5% RAS	2.617	2.299	2.460	6.6	17.0	61.2	10.4
30	IA	5% RAS	2.617	2.290	2.460	6.9	17.3	60.2	10.4
31	IA	6% RAS	2.617	2.277	2.451	7.1	17.6	59.7	10.5
32	IA	6% RAS	2.617	2.272	2.451	7.3	17.8	58.9	10.5
33	IA	6% RAS	2.617	2.273	2.451	7.3	17.7	58.8	10.4
34	IA	6% RAS	2.617	2.287	2.451	6.7	17.2	61.1	10.5
35	IA	6% RAS	2.617	2.277	2.451	7.1	17.6	59.7	10.5
36	MO	15% RAP	2.630	2.295	2.471	7.1	17.0	58.2	9.9
37	MO	15% RAP	2.630	2.293	2.471	7.2	17.1	57.9	9.9
38	MO	15% RAP	2.630	2.301	2.471	6.9	16.8	59.1	9.9

Table 16: Volumetric Properties of Compacted Sample Cylinder (Continued)

39	MO	15% RAP	2.630	2.295	2.471	7.1	17.0	58.2	9.9
40	MO	15% RAP	2.630	2.298	2.471	7.0	16.9	58.6	9.9
41	MO	5% Fine RAS	2.632	2.295	2.547	6.8	17.3	60.6	10.5
42	MO	5% Fine RAS	2.632	2.298	2.547	6.7	17.1	61.2	10.5
43	MO	5% Fine RAS	2.632	2.294	2.547	6.8	17.3	60.6	10.5
44	MO	5% Fine RAS	2.632	2.293	2.547	6.8	17.3	60.4	10.5
45	MO	5% Fine RAS	2.632	2.293	2.547	6.8	17.3	60.4	10.5
46	MO	5% Coarse RAS	2.632	2.293	2.527	6.5	17.3	62.8	10.9
47	MO	5% Coarse RAS	2.632	2.287	2.527	6.7	17.5	61.8	10.8
48	MO	5% Coarse RAS	2.632	2.281	2.527	7.0	17.8	60.9	10.8
49	MO	5% Coarse RAS	2.632	2.284	2.527	6.8	17.6	61.4	10.8
50	MO	5% Coarse RAS	2.632	2.274	2.527	7.2	18.0	59.8	10.8
51	IN	15% RAP	2.647	2.301	2.468	6.8	18.3	63.0	11.5
52	IN	15% RAP	2.647	2.292	2.468	7.1	18.6	61.6	11.5
53	IN	15% RAP	2.647	2.299	2.468	6.8	18.4	62.7	11.5
54	IN	3% RAS&HMA	2.618	2.279	2.448	6.9	18.3	62.4	11.4
55	IN	3% RAS&HMA	2.618	2.277	2.448	7.0	18.4	62.1	11.4
56	IN	3% RAS&HMA	2.618	2.285	2.448	6.7	18.1	63.3	11.5
57	IN	3% RAS&HMA	2.618	2.275	2.448	7.1	18.5	61.7	11.4
58	IN	3% RAS&HMA	2.618	2.276	2.448	7.0	18.5	61.9	11.4
59	IN	3% RAS&WMA	2.618	2.299	2.463	6.6	17.6	62.3	11.0
60	IN	3% RAS&WMA	2.618	2.293	2.463	6.9	17.8	61.4	10.9
61	IN	3% RAS&WMA	2.618	2.294	2.463	6.9	17.8	61.4	10.9
62	IN	3% RAS&WMA	2.618	2.294	2.463	6.9	17.8	61.4	10.9
63	IN	3% RAS&WMA	2.618	2.296	2.463	6.8	17.8	61.7	11.0

Viscosity (η)

Binder viscosities are calculated from DSR tests results through Equation 16 The procedures to test high temperature performance grade of RTFO aged binder were applied. Binder shear modulus and phase angle values were observed at temperatures ranging from 58 ℃ to 82 ℃ with increments of 6 ℃. Three or four viscosity values were tested for each type of binder. The A-VTS method is used to predict the binder viscosities at the interested temperatures which are the temperatures that the dynamic moduli of compacted samples were tested. The A-VTS method assumes that the binder viscosity is linearly related to temperature on a log-log to log scale. The expression of the method is presented in Equation 17. The VTS coefficients, A and VTS, are summarized in Table 17 and graphically presented in Figure 36.

$$\eta = \frac{|G^*|}{10}\left(\frac{1}{\sin\delta}\right)^{4.8628}$$

Equation 16

where η = viscosity (Poise),

$|G^*|$= binder complex shear modulus (Pa), and

δ = phase angle.

$$\log(\log(\eta)) = A + VTS \times \log(t_r)$$

Equation 17

where A, VTS = VTS coefficients,

t_r = temperature (°Rankin), and

η = viscosity (centipoises).

Table 17: VTS Coefficients of Recovered Asphalt Binder

Mix Number	Project	Description	A	VTS
BC-21	MN	5% Mfr. RAS	10.53205	-3.50984
BC-22		5% Tear-off RAS	10.88701	-3.63714
BC-23		30% RAP	11.05463	-3.70279
BC-24	IA	0% RAS	11.05398	-3.69434
BC-25		4% RAS	10.5888	-3.52328
BC-26		5% RAS	10.35324	-3.43054
BC-27		6% RAS	9.783821	-3.22009
BC-28	MO	15% RAP	10.92817	-3.64293
BC-29		5% Fine RAS	9.692357	-3.18057
BC-30		5% Coarse RAS	9.842163	-3.23768
BC-31	IN	15% FRAP	10.96405	-3.65855
BC-32		3% RAS&HMA	10.77171	-3.58458
BC-33		3% RAS&WMA	10.83753	-3.60935

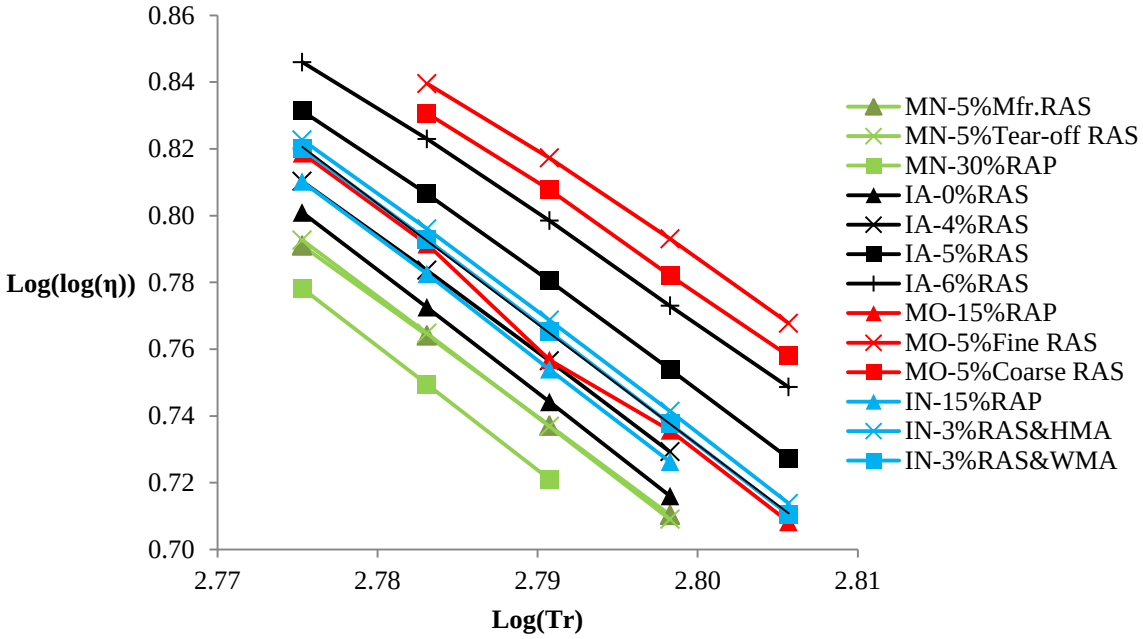

Figure 36: VTS Curves of Recovered Asphalt Binder

Complex Shear Modulus (G)*

DSR frequency sweep tests were performed at multiple temperatures and frequencies. Binder complex shear modulus master curves are developed by shifting G* values at different temperatures to a reference temperature using shift factors (a(T)). The selected reference temperatures are the interested temperatures, 4 ℃, 21 ℃, and 37 ℃. Figure 37 shows the actual observed G* values for binder extracted from Iowa 0% RAS mix. The G* curves are horizontally moved by factoring the actual testing frequencies with a(T) to achieve a smooth curve as shown in Figure 38. Figure 37 and Figure 38 provide an example of the master curve construction process. Master curves for other recovered binders were constructed and included in the Appendix. The a(T) values at 37 ℃ are summarized in Table 18. At reference temperature, the corresponding frequencies of G* values are the actual testing frequencies. It is not necessary to factor the frequencies at the reference temperature. Therefore, the shift factor at the reference temperature is equal to 1. To calculate the shift factors for 4 ℃ or 21 ℃reference temperatures, simply divide each shift factor for the 37 ℃ reference temperature by the shift factor at 4 ℃ or 21 ℃ for the 37 ℃ reference temperature. Lab G* tests were not performed at 4 ℃ because it takes significantly longer time to lower the water bath temperature to 4 ℃ than other

temperatures. As shown in Figure 39, the log shift factor values are linearly correlated to temperature. The shift factor at 4 ℃ is estimated for each recovered binder. The G* used for E* predictive models is the corresponding G* of a particular frequency and temperature on the master curve.

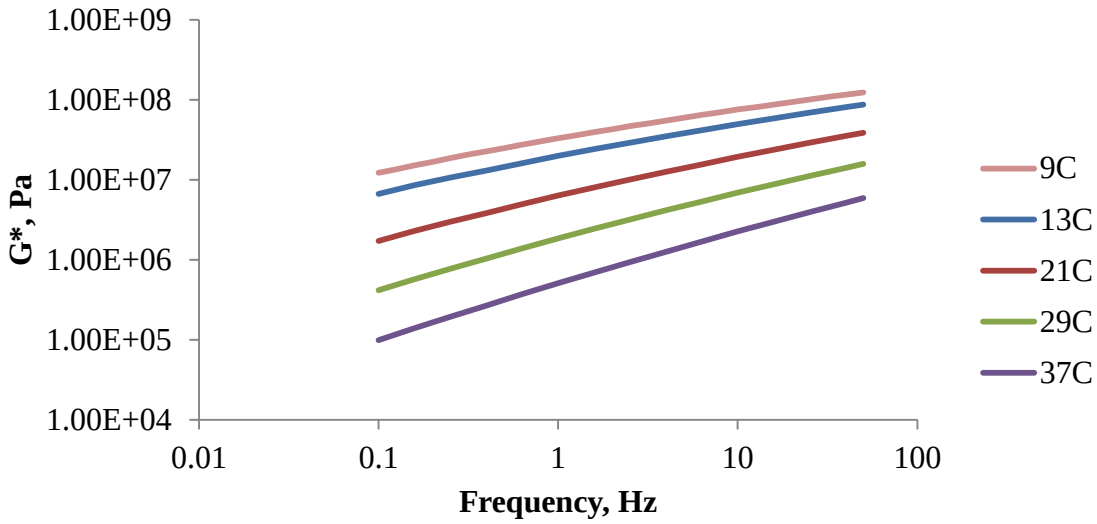

Figure 37: Lab Tested G* Values of Asphalt Binder Recovered from Iowa 0% RAS Mix

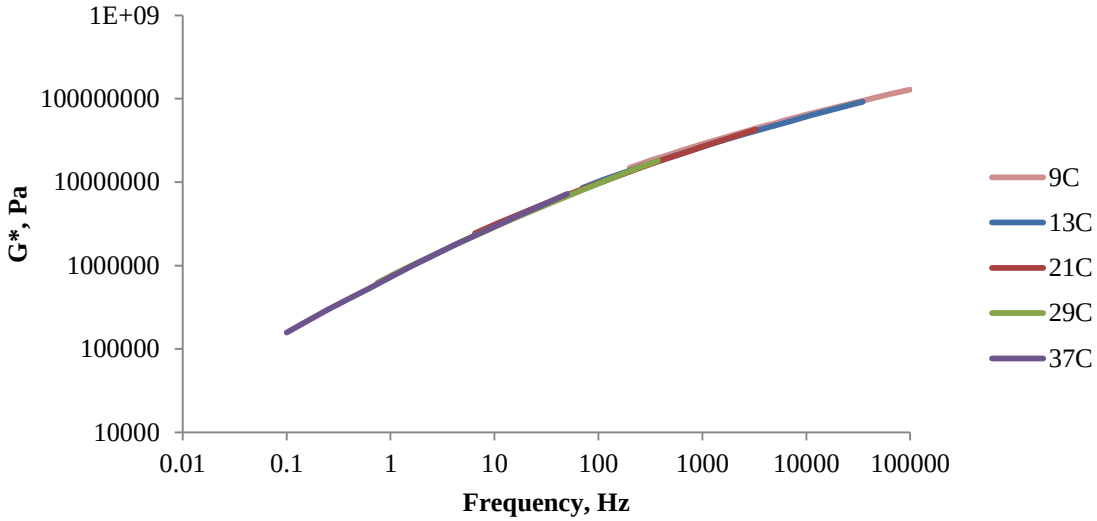

Figure 38: G* Master Curve for Mix BC24 (Reference Temperature is 37 ℃)

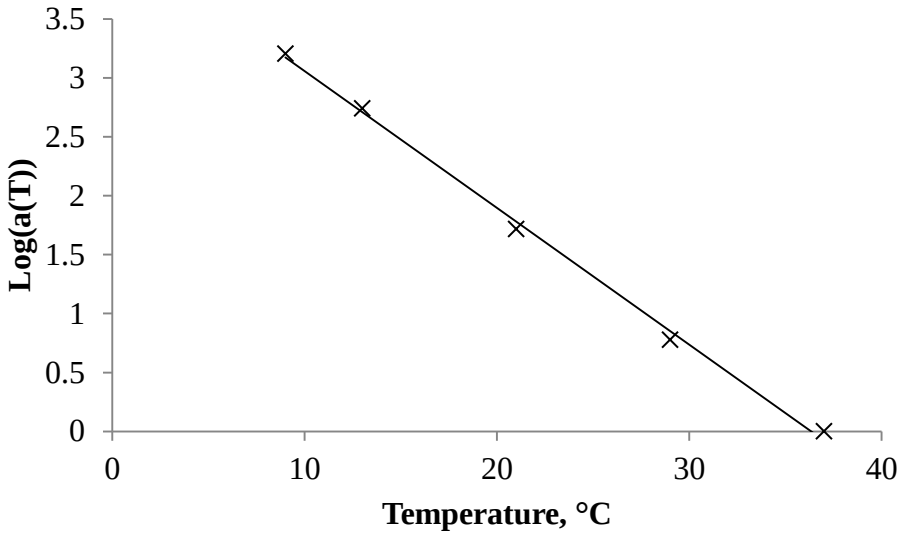

Figure 39: Shift Factors for Mix BC-25

Table 18: G* Shift Factors for Recovered Binders at Reference Temperature of 37 ℃

Mix Number	A(4 ℃)	A(9 ℃)	A(13 ℃)	A(21 ℃)	A(29 ℃)	A(37 ℃)
BC-21	2243	736	550	56	6.7	1
BC-23	3172	1700	550	55	7.0	1
BC-24	4804	1400	480	50	6.5	1
BC-25	5666	1600	550	52	6.0	1
BC-27	2972	908	550	55	7.0	1
BC-28	6638	3000	1000	80	8.5	1
BC-29	12066	3000	900	90	8.0	1
BC-30	4804	3500	1200	95	8.0	1
BC-31	7278	2000	650	60	7.0	1
BC-32	8674	2500	700	60	7.5	1
BC-33	7667	2000	700	65	7.5	1

Phase Angle (δ)

Models to estimate the value of phase angle are developed using the same method as the aforementioned method to estimate G*. Figure 40 shows an example of the phase angle master curves at reference temperature equal to 4 ℃, 21 ℃, and 37 ℃. The determined phase angle shift factors are summarized in Table 19.

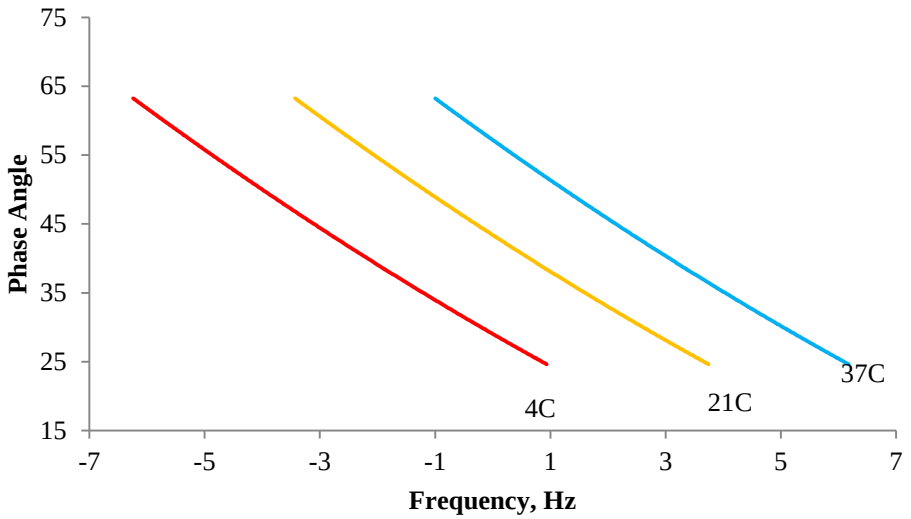

Figure 40: Phase Angle Master Curves for Asphalt Binder Recovered from Mix BC24

Table 19: Phase Angle Shifting Factors at Reference Temperature of 37 ℃

Mix Number	A(9 ℃)	A(13 ℃)	A(21 ℃)	A(29 ℃)	A(37 ℃)	A(4 ℃)
BC-21	11162	5500	280	15	1	56396
BC-23	15000	3900	250	15	1	39709
BC-24	10000	2600	160	12	1	49180
BC-25	19000	4000	200	14	1	95693
BC-27	17585	8000	350	16	1	96286
BC-28	22000	5500	250	14	1	72175
BC-29	75000	15000	400	18	1	511328
BC-30	120000	22000	600	20	1	49180
BC-31	17000	4000	220	14	1	91124
BC-32	25000	5500	250	16	1	139583
BC-33	30000	6500	270	15	1	173797

Witczak Model

The Witczak models are developed form of a sigmoid function. The basic form of the sigmoid function is shown in Equation 18 The shape of the sigmoid function is controlled by the four fitting parameters: δ, α, β, and γ. In this function, δ is the smallest E* value. In a scenario that HMA is subjected to a very high temperature and a slow moving traffic, the E* of the HMA is very close to δ. In this situation, the stiffness of asphalt binder is very low which the stiffness of HMA is governed by the aggregate and mixture volumetric properties. Equation 19 is the

developed form of δ in the 1999 Witczak Model. In the 2006 Witczak Model, the form of δ is written as Equation 20 The value of δ + α is the theoretical largest E*. Therefore, α represents the largest change of E* that a HMA pavement can have. The developed forms of α for 1999 and 2006 Witczak models are shown in Equation 21 and Equation 22, respectively. Parameter δ and δ + α define the lower and upper bounds of the sigmoid curve. Parameter β and γ are empirical constants that are used to define the shape of the curve.

$$\log(|E^*|) = \delta + \frac{\alpha}{1 + e^{\beta+\gamma\times\log(t_r)}}$$

Equation 18

where $|E^*|$ = dynamic modulus,

t_r = reduced time, and

δ, α, β, γ = fitting parameters.

$$\delta = 3.750063 + 0.02932\rho_{200} - 0.001767(\rho_{200})^2 - 0.002841\rho_4 - 0.058097V_a - 0.802208\left(\frac{V_{beff}}{V_{beff} + V_a}\right)$$

Equation 19

where ρ_{200} = percent mass of aggregates passing through a #200 sieve,

ρ_4 = cumulative percent mass of aggregates retained on a # 4 sieve,

V_a = air voids, and

V_{beff} = effective binder content by volume of the mix.

$$\delta = -0.349 + 0.754\left(|G_b^*|^{-0.0052}\right) \times \left(6.65 - 0.032\rho_{200} + 0.0027\rho_{200}^2 + 0.011\rho_4 - 0.0001\rho_4^2 + 0.006\rho_{38} - 0.00014\rho_{38}^2 - 0.08V_a - 1.06\left(\frac{V_{beff}}{V_a + V_{beff}}\right)\right)$$

Equation 20

where $|G_b^*|$ = dynamic shear modulus of the binder,

ρ_{38} = cumulative percent mass of aggregates retained on a 3/8" sieve, and

ρ_{200}, ρ_4, V_a, and V_{beff} = as previously defined.

$$\alpha = 3.871977 - 0.0021\rho_4 + 0.003958\rho_{38} - 0.000017(\rho_{38})^2 + 0.00547\rho_{34}$$

Equation 21

where ρ_{34} = cumulative percent mass of aggregates retained on a¾" sieve, and

ρ_{38}, and ρ_4 = as previously defined.

$$\alpha = 2.56 + 0.03V_a + 0.71\left(\frac{V_{beff}}{V_a + V_{beff}}\right) + 0.012\rho_{38} - 0.0001{\rho_{38}}^2 - 0.01\rho_{34}$$

Equation 22

where ρ_{38}, ρ_{34}, V_a, and V_{beff} = as previously defined.

The independent variable t_r is the multiplicative inverse of the reduced frequency (f_r). *The* reduced frequency is the equivalent frequency of an E* value at reference temperature. Reduced frequency is calculated using the real frequency factored by a shift factor (a(T)) which is determined by the binder rheological properties using the viscosity-temperature superposition method. Therefore, the variable t_r represents the binder stiffness effect on the mixture stiffness. Because the asphalt binder stiffness is dependent on temperature and loading frequency, t_r is also a simulation factor for the temperature and traffic loading rate. In the 1999 Witczak Model, t_r is a function of the loading rate and the binder viscosity as shown in Equation 23 In the 2006 Witczak Model, the stiffness of asphalt binder is calculated from the binder complex shear modulus and phase angle by Equation 24 Substitute t_r in Equation 18 by Equation 23 and Equation 24, a general form of the Witczak model can be obtained in Equation 25 The values of parameter b, g_1, and g_2 are equal to -0.604414, -0.313351, and -0.393532 for the 1999 Witczak Model. In the 2006 Witczak Model, the values of the three parameters, b, g_1, and g_2, are -0.7814, -0.5785, and 0.8834, respectively.

$$\log(t_r) = a\log(f) + b\log(\eta)$$

Equation 23

where f = loading frequency,

η = asphalt binder viscosity,

a, b = fitting parameters, and

t_r = as previously defined.

$$\mathbf{log(t_r) = alog(|G^*|) + blog(\phi)}$$

Equation 24

where Φ = phase angle,

a, b = fitting parameters, and

t_r, |G*| = as previously defined.

$$\mathbf{log(|E^*|) = \delta + \frac{\alpha}{1 + e^{b+g_1 log(x_1)+g_2(x_2)}}}$$

Equation 25

where x_1 = frequency in the 1999 Witczak Model or binder complex shear modulus in the 2006 Witczak Model,

x_2 = binder viscosity in the 1999 Witczak Model or phase angle in the 2006 Witczak Model,

b, g_1, g_2 = fitting parameters, and

|E*|, δ, α = as previously defined.

Therefore, dummy variables can be added to the δ, α, b, g_1 and g_2 terms to change the shape of the sigmoid function to match the laboratory tested E* values. The E* values of the control mixes which contain 0% RAS are used to determine the coefficients of the 0%-RAS-effect calibration variable $D_{IN,}$ D_{IA}, D_{MN}, and D_{MO} in Equation 26 After the coefficients of $D_{IN,}$ D_{IA}, D_{MN}, and D_{MO} were determined, Equation 26 can be used to calculate the predicted E* which the prediction accuracy variability from project differences is eliminated. The values of the coefficients in Equation 26 are determined through non-linear multiple variable regression of the lab data; and the results are listed in Table 20 for the 1999 Witczak Model and Table 21 for the 2006 Witczak Model.

$$\log(|E^*|) = \delta_c + \frac{\alpha_c}{1 + e^{b_c + g1_c \log(x_1) + g2_c(x_2)}}$$

$$\delta_c = \delta + C\delta_{IN}D_{IN} + C\delta_{IA}D_{IA} + C\delta_{MN}D_{MN} + C\delta_{MO}D_{MO}$$

$$\alpha_c = \alpha + C\alpha_{IN}D_{IN} + C\alpha_{IA}D_{IA} + C\alpha_{MN}D_{MN} + C\alpha_{MO}D_{MO}$$

$$b_c = b + Cb_{IN}D_{IN} + Cb_{IA}D_{IA} + Cb_{MN}D_{MN} + Cb_{MO}D_{MO}$$

$$g1_c = g_1 + Cg1_{IN}D_{IN} + Cg1_{IA}D_{IA} + Cg1_{MN}D_{MN} + Cg1_{MO}D_{MO}$$

$$g2_c = g_2 + Cg2_{IN}D_{IN} + Cg2_{IA}D_{IA} + Cg2_{MN}D_{MN} + Cg2_{MO}D_{MO}$$

Equation 26

where D_{IN} = 1 for Indiana mixes and 0 for others,

D_{IA} = 1 for Iowa mixes and 0 for others,

D_{MN} = 1 for Minnesota mixes and 0 for others,

D_{MO} = 1 for Missouri mixes and 0 for others,

$C\delta_{IN}$, $C\delta_{IA}$, $C\delta_{MN}$, $C\delta_{MO}$, $C\alpha_{IN}$, $C\alpha_{IA}$, $C\alpha_{MN}$, $C\alpha_{MO}$, Cb_{IN}, Cb_{IA}, Cb_{MN}, Cb_{MO}, Cg_{1IN}, Cg_{1IA}, Cg_{1MN}, Cg_{1MO}, Cg_{2IN}, Cg_{2IA}, Cg_{2MN}, Cg_{2MO} = coefficient of the dummy variable D_{IN}, D_{IA}, D_{MN}, and D_{MO}, and

δ,α,$|E^*|$, x_1, x_2, $|G_b^*|$,b, g_1, g_2= as previously defined.

Table 20: Regression Results of 0%-RAS-Effect for the 1999 Witczak Model

Parameter	Estimation	Standard Error	P-value
$C\delta_{IN}$	-2.4475	3.21572	0.4488
$C\delta_{IA}$	-2.4136	2.18329	0.2709
$C\delta_{MN}$	-0.3767	1.56535	0.8102
$C\delta_{MO}$	-2.1956	1.56179	0.1621
$C\alpha_{IN}$	2.41062	3.25415	0.461
$C\alpha_{IA}$	2.45945	2.25627	0.2776
$C\alpha_{MN}$	0.30519	1.68828	0.8568
$C\alpha_{MO}$	2.14614	1.5788	0.1763
Cb_{IN}	-0.8283	0.60855	0.1773
Cb_{IA}	-0.4255	0.42872	0.3228
Cb_{MN}	0.10558	0.5454	0.8468
Cb_{MO}	-0.7409	0.31634	0.0206
Cg_{1IN}	-0.0531	0.05045	0.2962
Cg_{1IA}	-0.0357	0.0524	0.4972
Cg_{1MN}	-0.1367	0.12542	0.2776
Cg_{1MO}	-0.0674	0.02645	0.0120
Cg_{2IN}	0.02603	0.04846	0.5927
Cg_{2IA}	0.05663	0.0487	0.2469
Cg_{2MN}	-0.0917	0.12768	0.4737
Cg_{2MO}	-0.0144	0.02681	0.5923

Table 21: Regression Results of 0%-RAS-Effect for the 2006 Witczak Model

Parameter	Estimation	Standard Error	P-value
$C\delta_{IN}$	-2.084	1.61254	0.2
$C\delta_{IA}$	-4.4766	3.35436	0.1843
$C\delta_{MN}$	-0.8869	0.39381	0.0259
$C\delta_{MO}$	-1.4828	1.05076	0.1605
$C\alpha_{IN}$	2.32134	1.81791	0.2053
$C\alpha_{IA}$	3.92956	3.41124	0.2514
$C\alpha_{MN}$	0.52512	0.4388	0.2335
$C\alpha_{MO}$	1.87323	1.31158	0.1556
Cb_{IN}	0.09357	0.52829	0.8599
Cb_{IA}	-6.6804	0.5422	<0.0001
Cb_{MN}	-3.5158	1.34441	0.0099
Cb_{MO}	1.72603	0.52612	0.0013
Cg_{1IN}	0.16969	0.08427	0.0474
Cg_{1IA}	0.3434	0.05092	<0.0001
Cg_{1MN}	0.04846	0.09017	0.5918
Cg_{1MO}	0.08525	0.10586	0.4221
Cg_{2IN}	-0.4511	0.25582	0.0816
Cg_{2IA}	2.86933	0.51064	<0.0001
Cg_{2MN}	2.00793	0.64926	0.0024
Cg_{2MO}	-1.012	0.05708	<0.0001

Figure 41 through Figure 44show the prediction accuracies of the Witczak models that calibrations are made to eliminate the project variability. Compared to Figure 30 through Figure 33, the linear trend lines for different projects tend to approach each other. This indicates that the Witczak models tend to have the same prediction accuracies for different projects. The real variability in prediction accuracies caused by changes in RAS contents is more detectable. The calibrated models will be further modified to account for the effects of the RAS content.

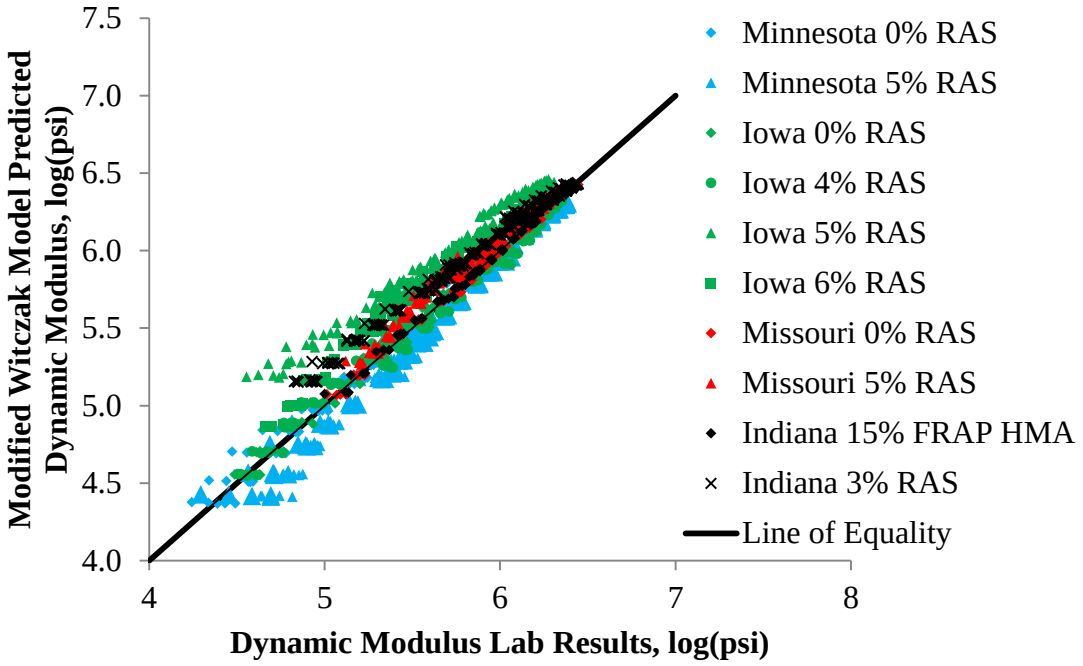

Figure 41: Project Effects Calibrated 1999 Witczak Model Accuracy on Logarithm Scale

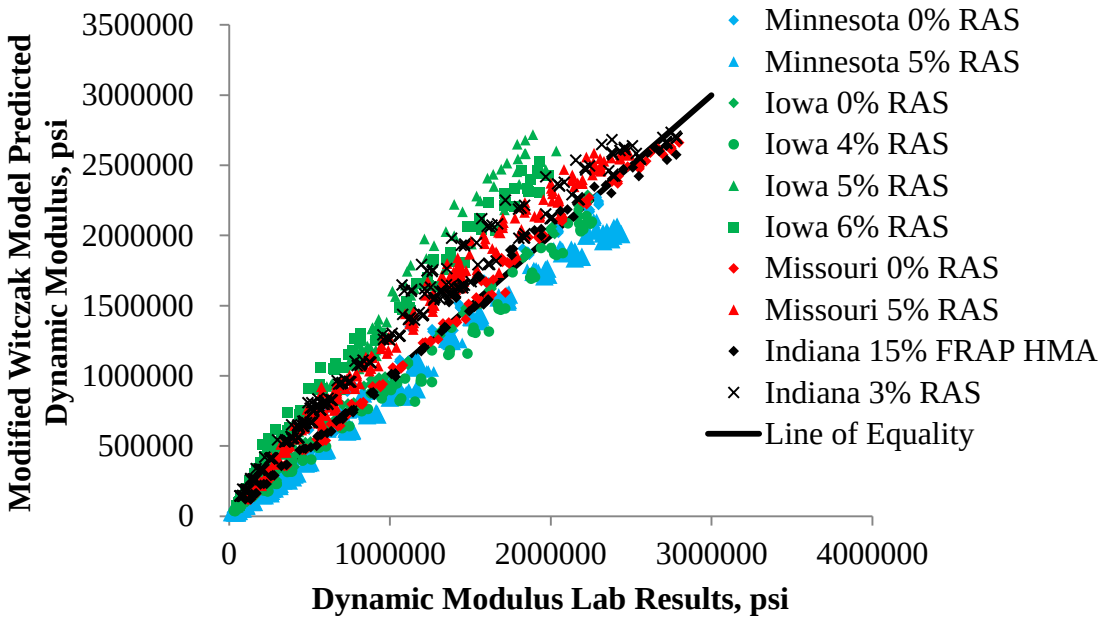

Figure 42: Project Effects Calibrated 1999 Witczak Model Accuracy on Normal Scale

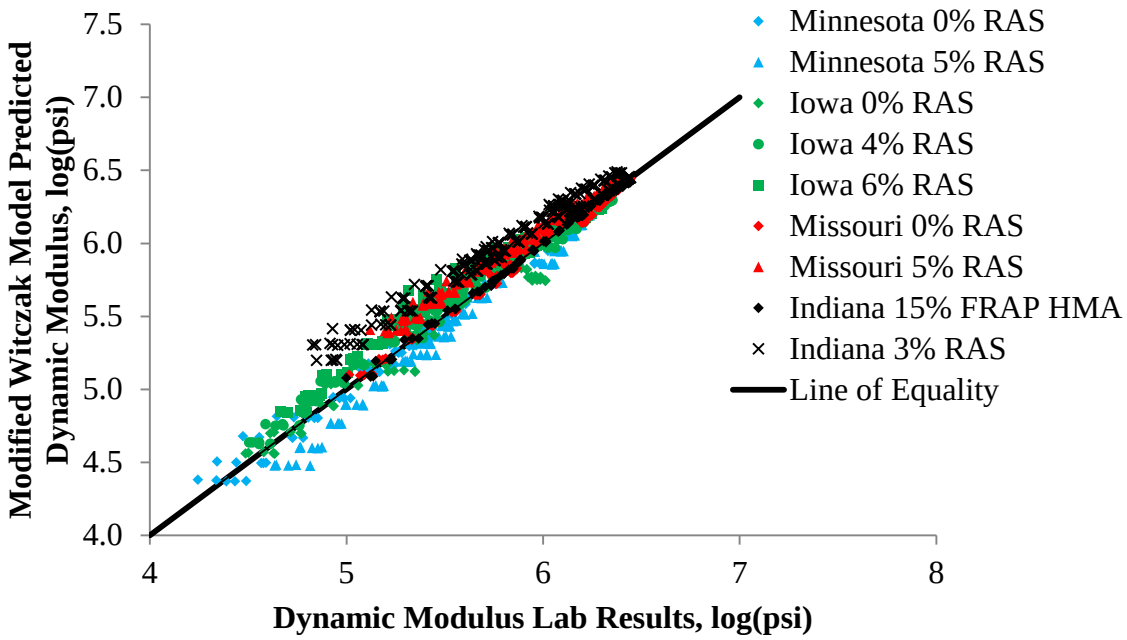

Figure 43: Project Effects Calibrated 2006 Witczak Model Accuracy on Logarithm Scale

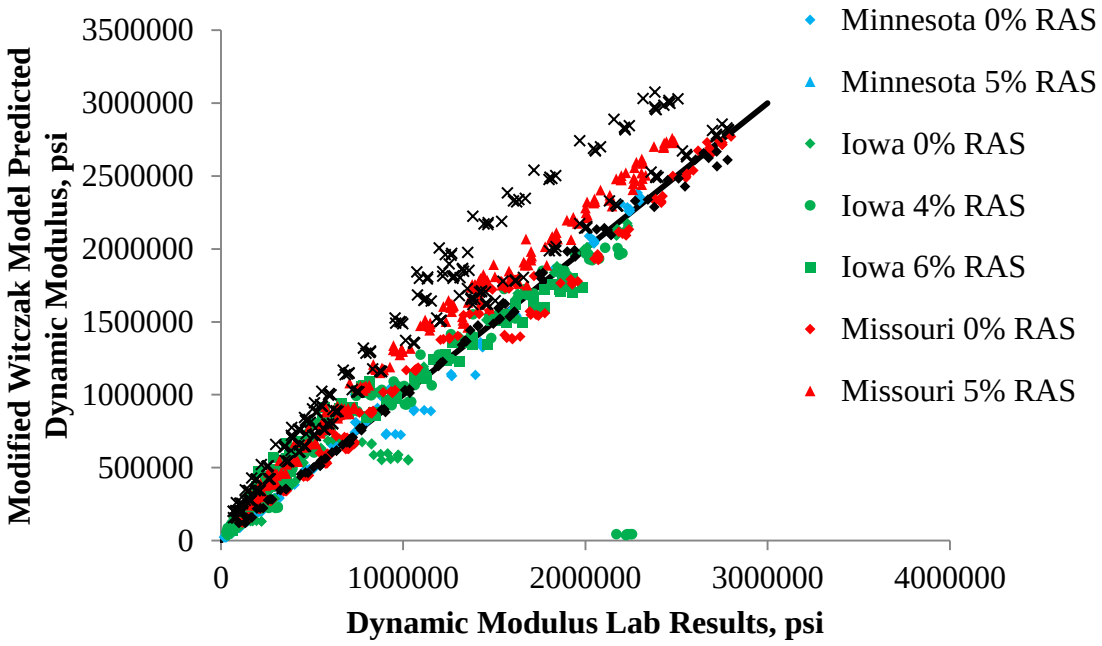

Figure 44: Project Effects Calibrated 2006 Witczak Model Accuracy on Normal Scale

Let δ_c, α_c, b_c, g_{1c}, and g_{2c} represent the calibrated δ, α, b, g_1, and g_2 terms identified in previous steps. Variables that represent different RAS contents are added to the δ_c, α_c, b_c, g_{1c}, and

g_{2c} terms to simulate the effects of RAS content. Lab tested E* values for each level of RAS content are used to determine the coefficients of the RAS effect variable $D_{3\%}$, $D_{4\%}$, $D_{5\%}$, and $D_{6\%}$ in Equation 27 The results of the regression analyses are shown in Table 22 and Table 23 for the 1999 and 2006 Witczak models, respectively. The prediction accuracies of modified Witczak models are shown in Figure 45 through Figure 48 on both normal and logarithm scales. The scatters on Figure 45 through Figure 48 are concentrated along the line of equality indicating the modified models have high accuracy of prediction. The modified 1999 Witczak Model achieves an R^2 value of 0.99 on a logarithm scale and 0.98 on a normal scale. The corresponding Se/Sy values are 0.11 and 0.15 for the logarithm and normal scales, respectively. The R^2 of the modified 2006 Witczak Model is 0.99 on a logarithm scale or 0.98 on a normal scale. The Se/Sy value is 0.08. According to Table 10, both the modified 1999 and 2006 Witczak models arrive at excellent goodness-of-fit.

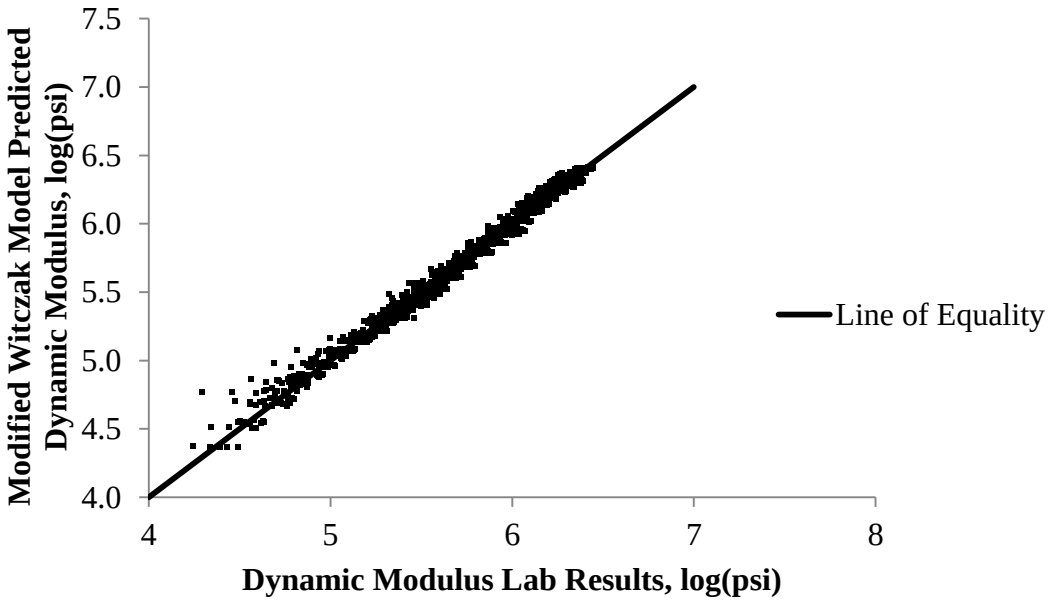

Figure 45: Modified 1999 Witczak Model Accuracy on Logarithm Scale

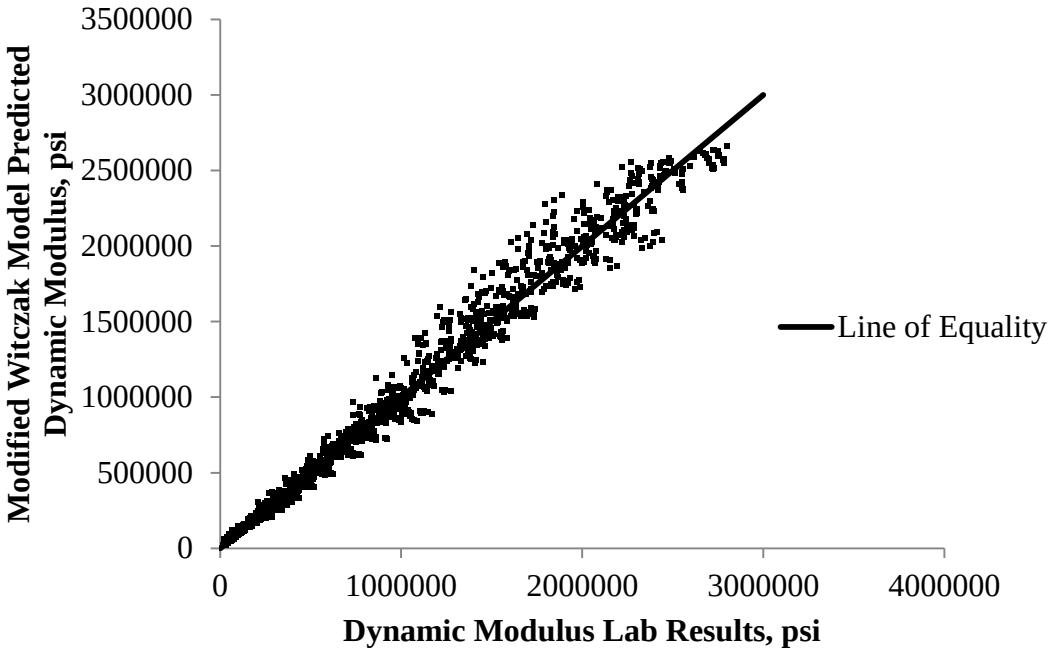

Figure 46: Modified 1999 Witczak Model Accuracy on Normal Scale

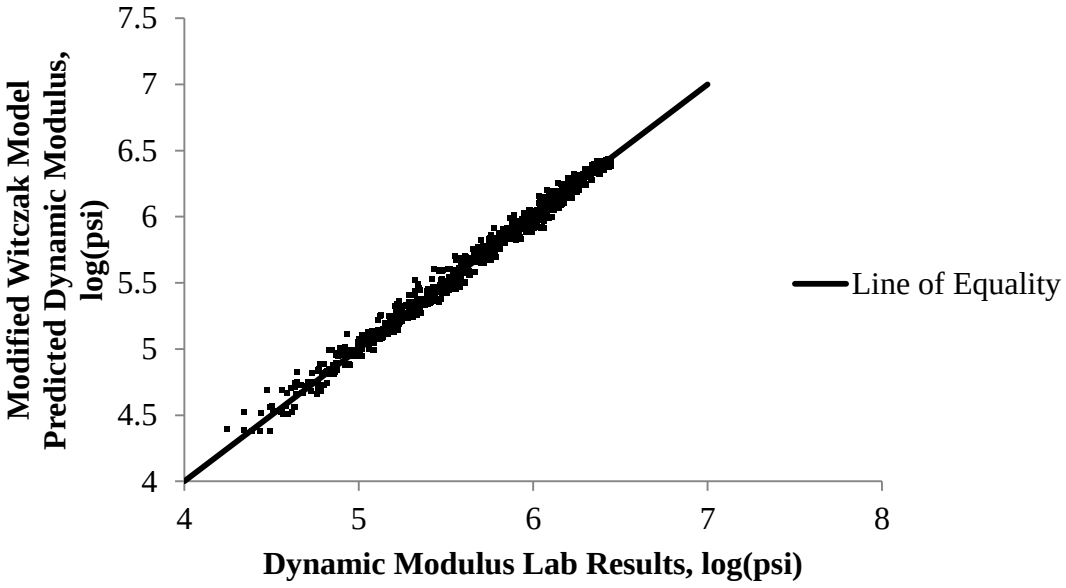

Figure 47: Modified 2006 Witczak Model Accuracy on Logarithm Scale

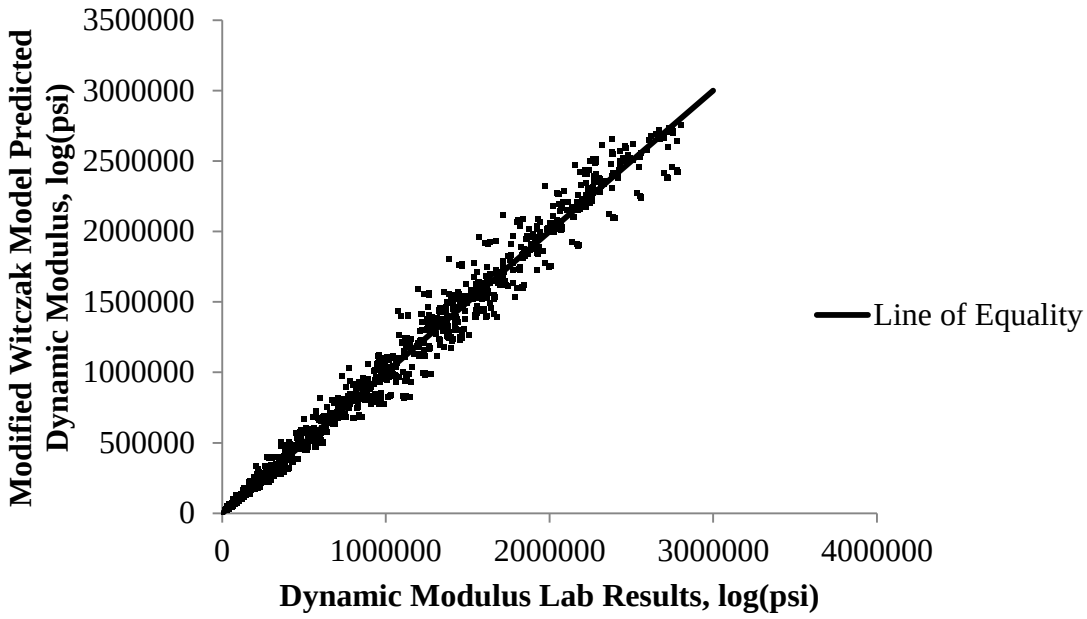

Figure 48: Modified 2006 Witczak Model Accuracy on Normal Scale

$$\log(|E^*|) = \delta_c + \delta_{RAS} + \frac{\alpha_c + \alpha_{RAS}}{1 + e^{b_c + b_{RAS} + (g_{1_c} + g_{1_{RAS}})\log(x_1) + (g_{2_c} + (g_{2_{RAS}})(x_2)}}$$

$$\delta_{RAS} = C\delta_{3\%}D_{3\%} + C\delta_{4\%}D_{4\%} + C\delta_{5\%}D_{5\%} + C\delta_{6\%}D_{6\%}$$

$$\alpha_{RAS} = C\alpha_{3\%}D_{3\%} + C\alpha_{4\%}D_{4\%} + C\alpha_{5\%}D_{5\%} + C\alpha_{6\%}D_{6\%}$$

$$b_{RAS} = Cb_{3\%}D_{3\%} + Cb_{4\%}D_{4\%} + Cb_{5\%}D_{5\%} + Cb_{6\%}D_{6\%}$$

$$g_{1_{RAS}} = Cg_{1_{3\%}}D_{3\%} + Cg_{1_{4\%}}D_{4\%} + Cg_{1_{5\%}}D_{5\%} + Cg_{1_{6\%}}D_{6\%}$$

$$g_{2_{RAS}} = Cg_{2_{3\%}}D_{3\%} + Cg_{2_{4\%}}D_{4\%} + Cg_{2_{5\%}}D_{5\%} + Cg_{2_{6\%}}D_{6\%}$$

Equation 27

where $D_{3\%}$ = 1 for mixes containing 3% RAS and 0 for others,

$D_{4\%}$ = 1 for mixes containing 4% RAS and 0 for others,

$D_{5\%}$ = 1 for mixes containing 5% RAS and 0 for others,

$D_{6\%}$ = 1 for mixes containing 6% RAS and 0 for others,

$C\delta_{3\%}$, $C\delta_{4\%}$, $C\delta_{5\%}$, $C\delta_{6\%}$, $C\alpha_{3\%}$, $C\alpha_{4\%}$, $C\alpha_{5\%}$, $C\alpha_{6\%}$, $C\beta_{3\%}$, $C\beta_{4\%}$, $C\beta_{5\%}$, $C\beta_{6\%}$, $C\gamma_{3\%}$, $C\gamma_{4\%}$, $C\gamma_{5\%}$, $C\gamma_{6\%}$, $Cc_{3\%}$, $Cc_{4\%}$, $Cc_{5\%}$, $Cc_{6\%}$ = coefficient of the dummy variable $D_{3\%}$, $D_{4\%}$, $D_{5\%}$, and $D_{6\%}$, and

$|E^*|$, $|G_b^*|$, δ_b, t_r, δ_c, α_c, β_c, $\gamma_{c,}$ f =as previously defined.

Table 22: Regression Results of RAS-Effect for the 1999 Witczak Model

Parameter	Estimation	Standard Error	P-value
$C\delta_{3\%}$	-1.6934	3.43166	0.6221
$C\delta_{4\%}$	2.338807	0.346263	<0.0001
$C\delta_{5\%}$	1.298827	0.02642	<0.0001
$C\delta_{6\%}$	2.371782	0.747357	0.0019
$C\alpha_{3\%}$	1.735896	3.466848	0.617
$C\alpha_{4\%}$	-2.52605	0.368664	<0.0001
$C\alpha_{5\%}$	-1.25625	0.031908	<0.0001
$C\alpha_{6\%}$	-2.37209	0.839104	0.0054
$Cb_{3\%}$	-0.05575	0.50377	0.9120
$Cb_{4\%}$	0.63665	0.141449	<0.0001
$Cb_{5\%}$	0.487354	0.013035	<0.0001
$Cb_{6\%}$	0.918556	0.305215	0.0031
$Cg1_{3\%}$	0.028509	0.035197	0.4187
$Cg1_{4\%}$	-0.09271	0.028679	0.0015
$Cg1_{5\%}$	0.022702	0.006049	0.0002
$Cg1_{6\%}$	0.012533	0.052773	0.8126
$Cg2_{3\%}$	0.024398	0.034317	0.4777
$Cg2_{4\%}$	-0.20079	0.03225	<0.0001
$Cg2_{5\%}$	0.01138	0.005911	0.0546
$Cg2_{6\%}$	-0.02292	0.054009	0.6719

Statistics in Table 22 indicates that the coefficients with p-value greater than 0.05 include $C\delta_{4\%}$, $C\delta_{5\%}$, $C\delta_{6\%}$, $C\alpha_{4\%}$, $C\alpha_{5\%}$, $Cb_{4\%}$, $Cb_{5\%}$, $Cb_{6\%}$, $Cg1_{4\%}$, $Cg1_{5\%}$,and $Cg2_{4\%}$. It is noticed that p-values of coefficients for 3% RAS content are greater than 0.05. None of the 3% RAS calibration factors are considered statistically significant factors. The coefficients for 5% RAS except for $Cg2_{5\%}$are considered statistically significant with a confidence level of 95%. The 5%RAS coefficients also have the lowest standard errors. This resulted from the large sample size of the laboratory tested E* values for mixes containing 5% RAS. The overall trend of the p-value for parameters except for g_2 is decreasing with increasing RAS content. This indicates that a RAS content of 3% may not be large enough to cause significant decrease in the prediction accuracy of the 1999 Witczak model. The p-values of the g_2 coefficients except for $Cg2_{4\%}$ are greater than

0.05. There is not an obvious trend in the p-values. Although the standard error is very small, $Cg2_{5\%}$ is still not a significant factor. This indicates that the RAS content may not have an effect on the parameter g_2. The conclusions need to be verified by a larger sample space.

Table 23: Regression Results of RAS-Effect for the 2006 Witczak Model

Parameter	Estimation	Standard Error	P-value
$C\delta_{3\%}$	1.56497	0.540942	0.0041
$C\delta_{4\%}$	0.60657	1.63964	0.7120
$C\delta_{5\%}$	0.83865	1.093461	0.4434
$C\delta_{6\%}$	2.182726	0.907241	0.0175
$C\alpha_{3\%}$	-1.95661	0.618857	0.0017
$C\alpha_{4\%}$	-0.63047	1.672241	0.7068
$C\alpha_{5\%}$	-0.8366	1.116441	0.4539
$C\alpha_{6\%}$	-0.82806	0.230407	0.0005
$Cb_{3\%}$	-0.52857	1.046937	0.6141
$Cb_{4\%}$	-1.81861	1.567145	0.2479
$Cb_{5\%}$	0.574334	0.99932	0.5657
$Cb_{6\%}$	5.866697	1.676873	0.0006
$Cg1_{3\%}$	-0.17666	0.094207	0.0618
$Cg1_{4\%}$	-0.00774	0.970961	0.9937
$Cg1_{5\%}$	-0.06169	0.250851	0.8058
$Cg1_{6\%}$	-0.07247	1.35486	0.9574
$Cg2_{3\%}$	0.848671	0.509028	0.0966
$Cg2_{4\%}$	1.1913	0.97377	0.2233
$Cg2_{5\%}$	-0.01117	0.373595	0.9762
$Cg2_{6\%}$	-2.5251	0.569046	0.1099

Statistics in Table 23 show that the coefficients having a p-value greater than 0.05 include $C\delta_{3\%}$, $C\delta_{6\%}$, $C\alpha_{3\%}$, $C\alpha_{6\%}$, and $Cb_{6\%}$. The general p-value trend for the δ, α, and b coefficients are decreasing with increasing RAS content. There are no distinct trends for the p-values of the g_1 and g_2 coefficients. This indicates that RAS content less than 5% may not result in significant

decrease in the prediction accuracy of the 2006 Witczak Model. Adding shingles to HMA may not change the g_1 and g_2 parameters in the model.

Hirsch Model

The Hirsch model is developed from the Hirsch's law of mixture. The basic equation is Equation 28 The model contains four empirical constants, E_a, p_0, p_1, and p_2. The values of the four constants determined by Christensen (2003) are 4,200,000, 20, 0.58, and 650 for E_a, p_0, p_1, and p_2, respectively. Dummy variables which are used to simulate different projects are added to the four constants in order to match the lab testing results. The 0%-RAS-effect calibration equations for E_a, p_0, p_1, and p_2 are shown in Equation 29 through Equation 32 Lab tested E* values for mixes containing 0% RAS are used to determine the value of each coefficient. The regression results are shown in Table 24. Figure 49 shows the prediction accuracies of the calibrated Hirsch Model. There are no distinct linear trend lines for different projects. Variables are added to the calibrated E_a, p_0, p_1, and p_2 to account for the effects of the RAS. The modified predicted E* values are calculated by Equation 28 with modified E_a, p_0, p_1, and $p_2$as shown in Equation 33 to Equation 36 Lab E* values for each RAS content are used for regression of the modified Hirsch function. The coefficients of the dummy variables are determined and summarized in Table 25. Figure 50 shows the lab tested E* vs. the predicted E* from the modified Hirsch model. Data points on Figure 50 are concentrated along the line of equality. The R^2 of the modified Hirsch model is 0.97 and the Se/Sy value is 0.19 on a normal scale. On a logarithm scale, the model achieves R^2 value of 0.51 and Se/Sy value of 0.76. According to Table 10, the goodness-of-fit for the modified Hirsch model is excellent on normal scale and fair on logarithm scale.

$$\boldsymbol{Ec = Pc(Va'Ea + VmEm) + (1 - Pc)\left[\frac{Va'}{Ea} + \frac{(Vm + Vv)^2}{VmEm}\right]^{-1}}$$

$$\mathbf{Pc = \frac{\left(P_0 + \frac{VFM \times Em}{VMA'}\right)^{P_1}}{P_2 + \left(\frac{VFM \times Em}{VMA'}\right)^{P_1}}}$$

Equation 28

where Ec = mixture modulus,

Ea = aggregate modulus,

Em = mastic modulus,

Va' = volume fraction of aggregate excluding the contact volume and mineral filler,

Vm = volume fraction of mastic,

Vv = volume fraction of air voids,

VMA' = voids in mineral aggregate,

VFM = voids filled by mastic, and

P_0, P_1, P_2 = empirical constant.

$$\mathbf{Eac = 4200000 + CEa_{IN}D_{IN} + CEa_{IA}D_{IA} + CEa_{MN}D_{MN} + CEa_{MO}D_{MO}}$$

Equation 29

where Eac = 0%-RAS-effect calibrated Ea,

D_{IN} = 1 for Indiana mixes and 0 for others,

D_{IA} = 1 for Iowa mixes and 0 for others,

D_{MN} = 1 for Minnesota mixes and 0 for others,

D_{MO} = 1 for Missouri mixes and 0 for others, and

CEa_{IN}, CEa_{IA}, CEa_{MN}, CEa_{MO} = coefficient of the dummy variable D_{IN}, D_{IA}, D_{MN}, and D_{MO}.

$$\mathbf{P_0c = 20 + CP0_{IN}D_{IN} + CP0_{IA}D_{IA} + CP0_{MN}D_{MN} + CP0_{MO}D_{MO}}$$

Equation 30

where P_0c = 0%-RAS-effect calibrated P_0,

CEa_{IN}, CEa_{IA}, CEa_{MN}, CEa_{MO} = coefficient of the dummy variable D_{IN}, D_{IA}, D_{MN}, and D_{MO}, and

D_{IN}, D_{IA}, D_{MN}, D_{MO} = as previously defined.

$$\mathbf{P_1c = 0.58 + CP1_{IN}D_{IN} + CP1_{IA}D_{IA} + CP1_{MN}D_{MN} + CP1_{MO}D_{MO}}$$

Equation 31

where P_1c = 0%-RAS-effect calibrated P_1,

$CP1_{IN}$, $CP1_{IA}$, $CP1_{MN}$, $CP1_{MO}$ = coefficient of the dummy variable D_{IN}, D_{IA}, D_{MN}, and D_{MO}

D_{IN}, D_{IA}, D_{MN}, D_{MO} = as previously defined.

$$\mathbf{P_2c = 650 + CP2_{IN}D_{IN} + CP2_{IA}D_{IA} + CP2_{MN}D_{MN} + CP2_{MO}D_{MO}}$$

Equation 32

where P_2c = 0%-RAS-effect calibrated P_2,

$CP2_{IN}$, $CP2_{IA}$, $CP2_{MN}$, $CP2_{MO}$ = coefficient of the dummy variable D_{IN}, D_{IA}, D_{MN}, and D_{MO}

D_{IN}, D_{IA}, D_{MN}, D_{MO} = as previously defined.

Table 24: Regression Results of 0%-RAS-Effect for Hirsch 2006 Model

Parameter	Estimation	Standard Error	P-value
CEa_{IN}	0.090722	584201.6	1
CEa_{IA}	-0.05654	571286.4	1
CEa_{MN}	-0.10356	424926.4	1
CEa_{MO}	0.194212	276180.1	1
$CP0_{IN}$	249.0332	367.5947	0.4982
$CP0_{IA}$	-23.3469	272.2187	0.9317
$CP0_{MN}$	-3.91492	218.532	0.9857
$CP0_{MO}$	139.2855	240.595	0.5627
$CP1_{IN}$	0.012657	0.079471	0.8735
$CP1_{IA}$	0.100167	0.064257	0.1193
$CP1_{MN}$	0.133187	0.052335	0.0110
$CP1_{MO}$	0.074322	0.036013	0.0392
$CP2_{IN}$	69.14189	437.4	0.8744
$CP2_{IA}$	2063.315	1300.127	0.1127
$CP2_{MN}$	3078.152	1540.125	0.0458
$CP2_{MO}$	755.1289	396.8387	0.0573

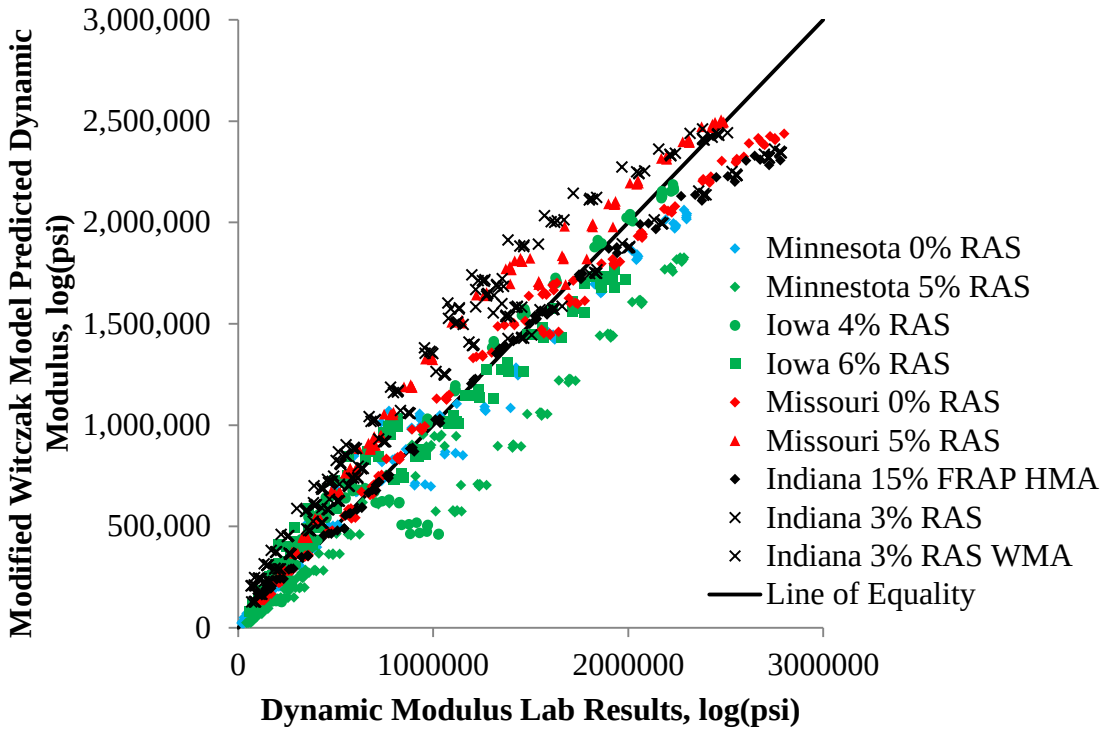

Figure 49: Lab Tested vs. Hirsch Predicted E* Values Calibrated for 0%-RAS-Effect

$$\mathbf{P_0' = P_0c + CP0_{3\%}D_{3\%} + CP0_{4\%}D_{4\%} + CP0_{5\%}D_{5\%} + CP0_{6\%}D_{6\%}}$$

Equation 33

where P_0c' = modified P_0,

$Eac' =$ modified Ea,

$D_{3\%}$ = 1 for mixes containing 3% RAS and 0 for others,

$D_{4\%}$ = 1 for mixes containing 4% RAS and 0 for others,

$D_{5\%}$ = 1 for mixes containing 5% RAS and 0 for others,

$D_{6\%}$ = 1 for mixes containing 6% RAS and 0 for others,

$CP0_{3\%}$, $CP0_{4\%}$, $CP0_{5\%}$, $CP0_{6\%}$ = coefficient of the dummy variable $D_{3\%}$, $D_{4\%}$, $D_{5\%}$, and $D_{6\%}$, and

P_0c as previously defined.

$$\mathbf{P_1c' = P_1c + CP1_{3\%}D_{3\%} + CP1_{4\%}D_{4\%} + CP1_{5\%}D_{5\%} + CP1_{6\%}D_{6\%}}$$

Equation 34

where P_1c = modified P_1,

$CP1_{3\%}$, $CP1_{4\%}$, $CP1_{5\%}$, $CP1_{6\%}$ = coefficient of the dummy variable $D_{3\%}$, $D_{4\%}$, $D_{5\%}$, and $D_{6\%}$, and

$D_{3\%}$, $D_{4\%}$, $D_{5\%}$, $D_{6\%}$, P_1c = as previously defined.

$$\mathbf{P_2c' = P_2c + CP2_{3\%}D_{3\%} + CP2_{4\%}D_{4\%} + CP2_{5\%}D_{5\%} + CP2_{6\%}D_{6\%}}$$

Equation 35

where P_2c = modified P_2,

$CP2_{3\%}$, $CP2_{4\%}$, $CP2_{5\%}$, $CP2_{6\%}$ = coefficient of the dummy variable $D_{3\%}$, $D_{4\%}$, $D_{5\%}$, and $D_{6\%}$, and

$D_{3\%}$, $D_{4\%}$, $D_{5\%}$, $D_{6\%}$, P_1c as previously defined.

$$\mathbf{Eac' = Eac + CEa_{3\%}D_{3\%} + CEa_{4\%}D_{4\%} + CEa_{5\%}D_{5\%} + CEa_{6\%}D_{6\%}}$$

Equation 36

where Eac' = modified Ea,

$CEa_{3\%}$, $CEa_{4\%}$, $CEa_{5\%}$, $CEa_{6\%}$ = coefficient of the dummy variable $D_{3\%}$, $D_{4\%}$, $D_{5\%}$, and $D_{6\%}$, and

$D_{3\%}$, $D_{4\%}$, $D_{5\%}$, $D_{6\%}$, Eac = as previously defined.

Table 25: Regression Results of RAS-Effect Calibration Parameters for Hirsch Model

Parameter	Estimation	Standard Error	P-value
$CEa_{3\%}$	0.852332	650984	1
$CEa_{4\%}$	0.298186	885596.7	1
$CEa_{5\%}$	0	356120.7	1
$CEa_{6\%}$	0.400577	1623160	1
$CP0_{3\%}$	-53.876	486.252	0.9118
$CP0_{4\%}$	0.73575	416.533	0.9986
$CP0_{5\%}$	659.784	364.327	0.0704

Table 25: Regression Results of RAS-Effect Calibration Parameters for Hirsch Model (Continued)

Parameter	Estimation	Standard Error	P-value
$CP0_{6\%}$	22.6821	589.209	0.9693
$CP1_{3\%}$	0.1109	0.09217	0.2291
$CP1_{4\%}$	0.02706	0.09873	0.7840
$CP1_{5\%}$	0.12435	0.05287	0.0188
$CP1_{6\%}$	0.01392	0.13396	0.9172
$CP2_{3\%}$	2324.44	1288.15	0.0714
$CP2_{4\%}$	910.952	2422.94	0.7070
$CP2_{5\%}$	5513.72	3011.19	0.0673
$CP2_{6\%}$	0.852332	650984	1

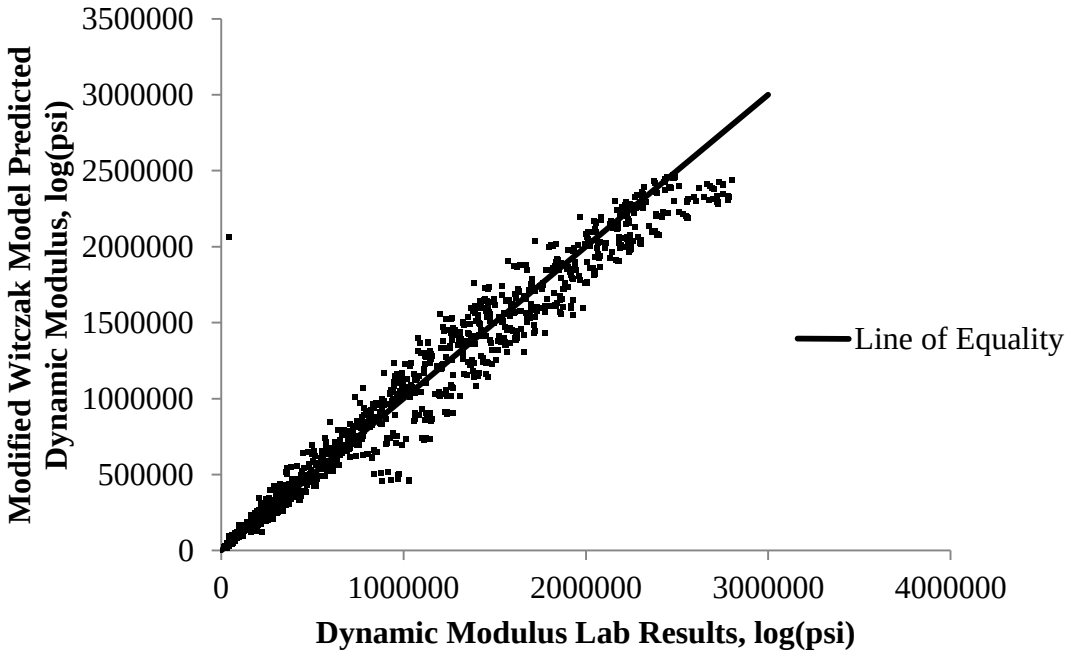

Figure 50: Lab Tested vs. Predicted E* Values of Modified Hirsch Model

The p-values of Ea coefficients in Table 25 that are equal to 1 indicating the all Ea coefficients are not significant factors. The estimations of coefficient values are very small compared to the value of Ea which is 4,200,000. Parameter Ea is the assumed aggregate modulus. The addition of shingles in HMA does not change the modulus of aggregate. There is only one p-

value in Table 25 that is less than 0.05 indicating that the coefficients to simulate the shingle effects are not significant factors. A RAS content which is smaller than 6% may not result in bias in the Hirsch prediction of E* values of RAS mixtures

MODIFIED MODEL EVALUATION

The aforementioned R^2 and Se/Sy values of the modified Witczak and Hirsch models indicate the three E* predictive models achieve excellent goodness-of-fit for this database containing 1701 data points. This section discusses the prediction efficiencies of modified Witczak and Hirsch models in terms of model accuracy and reliability. Dynamic modulus master curves and the plots of laboratory versus predicted E* are constructed to evaluate the model accuracy. Statistics of the dummy variable coefficients are analyzed to discuss the reliability of each parameter estimation and the correlations of parameters.

Model Efficiency Evaluation

Laboratory dynamic modulus values are tested at different temperatures and frequencies. In this section, the accuracies of modified Witczak and Hirsch models are evaluated at the corresponding temperatures and frequencies. Dynamic modulus master curves are often used to simulate HMA E* behavior over a wide range of temperatures. Therefore, master curves are used to discuss the model accuracies at different temperatures. The lab vs. predictve plots are developed at each loading frequency to evaluate the model accuracies at different frequencies.

Witczak Model

Dynamic modulus master curves are constructed for mixes containing shingles in order to evaluate the prediction accuracy of the modified Witczak models. A typical E* master curve has three components: upper tail, lower tail, and linear range. At the two tails of the curve, E* values are approaching a constant simulating extreme climate and traffic loading. The upper tail simulates HMA behavior under a fast moving traffic in a very cold winter day. The lower tail simulates the opposite situation. The accuracies of the model predicted master curve on the upper and lower tails are related to the accuracies of predicting HMA permanent deformation and thermal cracking, respectively. In between of the two tails, the slope of the master curve approaches a constant. The E* is changing with a constant rate on log to log scale. The accuracy of this range is related to the prediction accuracy of asphalt fatigue cracking. The original and modified 2006 and 1999 Witczak master curves in Figure 51 to Figure 59 conform very closely

to the lab master curves at the upper tail. The differences between the upper tails of the original and modified 1999 Witczak models and the modified 2006 Witczak Model are very small. The original 2006 Witczak Model tends to overestimate E* values at every range. The master curves of the 1999 Witczak Models are closer to the lab master curves than the 2006 Witczak models. Compared to the original Witczak models, the accuracies of modified models are increased at the upper tail and the linear range. However, Figure 51 to Figure 59 show low model accuracies on the lower tail. On the lower tail, the modified 1999 Witczak Model achieves better match with the lab curve for mix BC25, 26, 32, and 33. For the 2006 Witczak Model, the modified model has increased accuracy on the lower tail for mix BC29, 30, 32, and 33. For other mixes, modifications of original models do not increase the model accuracies. It should be noticed that E* values at the lower tail is very small. Small differences in two sets of E* values can cause significant difference in the lower tails of the developed master curves. In testing E* at high temperatures, the variability in test results is large and causes the inaccurate prediction of E* at lower tail of master curve.

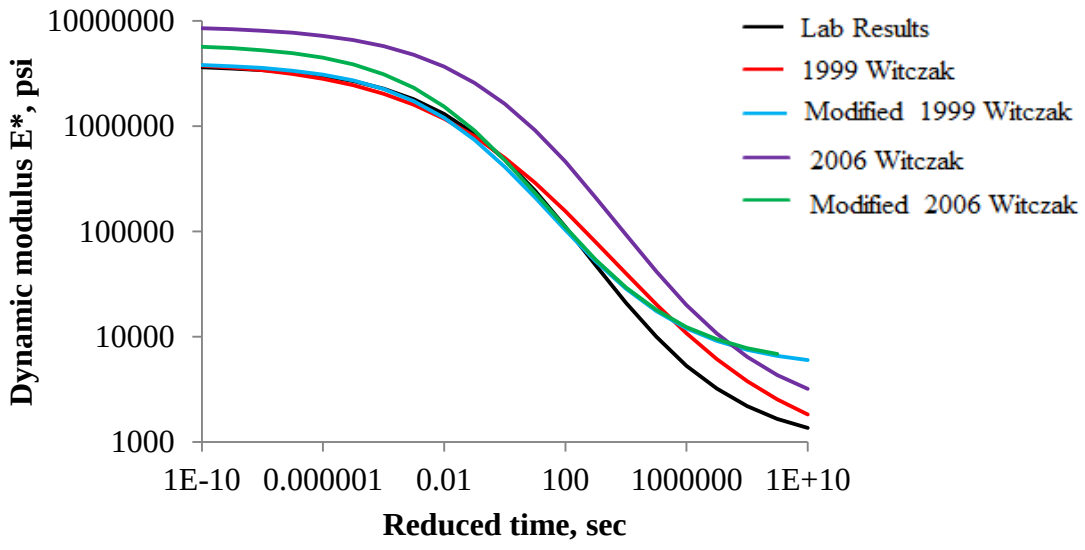

Figure 51: Witczak Model Master Curves for Minnesota Mfr. RAS Mix (Mix BC21)

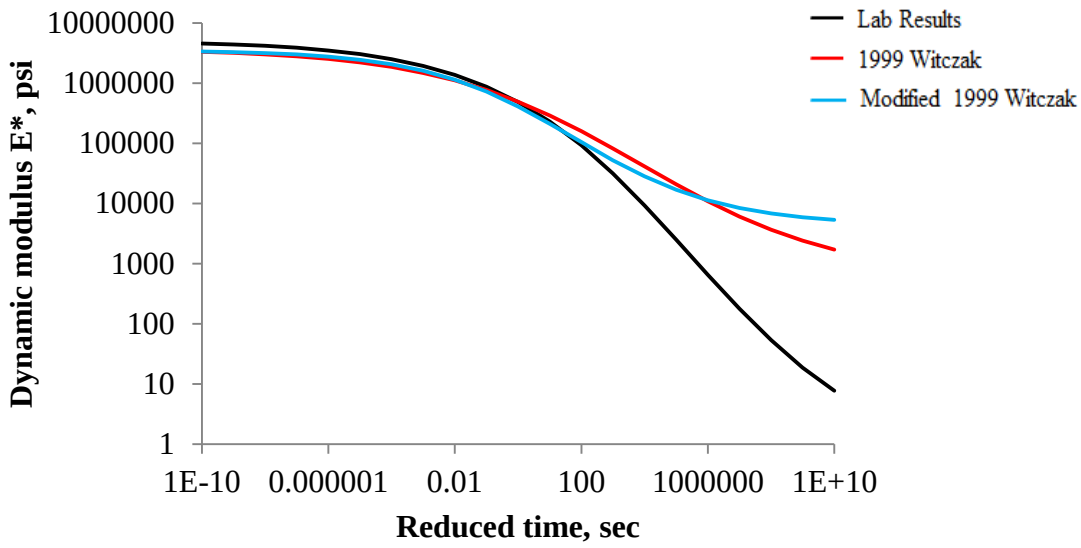

Figure 52: Witczak Model Master Curves for Minnesota Tear-off RAS Mix (Mix BC22)

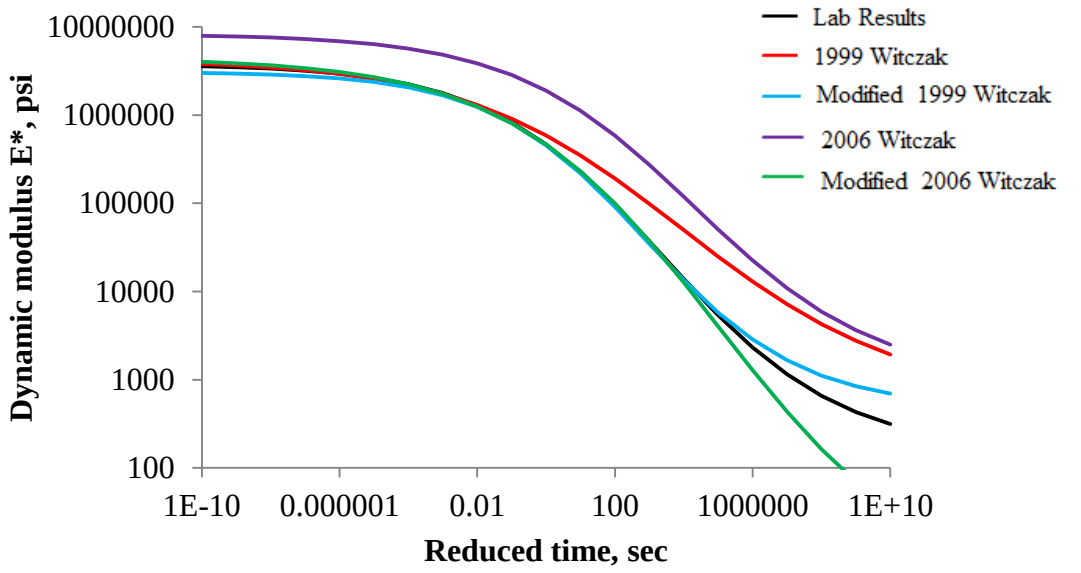

Figure 53: Witczak Model Master Curves for Iowa 4% RAS Mix (Mix BC25)

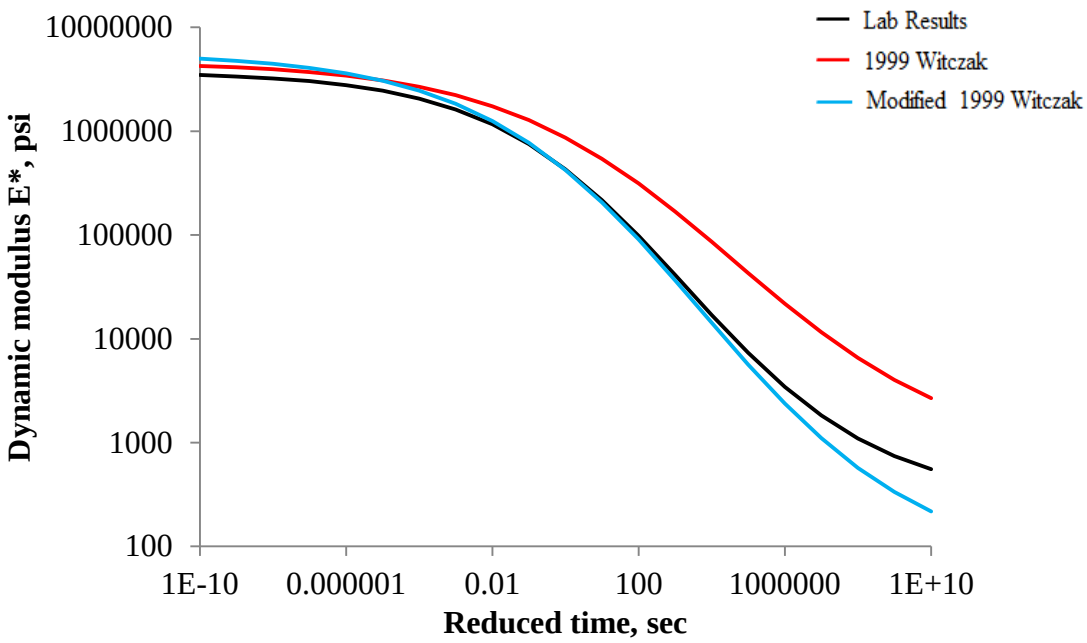

Figure 54: Witczak Model Master Curves for Iowa 5% RAS Mix (Mix BC26)

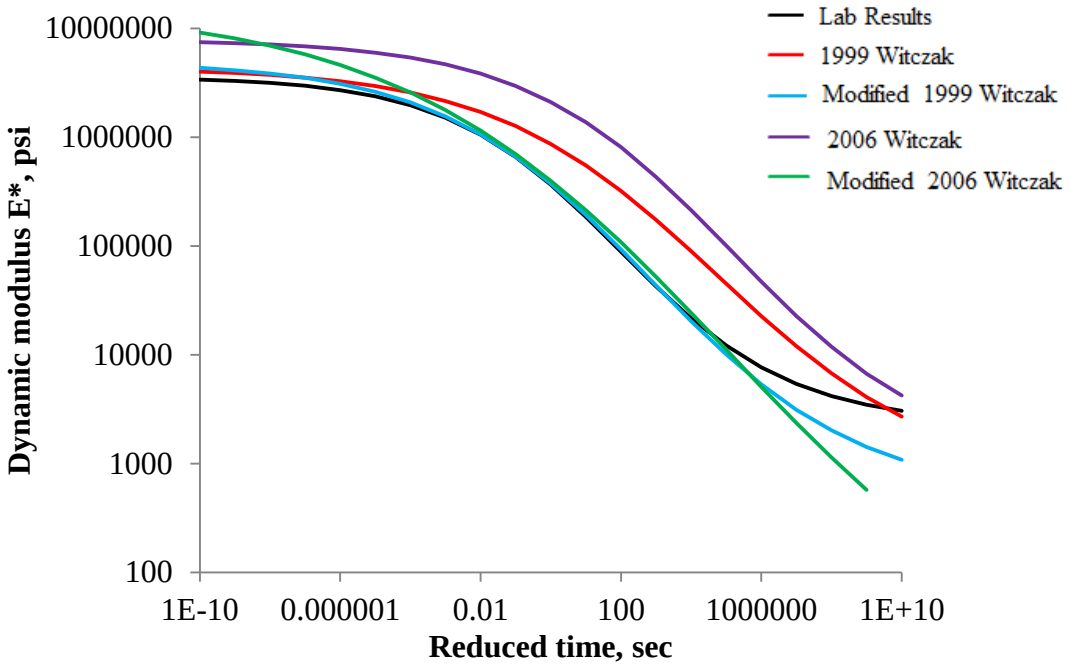

Figure 55: Witczak Model Master Curves for Iowa 6% RAS Mix (Mix BC27)

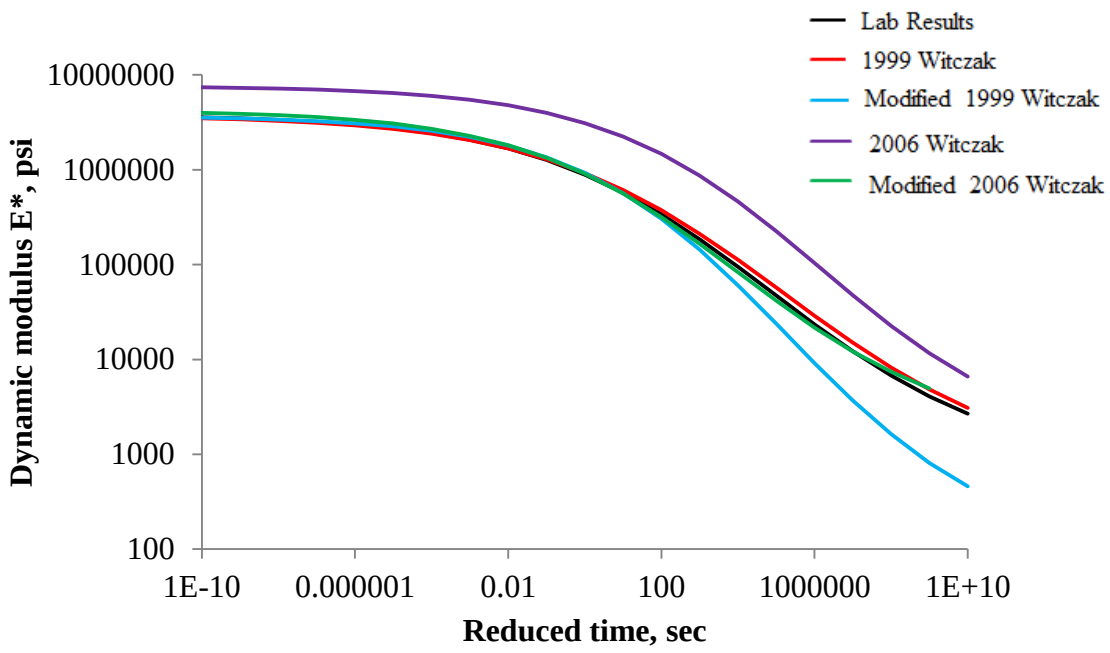

Figure 56: Witczak Model Master Curves for Missouri 5% Fine RAS Mix (Mix BC29)

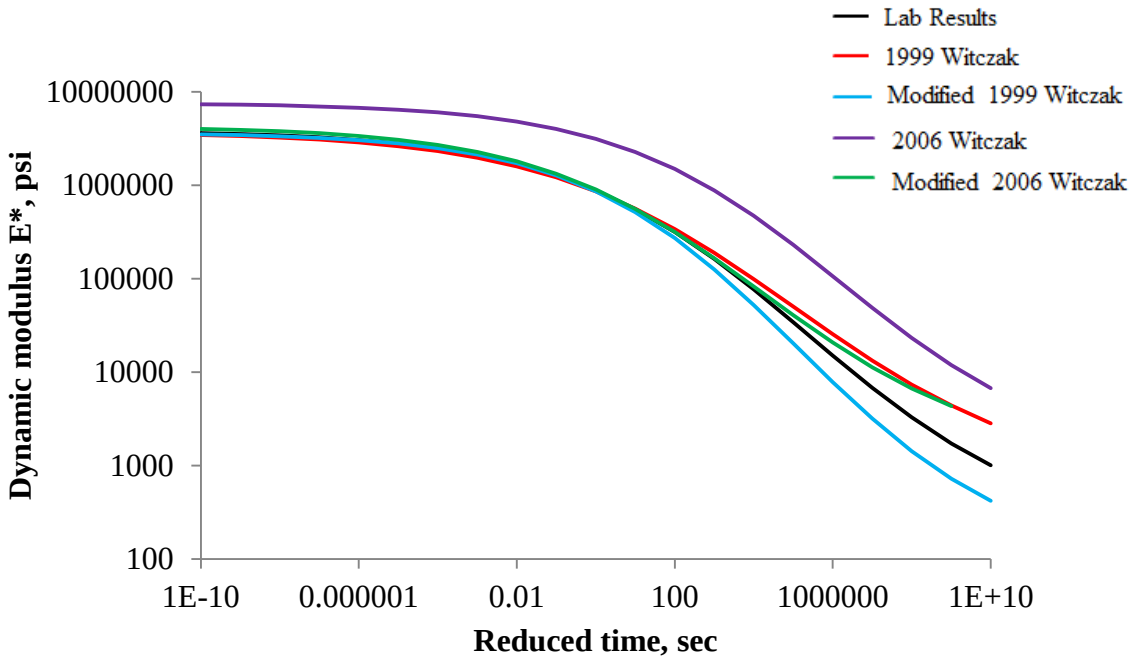

Figure 57: Witczak Model Master Curves for Missouri 5% Coarse RAS Mix (Mix BC30)

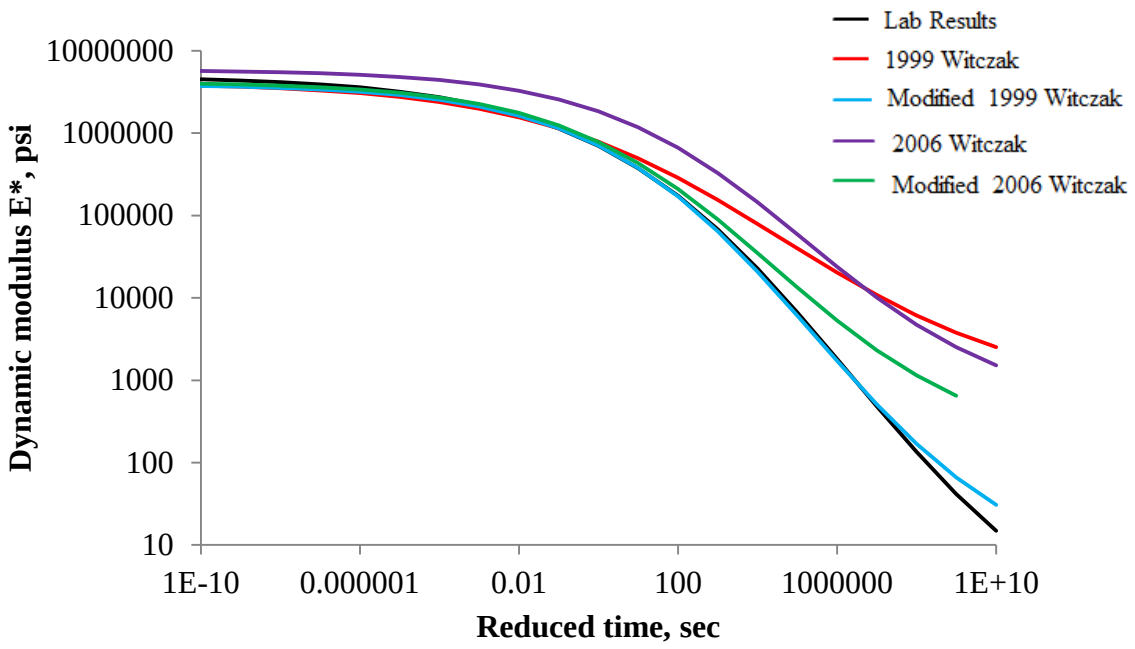

Figure 58: Witczak Model Master Curves for Indiana 3% RAS&HMA Mix (Mix BC32)

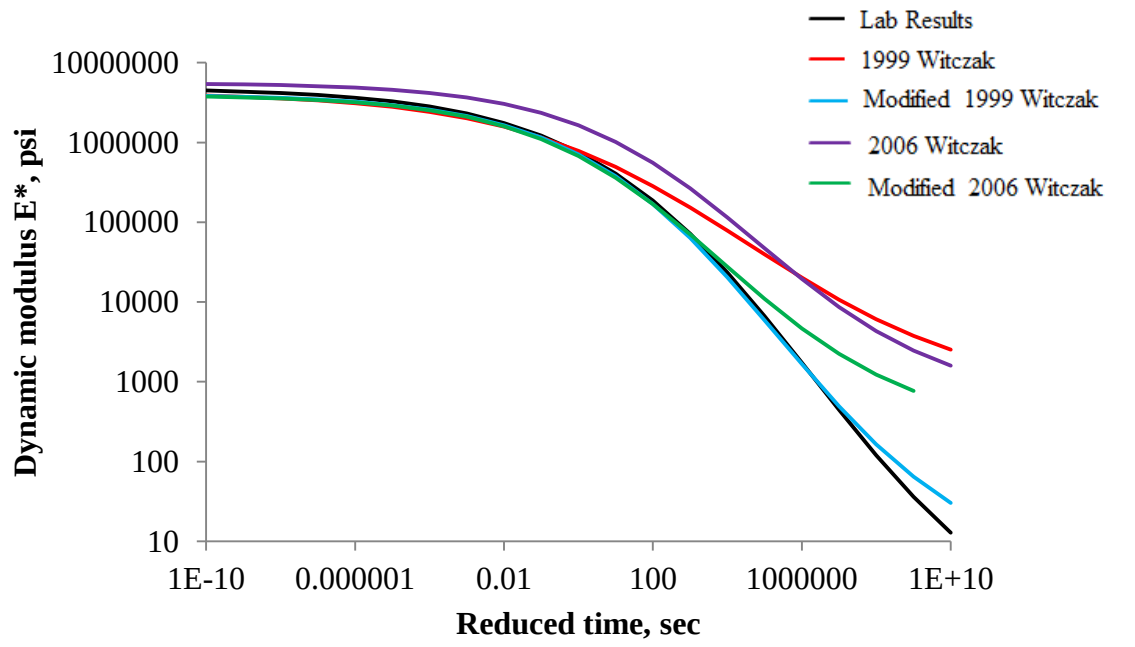

Figure 59: Witczak Model Master Curves for Indiana 3% RAS&WMA Mix (Mix BC33)

Figur includes nine individual plots of the tested results vs. the 1999 Witczak predictions of E* for the nine loading frequencies in laboratory testing. The data are plotted on a normal scale. The variability in predicting E* increases as the predicted E* increases. The scatters for the modified 1999 Witczak Model are closely distributed along the line of equality. The spreads of scatters for the original 1999 Witczak Model are wider indicating the variability in prediction accuracy for the original model is larger than that for the modified model. The linear trend lines of the original model predictions has a slope greater than 1 showing that the original model tends to overestimate the E* value. There effects of different frequencies on the prediction accuracies are not be able to visually identify from the plots in Figur.

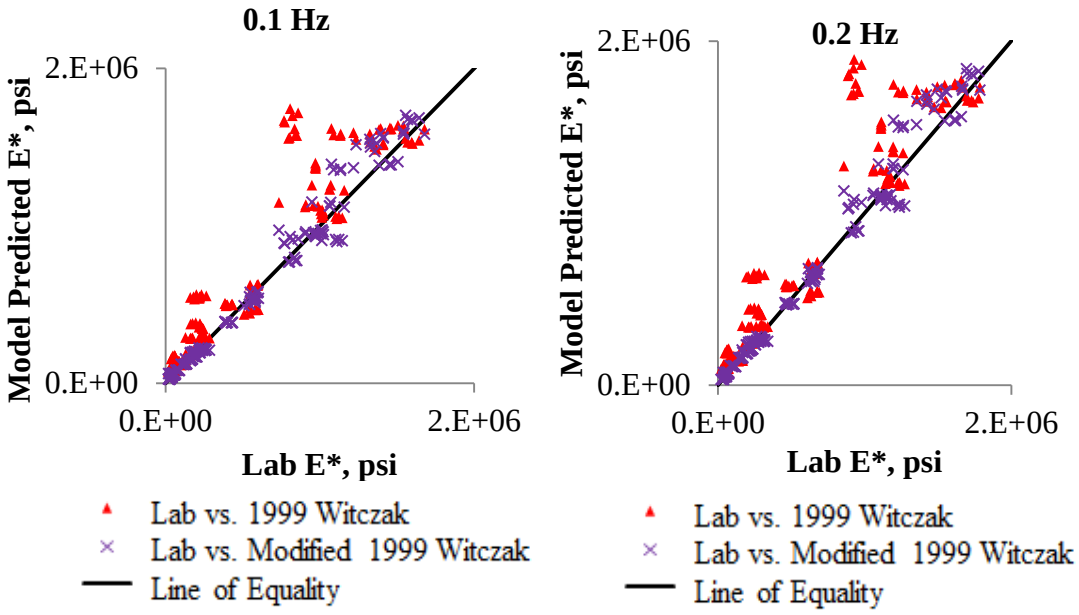

Figure 60: Lab E* vs. Predicted E* of Witczak 1999 Model

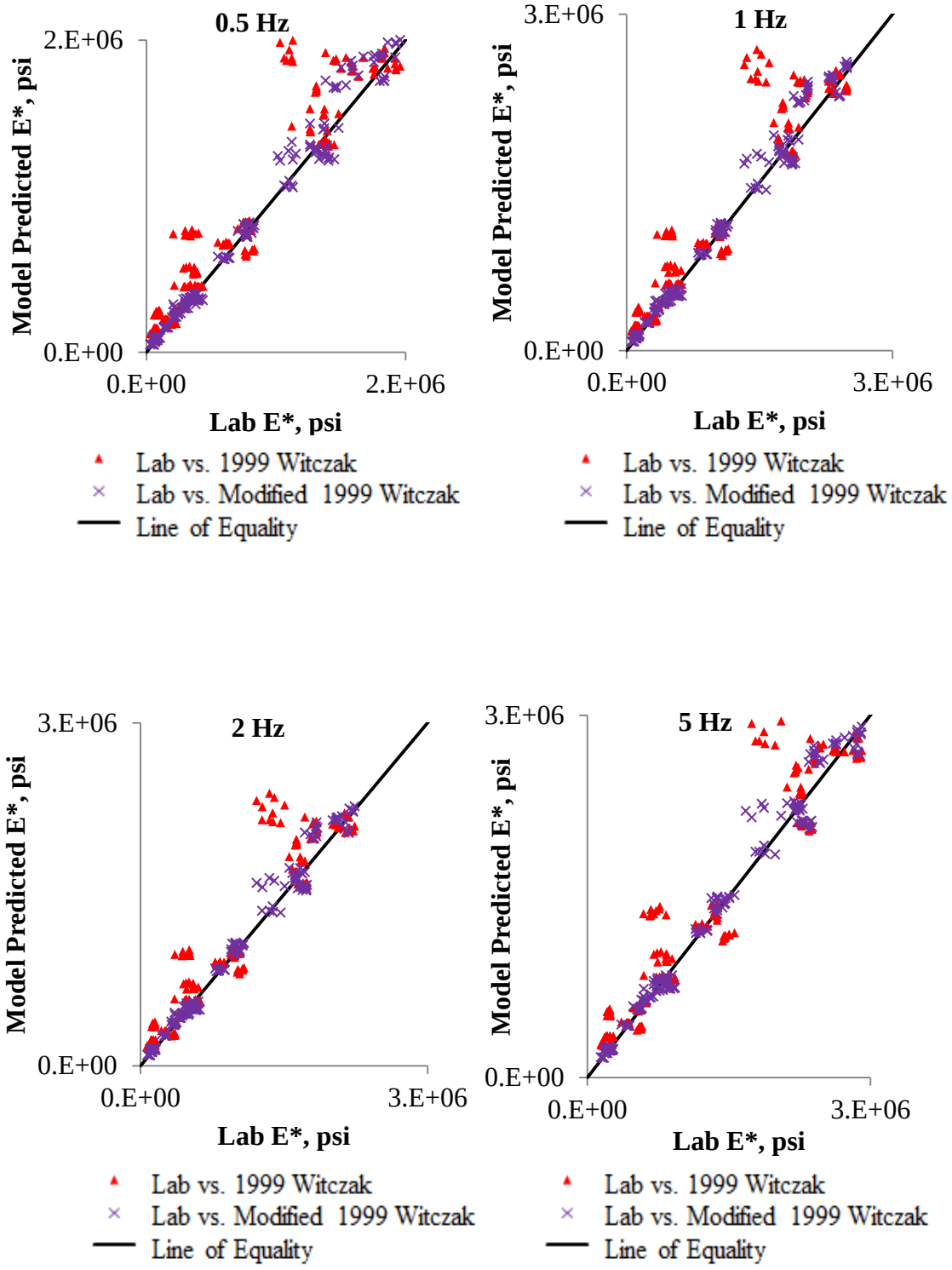

Figure 60: Lab E* vs. Predicted E* of Witczak 1999 Model (Continued)

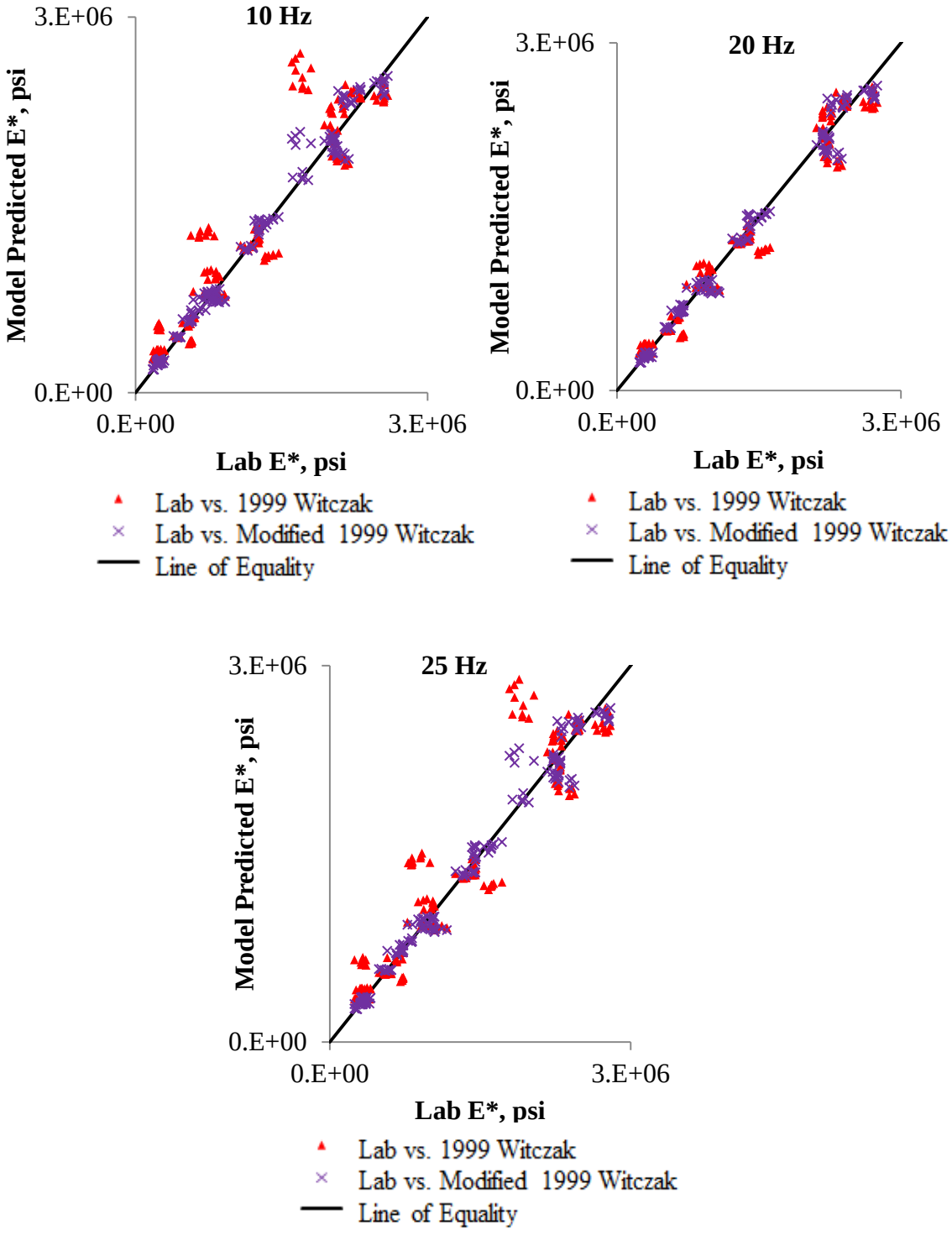

Figure 60: Lab E* vs. Predicted E* of Witczak 1999 Model (Continued)

The lab vs. prediction plots are prepared for the 2006 Witczak Model in Figure 61. The data are plotted on a normal scale. The variability in predicting E* increases as the predicted E*

increases. The original model obtains heavily biased E* values with large variability. Compared to the original model, the modified model has higher accuracy and precision. There effects of different frequencies on the prediction accuracies are not be able to visually identify from the plots in Figure 61.

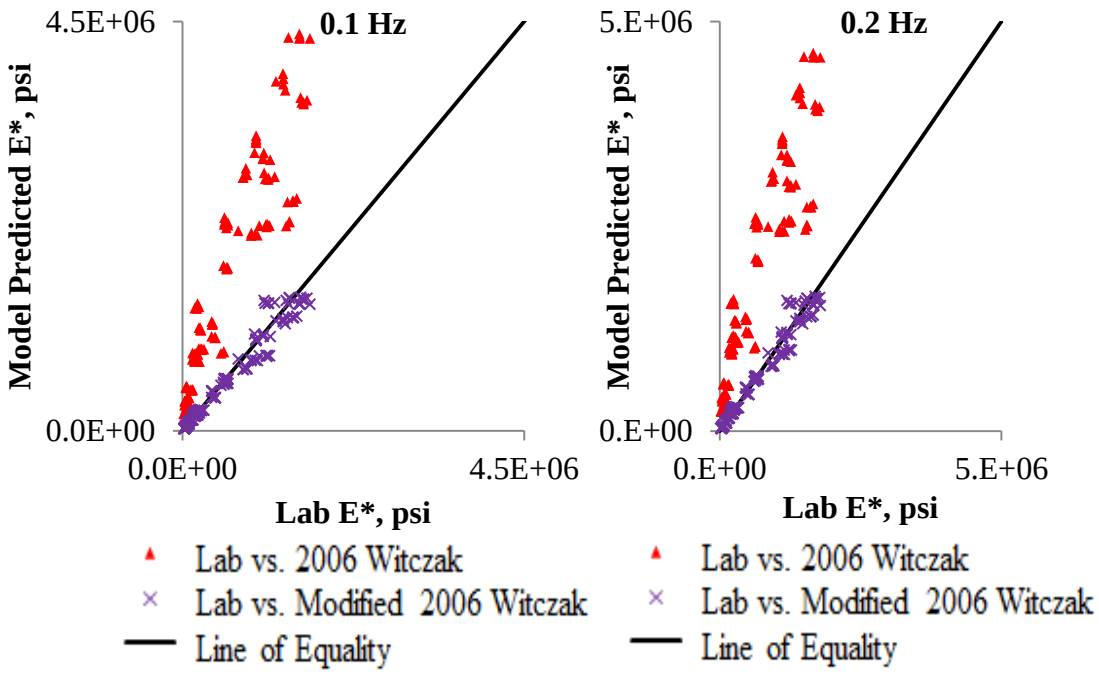

Figure 61: Lab E* vs. Predicted E* of Witczak 2006 Model

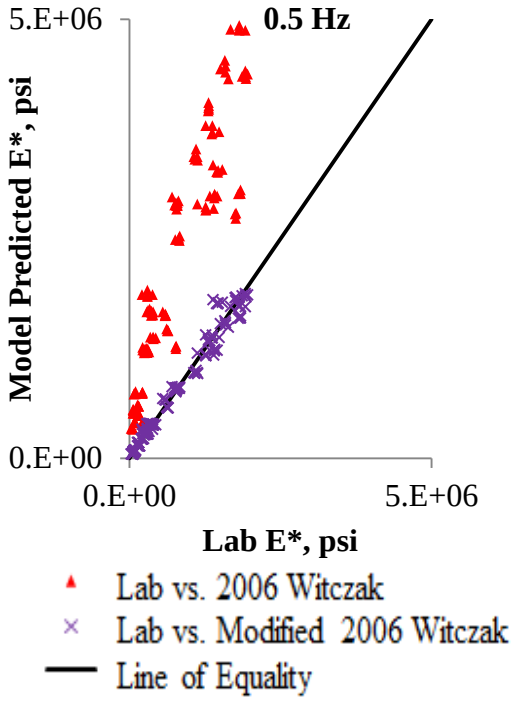

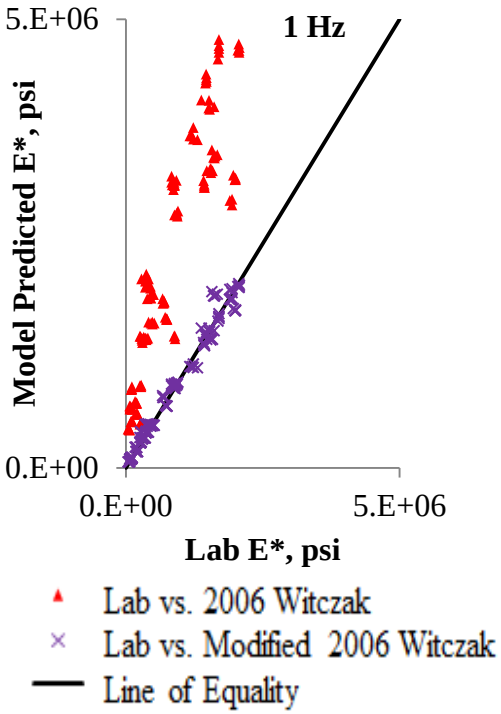

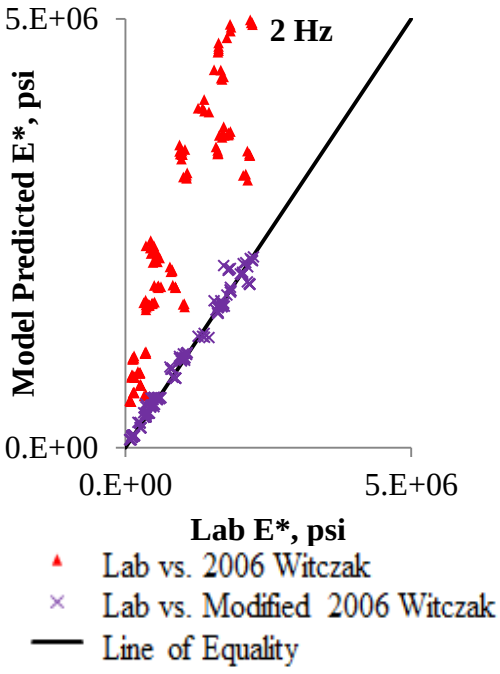

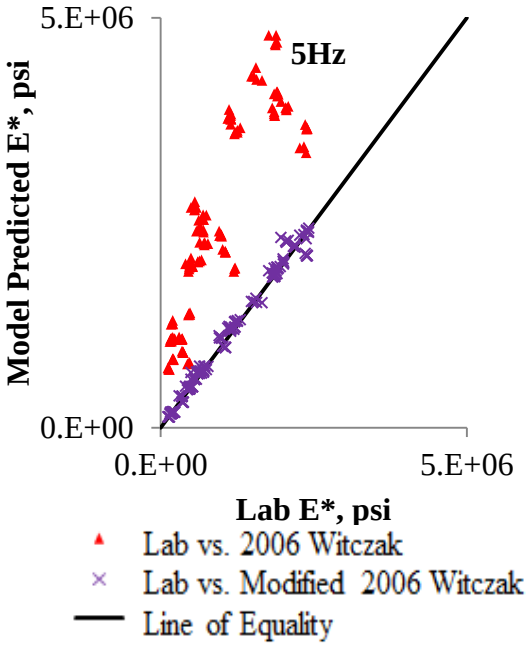

Figure 61: Lab E* vs. Predicted E* of Witczak 2006 Model (Continued)

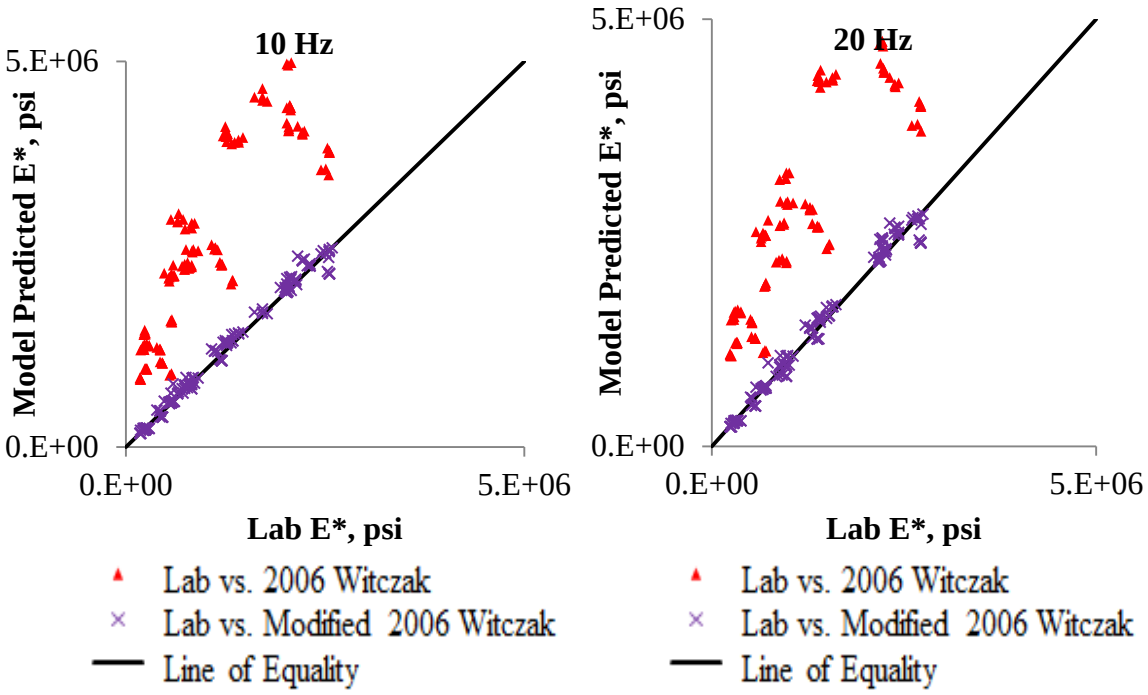

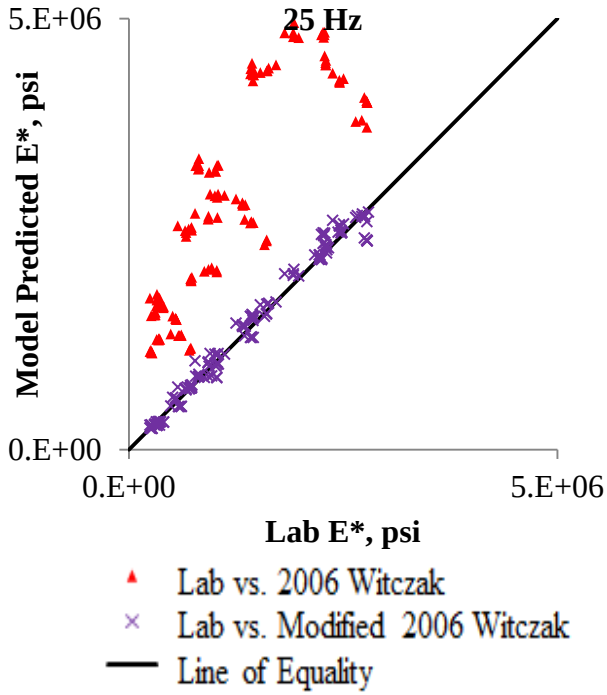

Table 61: Lab E* vs. Predicted E* of Witczak 2006 Model (Continued)

The R^2 values in Table 26 provide numerical evaluation of the model accuracies at each frequency level. Negative R^2 value means the differences between predicted and tested E* values are larger than the variability of the lab E*, which indicates the model is significantly biased. Therefore, the original 2006 Witczak Model has significantly biased predictions of E*. The R^2 for the original 1999 Witczak Model tends to be increased when the frequency increases. Calibration of the original Witczak models significantly improves predicting accuracy and precision. The R^2 values for the modified Witczak model are greater than 0.95 at every frequency level.

Table 26: Coefficient of Determination of the Witczak Models

Frequency	R^2 Values			
	Witczak 1999	**Modified Witczak 1999**	**Witczak 2006**	**Modified Witczak 2006**
0.1	0.78	0.97	*[7]	0.96
0.2	0.77	0.98	*	0.97
0.5	0.8	0.98	*	0.98
1	0.83	0.98	*	0.98
2	0.84	0.98	*	0.95
5	0.86	0.98	*	0.99
10	0.87	0.98	*	0.99
20	0.96	0.98	*	0.98
25	0.88	0.98	*	0.98

Hirsch Model

The upper tails of the Hirsch model master curves in Figure 62 to Figure 68 conforms very closely to the lab master curves. At the linear range, the original Hirsch model tends to overestimate E* values. The modified Hirsch model achieves improved accuracy for mix BC21, 25, 29, 30, 32, and 33. At the lower tail, the original Hirsch model has overwhelming biased predictions which can be more than 1000 times the E* values estimated from lab master curves. The modified Hirsch Model has more accurate predictions at the lower tail for mix BC25. For other mixes, the prediction accuracy of the modified Hirsch Model is equal to, or lower than that of the original model.

[7] * represents a very low coefficient of determination that the model becomes extremely unreliable.

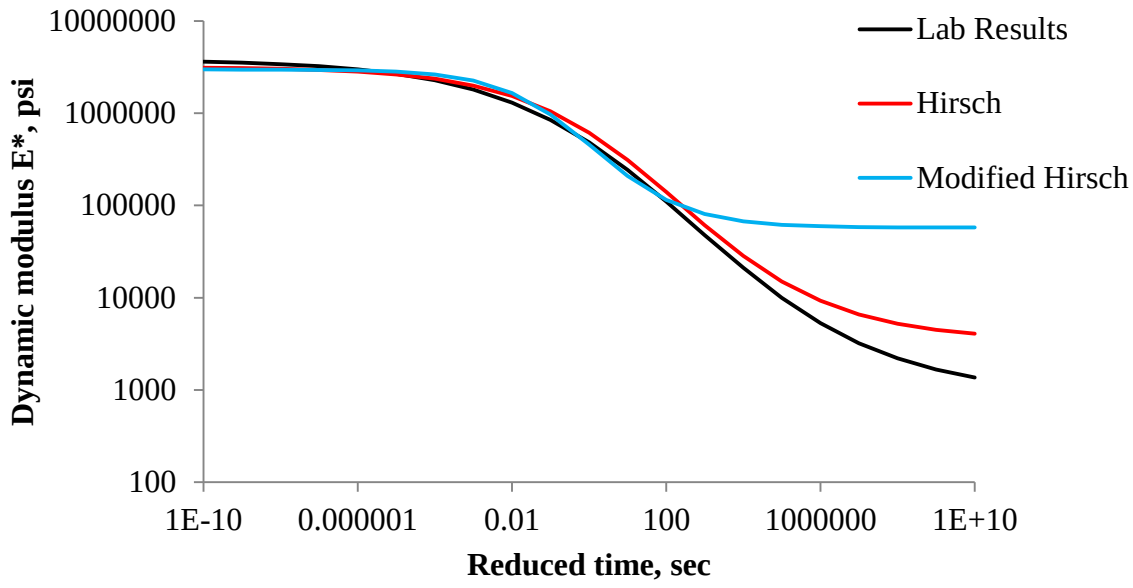

Figure 62: Hirsch Model Master Curves for Mix BC21

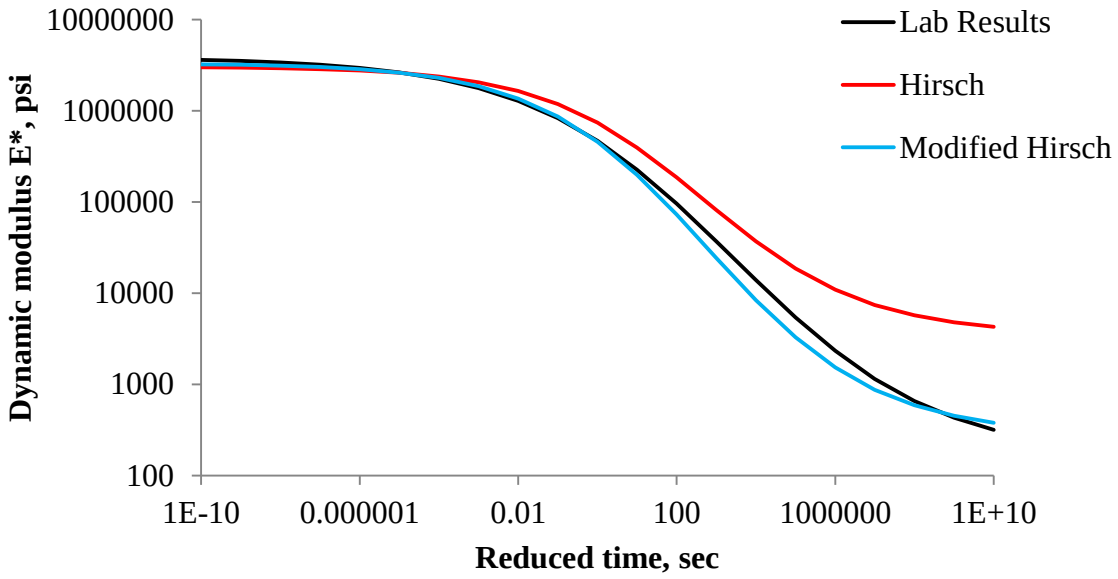

Figure 63: Hirsch Model Master Curves for Mix BC25

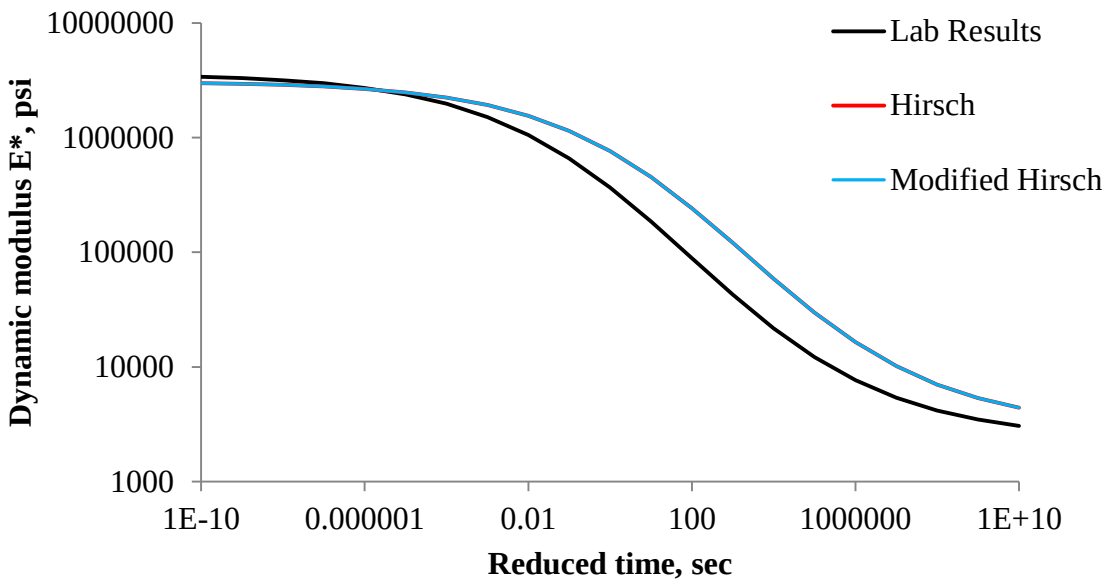

Figure 64: Hirsch Model Master Curves for Mix BC27

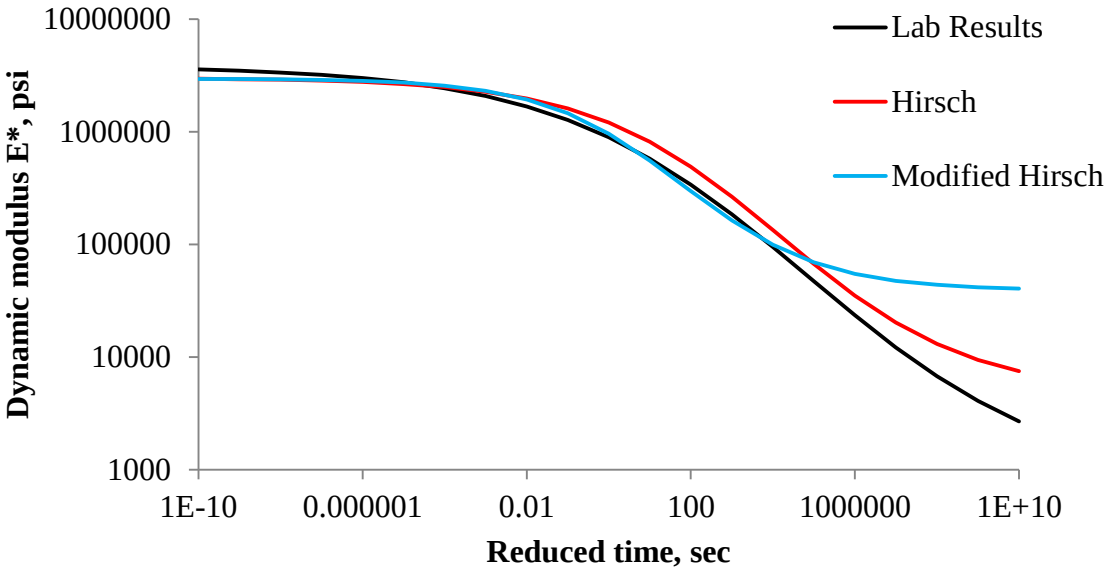

Figure 65: Hirsch Model Master Curves for Mix BC29

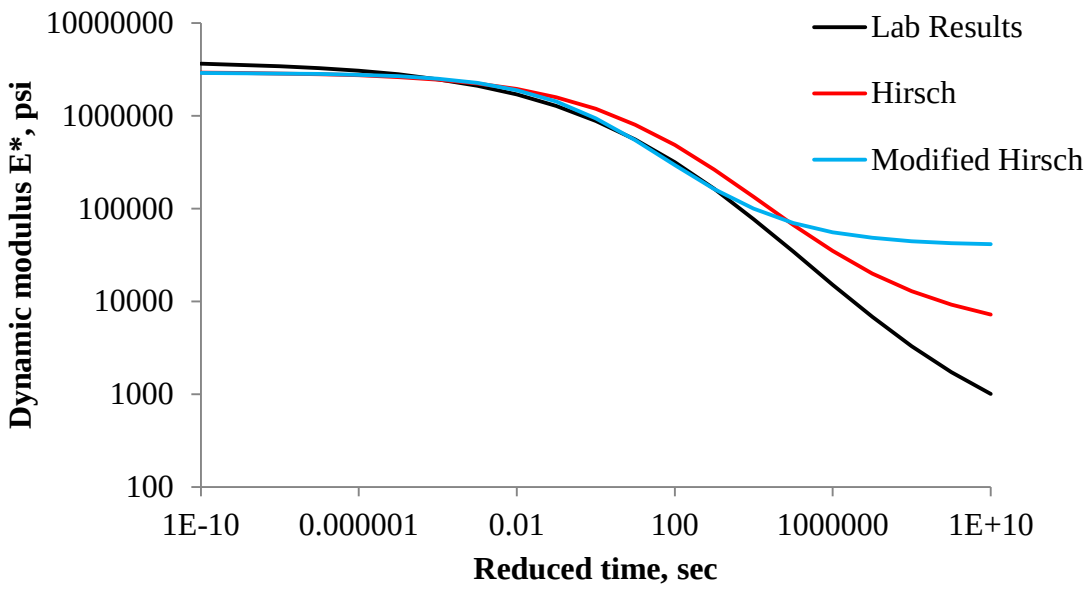

Figure 66: Hirsch Model Master Curves for Mix BC30

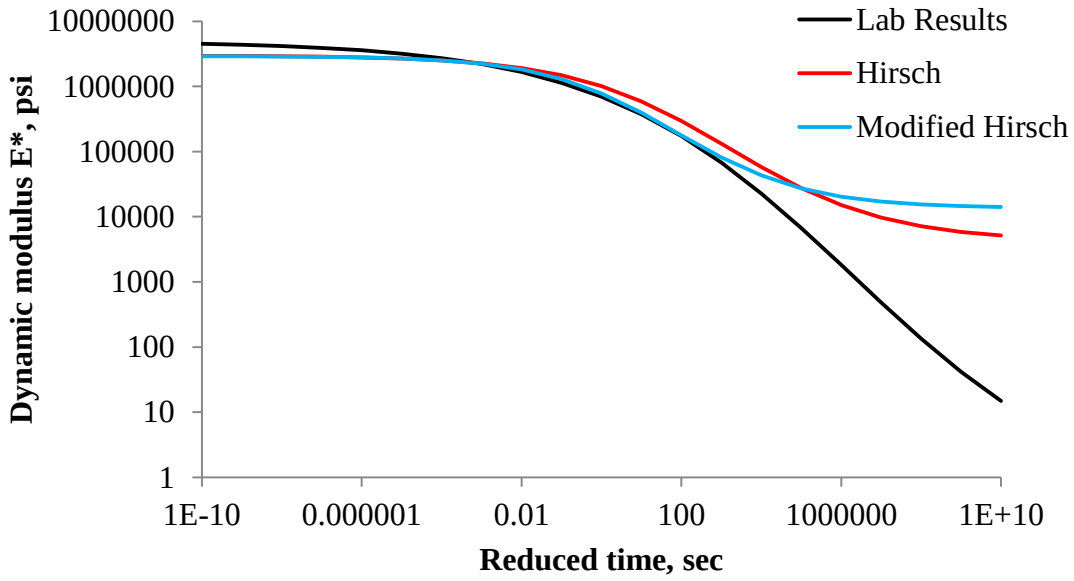

Figure 67: Hirsch Model Master Curves for Mix BC32

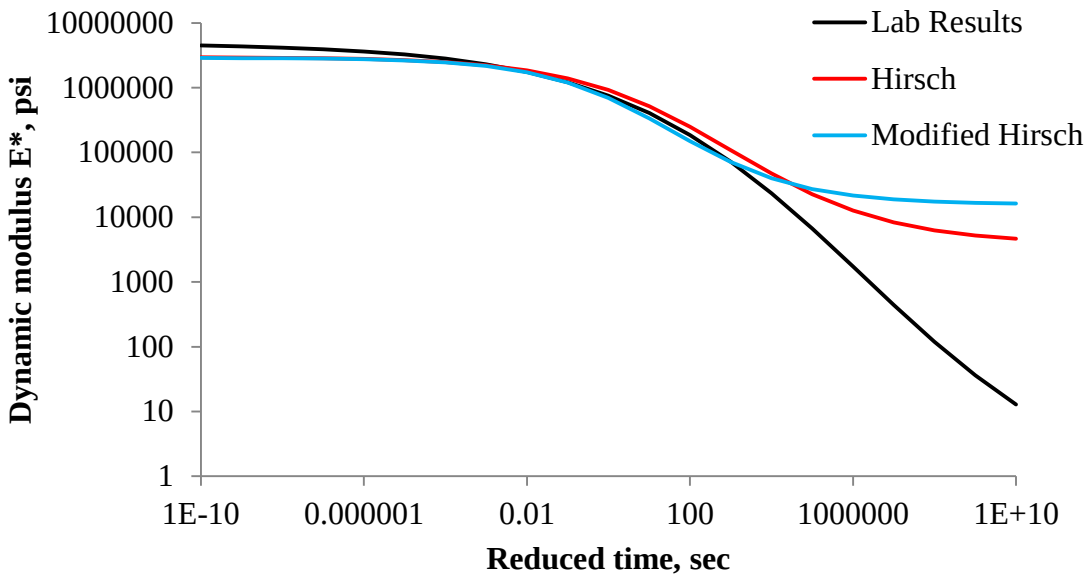

Figure 68: Hirsch Model Master Curves for Mix BC33

Hirsch model lab-prediction plots are prepared in Figure 69. The plots show accurate prediction for the Hirsch model. Data for both original and modified models closely confirm the line of equality indicating the bias of predicted E* is small. The modification does not significantly improve the accuracy of the Hirsch model. R^2 values in Table 27 indicate that the modified Hirsch model has slightly higher coefficient of determination. The improvement in prediction accuracy is primarily from the calibration of the project effects. The influence of loading frequency on model prediction accuracy and precision is not being able to visually identify from Figure 69.

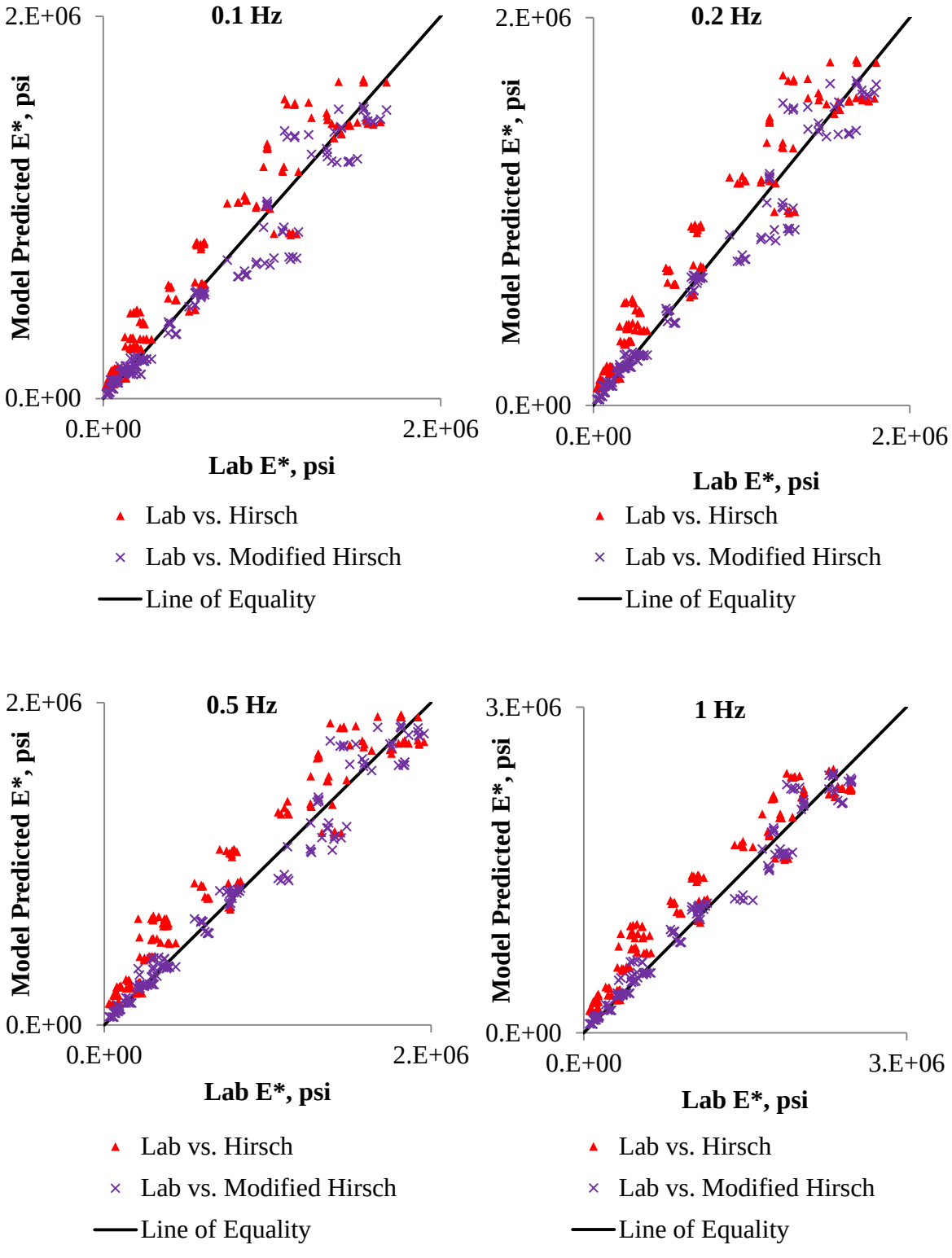

Figure 69: Lab E* vs. Predicted E* of Hirsch Model

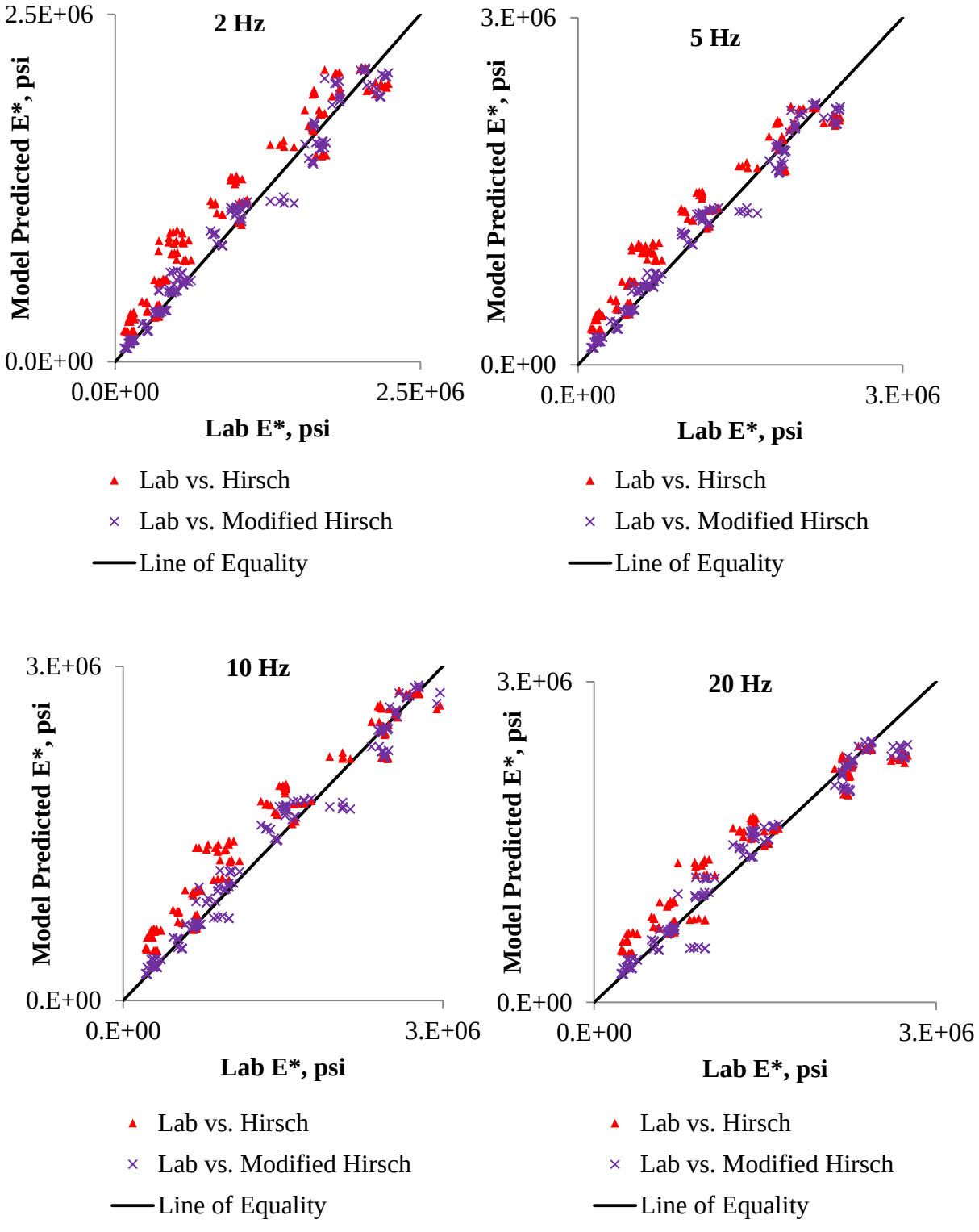

Figure 69: Lab E* vs. Predicted E* of Hirsch Model (Continued)

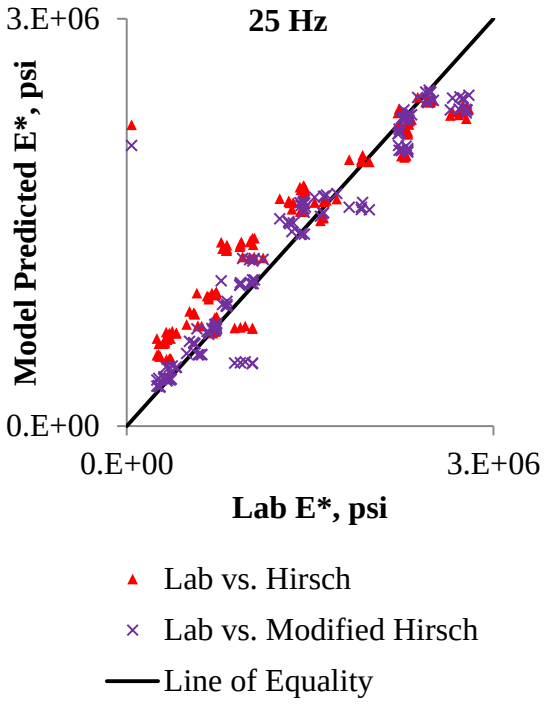

Figure 69: Lab E* vs. Predicted E* of Hirsch Model (Continued)

Table 27: Coefficient of Determination of the Hirsch Model

Frequency	R2 Values	
	Hirsch	Modified Hirsch
0.1	0.89	0.95
0.2	0.89	0.96
0.5	0.89	0.97
1	0.89	0.97
2	0.89	0.98
5	0.9	0.98
10	0.9	0.97
20	0.91	0.96
25	0.85	0.91

Parameter Evaluation of Models

Witczak 1999 Model

Figure 70 indicates that an increased δ in the 1999 Witczak Model needs to be used to predict E* when more than 4% RAS is added to HMA. The δ calibration coefficients are positive for 4%,

5%, and 6% RAS contents. The δ calibration coefficient for RAS content of 3% is negative. However, the standard error for 3% RAS is large indicating 3% RAS content may not change the δ parameter in the predictive equation. Figure 42 indicates that a decreased α in the 1999 Witczak Model needs to be used to predict E* when more than 4% RAS is added to HMA. Negative α calibration coefficients are obtained for 4%, 5%, and 6% RAS contents. The α calibration coefficient for RAS content of 3% is positive. However, the standard error for 3% RAS is large indicating 3% RAS content may not change the α parameter in the predictive equation. Figure 43 shows the b parameter in the 1999 Witczak Model needs to be increased to predict E* when more than 4% RAS is added to HMA. Positive b calibration coefficients are obtained for 4%, 5%, and 6% RAS contents. The b calibration coefficient for RAS content of 3% is negative. However, the standard error for 3% RAS is large indicating 3% RAS content may not change the b parameter in the predictive equation. The g_1 and g_2 calibration coefficients in Figure 44 for 3%, 5%, and 6% RAS contents are positive. The g_1 and g_2 calibration coefficients for 4% RAS are negative. The standard errors of g_1 and g_2 calibration coefficient for 3% and 6% RAS contents are large. The effects of 3% and 6% RAS contents on g_1 and g_2 parameters are not able to be identified. Therefore, the addition of shingles in HMA results in increased δ and decreased α parameters. The effects on the g_1 and g_2 parameters are not significant. Modification of the 1999 Witczak Model is recommended when a 4% or more RAS content is used.

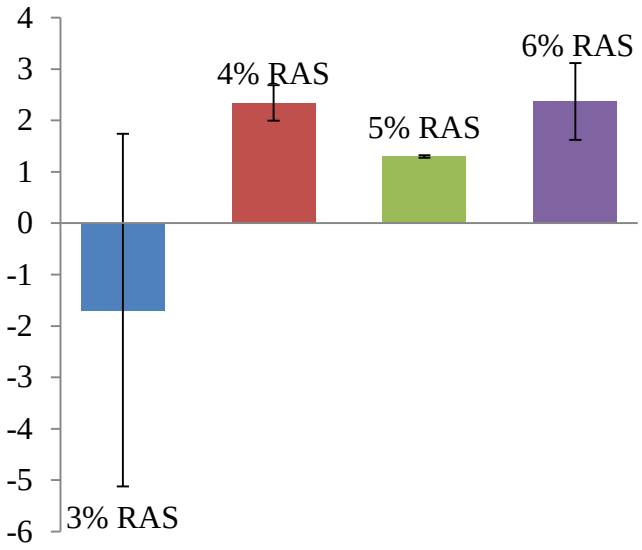

Figure 70: δ Calibration Coefficient for the 1999 Witczak Model

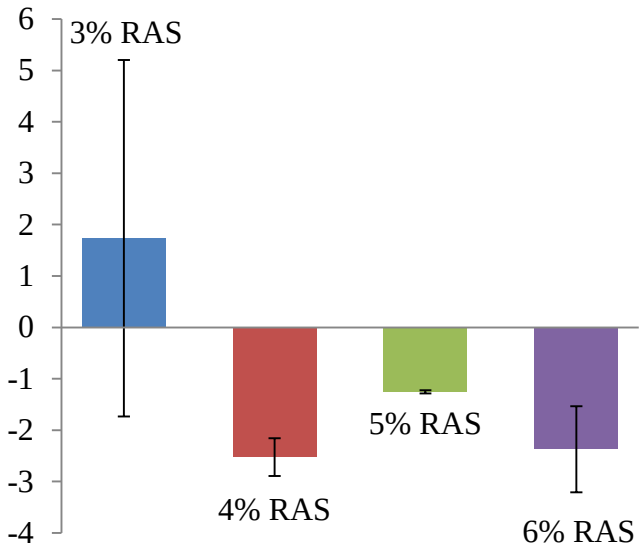

Figure 71: α Calibration Coefficient for the 1999 Witczak Model

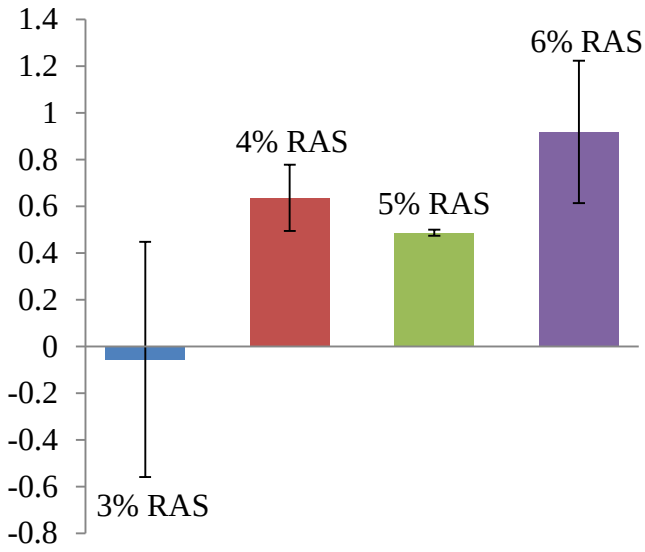

Figure 72: b Calibration Coefficient for the 1999 Witczak Model

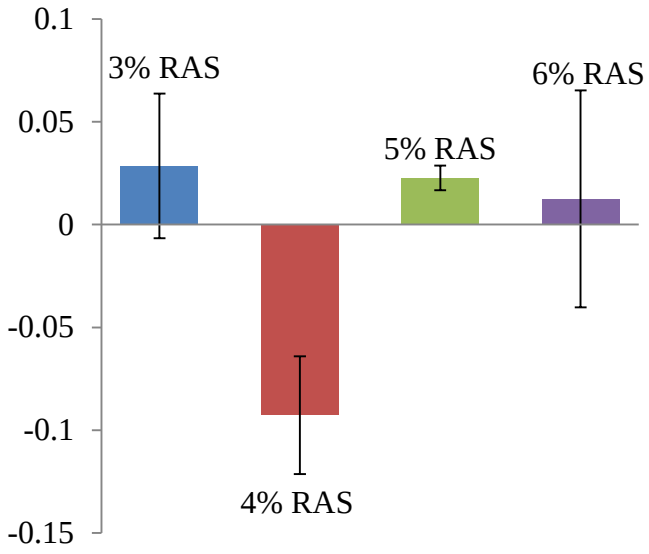

Figure 73: g_1 Calibration Coefficient for the 1999 Witczak Model

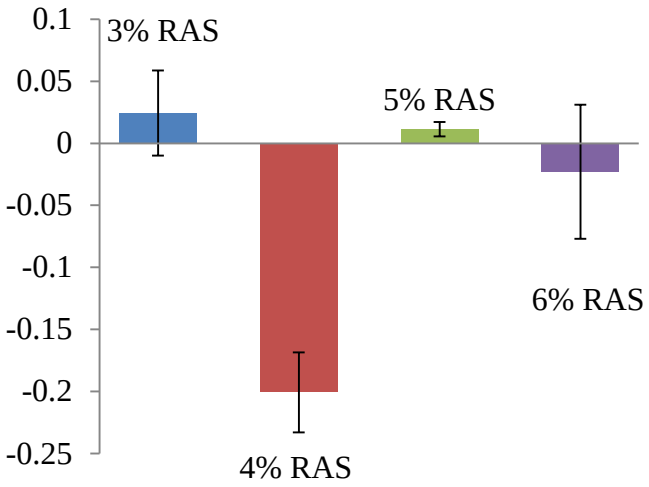

Figure 74: g_2 Calibration Coefficient for the 1999 Witczak Model

Table 28 shows the correlations between the calibration coefficients. The correlation between two coefficients is represented by a number ranging from -1 to 1. The absolute value of the correlation ratio represents the degree of the correlation. An absolute value of 1 means the correlation between two coefficients is perfectly linear; and a value of 0 means the two coefficients are independent. A positive number indicates one coefficient increases when the

other coefficient is increased; and a negative number indicates the opposite. The correlation ratios for coefficients of different RAS contents in Figure 46 are equal to zero indicating the calibration coefficients of different RAS contents are independent. Strong correlations are found within coefficients at each RAS content level. High correlation ratios of the δ and α coefficients indicate that δ and α are linearly correlated. The b, g_1, and g_2 coefficients for 3%, 4%, and 6% RAS have approximately perfectly linear correlations with absolute values of correlation ratios greater than 0.95. For 5% RAS, the coefficients are still correlated with a much lower correlation ratio. The chart also indicates that increase of δ will result in decreases of α, g_1, and g_2 and increase of b. An increase of α causes decreases of b and increases of g_1 and g_2. An increase of b will cause decreases of g_1 and g_2. An increased g_1 will cause an increased g_2.

Table 28: Coefficient Correlation Chart for the 1999 Witczak Model

	$C\delta_{3\%}$	$C\delta_{4\%}$	$C\delta_{5\%}$	$C\delta_{6\%}$	$C\alpha_{3\%}$	$C\alpha_{4\%}$	$C\alpha_{5\%}$	$C\alpha_{6\%}$	$Cb_{3\%}$	$Cb_{4\%}$	$Cb_{5\%}$	$Cb_{6\%}$	$Cg1_{3\%}$	$Cg1_{4\%}$	$Cg1_{5\%}$	$Cg1_{6\%}$	$Cg2_{3\%}$	$Cg2_{4\%}$	$Cg2_{5\%}$	$Cg2_{6\%}$
$C\delta_{3\%}$	1.00	0.00	0.00	0.00	-1.00	0.00	0.00	0.00	1.00	0.00	0.00	0.00	-0.99	0.00	0.00	0.00	-0.98	0.00	0.00	0.00
$C\delta_{4\%}$		1.00	0.00	0.00	0.00	-1.00	0.00	0.00	0.00	1.00	0.00	0.00	0.00	-0.97	0.00	0.00	0.00	-0.96	0.00	0.00
$C\delta_{5\%}$			1.00	0.00	0.00	0.00	-0.95	0.00	0.00	0.00	0.81	0.00	0.00	0.00	-0.36	0.00	0.00	0.00	-0.55	0.00
$C\delta_{6\%}$				1.00	0.00	0.00	0.00	-1.00	0.00	0.00	0.00	1.00	0.00	0.00	0.00	-0.98	0.00	0.00	0.00	-0.98
$C\alpha_{3\%}$					1.00	0.00	0.00	0.00	-1.00	0.00	0.00	0.00	0.99	0.00	0.00	0.00	0.98	0.00	0.00	0.00
$C\alpha_{4\%}$						1.00	0.00	0.00	0.00	-1.00	0.00	0.00	0.00	0.97	0.00	0.00	0.00	0.97	0.00	0.00
$C\alpha_{5\%}$							1.00	0.00	0.00	0.00	-0.63	0.00	0.00	0.00	0.51	0.00	0.00	0.00	0.74	0.00
$C\alpha_{6\%}$								1.00	0.00	0.00	0.00	-1.00	0.00	0.00	0.00	0.99	0.00	0.00	0.00	0.99
$Cb_{3\%}$									1.00	0.00	0.00	0.00	-0.98	0.00	0.00	0.00	-0.98	0.00	0.00	0.00
$Cb_{4\%}$										1.00	0.00	0.00	0.00	-0.96	0.00	0.00	0.00	-0.95	0.00	0.00
$Cb_{5\%}$											1.00	0.00	0.00	0.00	-0.12	0.00	0.00	0.00	-0.31	0.00
$Cb_{6\%}$												1.00	0.00	0.00	0.00	-0.98	0.00	0.00	0.00	-0.97
$Cg1_{3\%}$													1.00	0.00	0.00	0.00	0.99	0.00	0.00	0.00
$Cg1_{4\%}$														1.00	0.00	0.00	0.00	0.97	0.00	0.00
$Cg1_{5\%}$															1.00	0.00	0.00	0.00	0.60	0.00
$Cg1_{6\%}$																1.00	0.00	0.00	0.00	0.99
$Cg2_{3\%}$																	1.00	0.00	0.00	0.00
$Cg2_{4\%}$																		1.00	0.00	0.00
$Cg2_{5\%}$																			1.00	0.00
$Cg2_{6\%}$																				1.00

2006 Witczak Model

The δ calibration coefficients are all positive values as shown in Figure 75. The α calibration coefficients are all negative values as shown in Figure 76. The absolute value of the δ coefficient for 6% RAS is greater than other RAS contents, while the absolute value of α coefficient is approximately the same as that of 4% RAS and 5% RAS. The coefficients for 4% and 5% RAS contents have large standard errors compared to the value of the coefficients indicating the effects of 4% and 5% RAS contents on the parameter δ and α are not significant. The b calibration coeffcicients in Figure 77 for 3% and 4% RAS contents are negative. The coefficient values at 3%, 4%, and 5% RAS contents are small compared to their standard errors. The 6% RAS has a significant positive effect on the b parameter in the model. Figure 78 show very small g_1 calibration coefficients at 4%, 5%, and 6% RAS contents compared to their standard errors. Adding shingles to HMA may not cause changes in the g_1 parameter. Figure 79 indicates the g_2 calibration coefficient for 5% RAS is almost zero. The 6% RAS has a significant larger negative calibration coefficient than other RAS contents. To summarize, adding shingles to HMA increases the δ and decreases the α values in the 2006 Witczak Model. The g_1 parameter does not affected by addition of shingles in HMA. Modification of the original model is recommended when 6% or more RAS is used.

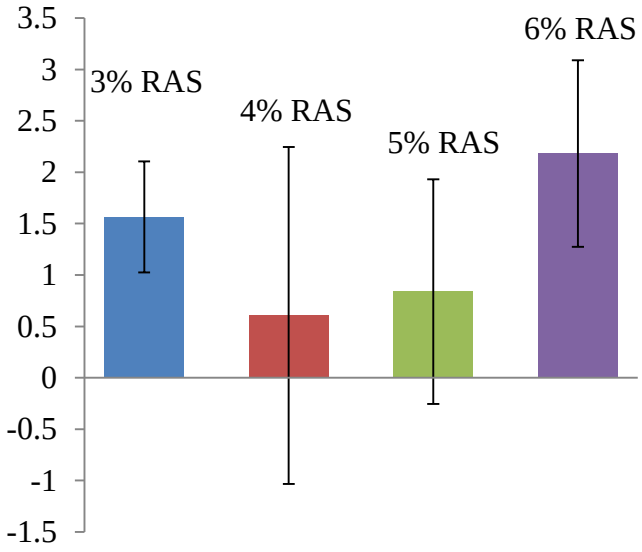

Figure 75: δ Calibration Coefficient for the 2006 Witczak Model

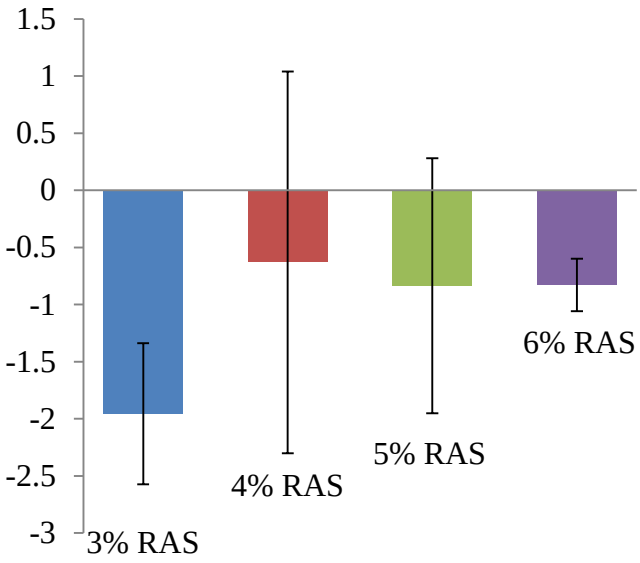

Figure 76: α Calibration Coefficient for the 2006 Witczak Model

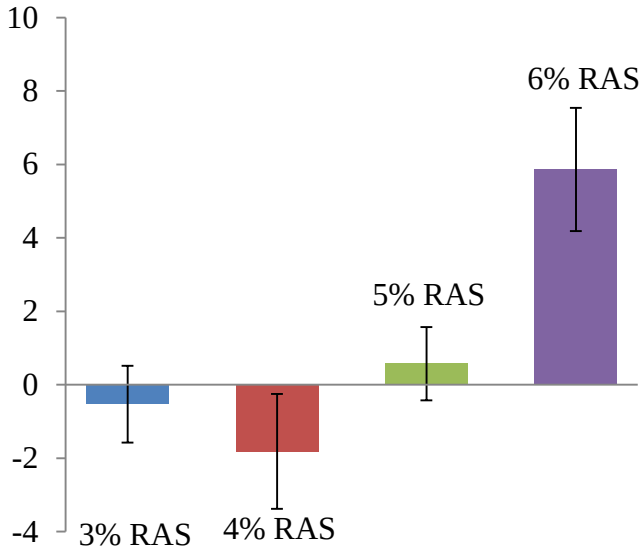

Figure 77: b Calibration Coefficient for the 2006 Witczak Model

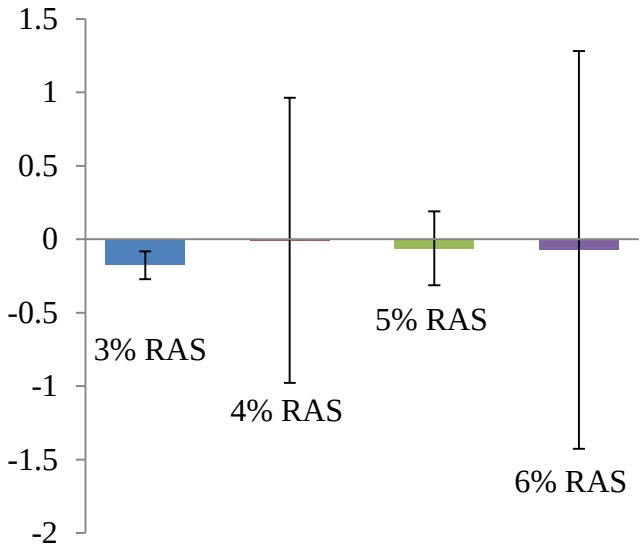

Figure 78: g_1 Calibration Coefficient for the 2006 Witczak Model

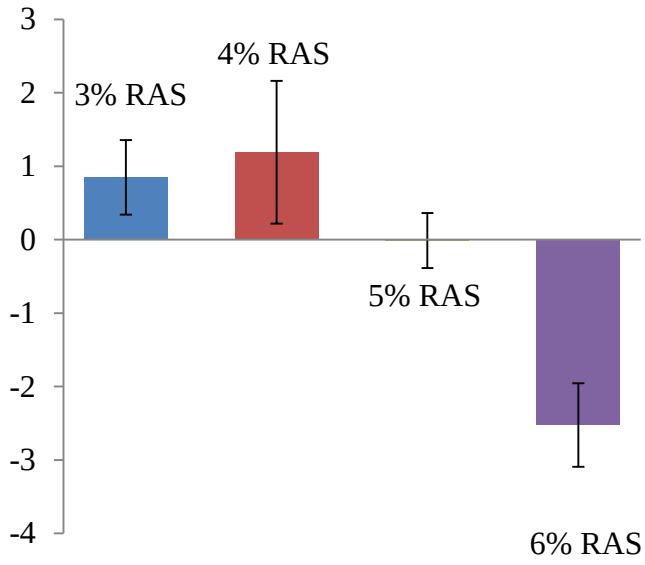

Figure 79: g_2 Calibration Coefficient for the 2006 Witczak Model

Table 29 shows that the δ and α calibration coefficients are strongly correlated. An increased δ will result in a decreased α. The δ coefficient is negatively correlated to the b coefficient. The α coefficient is positively correlated to the g_1 coefficient. The coefficient b is negatively correlated to the g_2 coefficient. Coefficients of different RAS contents are independent to each other.

Table 29: 2006 Witczak Modification Coefficient Correlation Table

	$C\delta_{3\%}$	$C\delta_{4\%}$	$C\delta_{5\%}$	$C\delta_{6\%}$	$C\alpha_{3\%}$	$C\alpha_{4\%}$	$C\alpha_{5\%}$	$C\alpha_{6\%}$	$Cb_{3\%}$	$Cb_{4\%}$	$Cb_{5\%}$	$Cb_{6\%}$	$Cg1_{3\%}$	$Cg1_{4\%}$	$Cg1_{5\%}$	$Cg1_{6\%}$	$Cg2_{3\%}$	$Cg2_{4\%}$	$Cg2_{5\%}$	$Cg2_{6\%}$
$C\delta_{3\%}$	1.00	0.00	0.00	0.00	-0.99	0.00	0.00	0.00	0.33	0.00	0.00	0.00	-0.95	0.00	0.00	0.00	0.08	0.00	0.00	0.00
$C\delta_{4\%}$		1.00	0.00	0.00	0.00	-1.00	0.00	0.00	0.00	0.26	0.00	0.00	0.00	-0.90	0.00	0.00	0.00	0.33	0.00	0.00
$C\delta_{5\%}$			1.00	0.00	0.00	0.00	-0.96	0.00	0.00	0.00	0.44	0.00	0.00	0.00	-0.59	0.00	0.00	0.00	-0.29	0.00
$C\delta_{6\%}$				1.00	0.00	0.00	0.00	-1.00	0.00	0.00	0.00	-0.14	0.00	0.00	0.00	-0.99	0.00	0.00	0.00	0.87
$C\alpha_{3\%}$					1.00	0.00	0.00	0.00	-0.19	0.00	0.00	0.00	0.92	0.00	0.00	0.00	-0.23	0.00	0.00	0.00
$C\alpha_{4\%}$						1.00	0.00	0.00	0.00	-0.25	0.00	0.00	0.00	0.89	0.00	0.00	0.00	-0.35	0.00	0.00
$C\alpha_{5\%}$							1.00	0.00	0.00	0.00	-0.55	0.00	0.00	0.00	0.70	0.00	0.00	0.00	0.41	0.00
$C\alpha_{6\%}$								1.00	0.00	0.00	0.00	0.21	0.00	0.00	0.00	0.99	0.00	0.00	0.00	-0.91
$Cb_{3\%}$									1.00	0.00	0.00	0.00	-0.53	0.00	0.00	0.00	-0.91	0.00	0.00	0.00
$Cb_{4\%}$										1.00	0.00	0.00	0.00	-0.64	0.00	0.00	0.00	-0.82	0.00	0.00
$Cb_{5\%}$											1.00	0.00	0.00	0.00	-0.97	0.00	0.00	0.00	-0.98	0.00
$Cb_{6\%}$												1.00	0.00	0.00	0.00	0.11	0.00	0.00	0.00	-0.60
$Cg1_{3\%}$													1.00	0.00	0.00	0.00	0.14	0.00	0.00	0.00
$Cg1_{4\%}$														1.00	0.00	0.00	0.00	0.09	0.00	0.00
$Cg1_{5\%}$															1.00	0.00	0.00	0.00	0.92	0.00
$Cg1_{6\%}$																1.00	0.00	0.00	0.00	-0.86

Hirsch Model

Regression statistics in Table 25 show that values of the Ea calibration coefficients are very small with significantly large standard errors. The absolute values of the coefficients are less than 1. Considering the value of Ea is 4,200,000 in the original Hirsch model, addition of shingles in HMA does not change the assumed aggregate modulus. The p_0 calibration coefficient for 5% RAS in Figure 80 is positive. However, the coefficients for other RAS contents are very small. Figure 81 and Figure 82 show RAS has positive effects on the p_1 and $p_2$parameters. The effects are very small at 6% RAS content. To summarize, the addition of RAS in HMA does not significantly decrease the prediction accuracy of the original Hirsch model.

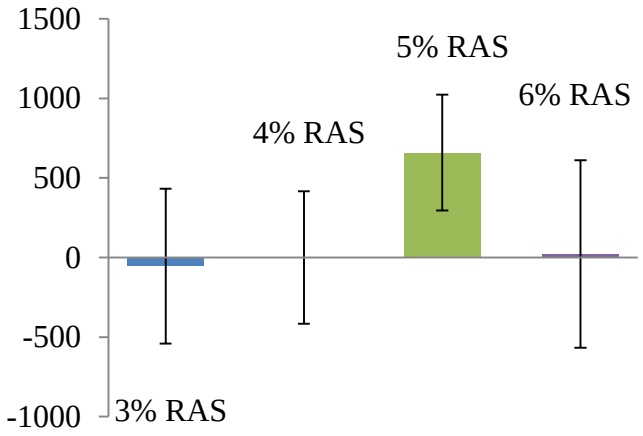

Figure 80: p_0 Calibration Coefficient for the Hirsch Model

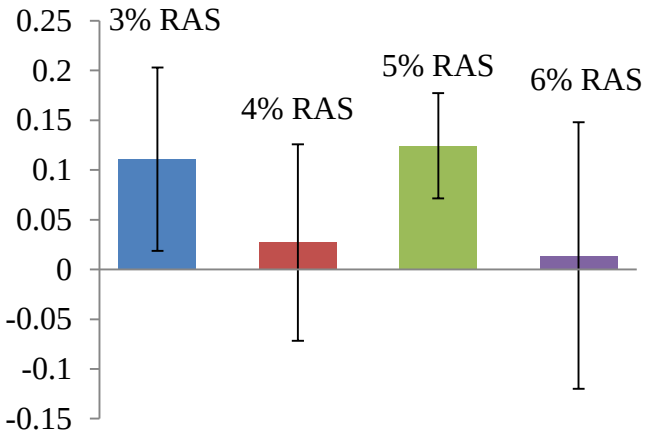

Figure 81: p_1 Calibration Coefficient for the Hirsch Model

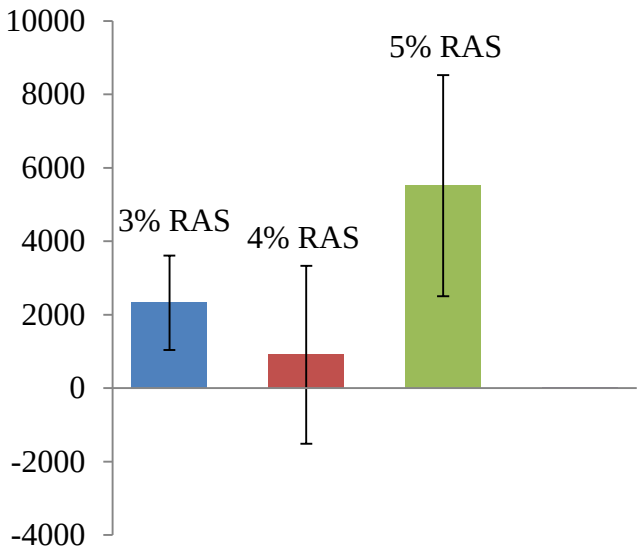

Figure 82: p_2 Calibration Coefficient for the Hirsch Model

CHAPTER 5: CONCLUSIONS AND RECOMMENDATIONS

The research was conducted to evaluate the accuracies of the commonly used dynamic modulus (E*) predictive models when recycled asphalt shingles are used in producing asphalt mixtures. The E* predictive models evaluated in this research are the 1999 Witczak Model, the 2006 Witczak Model, and the Hirsch Model. Modifications were proposed for the Witczak models. Model parameter statistics indicate that the Hirsch Model is not sensitive to mixtures RAS containing and thus modification of the Hirsch model is not necessary.

The mixes tested in this study were procured from demonstration projects of the National Pooled Fund Study #1208 which was conducted for the purpose of evaluating the effects of RAS on laboratory testing properties and field performances of asphalt mixtures. In the study, thirteen mixes were produced for four different demonstration projects constructed by state agencies including Indiana, Iowa, Minnesota, and Missouri. The Indiana mixes include two three percent RAS mixes of which one of them used a foaming warm mix asphalt technology and a control mix which contains 15 percent FRAP. The Iowa mixes include a control mix which does not contain any RAS and three experimental mixes with four, five, and six percent RAS contents. The Minnesota mixes include a control mix containing 30 percent FRAP, and two experimental mixes containing five percent manufactured and tear-off RAS, respectively. The Missouri mixes include a control mix containing 15 percent RAP, a mix containing ten percent RAP and five percent fine ground RAS, and a Mix containing ten percent RAP and five percent coarse ground RAS. The asphalt used in the Missouri demonstration project contains ground tire rubber and a vestenamer polymer to improve the binder performance grade from 64-22 to 70-22. Loose mixtures were obtained in the field and compacted to test cylinders in the laboratory for dynamic modulus testing. Asphalts were recovered from the field mixes through a centrifugal extraction method for the DSR tests. The DSR tests results were used to estimate the values of input parameters regarding binder rheological properties. The laboratory E* values were compared with the calculated E* values from the predictive models. A statistical analysis was performed on the accuracies of the models to determine if there were significant differences in mixes containing different percentages of RAS from different demonstration projects. Modifications of the original predictive models were made to change the empirically determined coefficients by introducing dummy variables to consider the use of RAS. Non-linear multiple variable regressions based on the least square method were performed to determine the coefficients of the

dummy variables. A statistical analysis was conducted to evaluate the effectiveness of the coefficients and their correlations. Based on the aforementioned analysis, the following conclusions are drawn in the ensuing sections.

Prediction Accuracies of the Original E* Predictive Models

The 1999 Witczak Model

The 1999 Witczak Model tends to overestimate E* values for mixes containing RAS. The master curves constructed on the model predicted E* values closely confirm the master curves constructed on the laboratory tested E* values at the low temperatures, while the master curves diverge at the high temperatures. These results are in agreement with Clyne et al. [29] and Kim et al. [30]. Birgisson et al. [31] indicated in their study on the influences of different binder viscosity measuring methods on the accuracy of the 1999 Witczak Model leads to underestimating E* values. However, this research shows a disagreement as the predictive accuracy of the 1999 Witczak Model is significantly affected by the projects, RAS contents, and environmental condition. Statistically significant differences were detected between every pair of projects and RAS contents suggesting modification is needed to account for the effects of the projects and shingles. Loading condition does not affect the model's prediction accuracy. The overall goodness-of-fit is statistically considered good.

The 2006 Witczak Model

The 2006 Witczak Model tends to overestimate the E* values. The master curves constructed on the model predicted E* values show the E* values are overestimated at every temperature range. The goodness-of-fit of the 2006 Witczak Model is fair. Statistically significant differences in predicting accuracies were detected between every pair of projects. The statistical analysis indicates the model has the same accuracy level of predicting E* values for mixes containing 0 percent RAS and four or five percent RAS. However, the predictive accuracy for mixes containing four percent RAS is significantly different from mixes containing five percent RAS. The predictive accuracy level for mixes containing six percent RAS is found to be the same as mixes containing three or five percent RAS. However, significant difference in model accuracies was detected between mixes containing three and five percent RAS. Significant differences were found for other comparisons. Failure to detect significant differences in the aforementioned

comparisons may be a result from variability in lab testing results. However, modification is needed to account for the effects of RAS and projects.

The Hirsch Model

The Hirsch Model tends to overestimate the E* values at the high temperatures. Master curves constructed by the Hirsch Model predictions closely conform to the laboratory data at low temperatures and diverge at high temperatures. The goodness-of-fit of the Hirsch Model is excellent. Demonstration project factor is a significant factor affecting the predicting accuracy of the model. Statistical differences in model accuracies of the Hirsch Model were detected between mixes containing zero and four percent RAS, zero and five percent RAS, three and five percent RAS, and four and five percent RAS. There is not a rational relationship between the prediction accuracy and RAS content for the Hirsch Model.

Modified E* Predictive Models

The three modified E* predictive models have high accuracies of predicting at low and intermediate temperatures and considerably lower accuracies at high temperatures. The modified models have the same level of predictive accuracies under different loading rates.

The Modified 1999 Witczak Model

The calibrated modified 1999 Witczak Model is presented in Equation 37. The values of the introduced parameters are listed in Table 30 and Table 31. The R^2 value of the model is improved from 0.87 to 0.99 on a logarithm scale by the calibration.

$$\log|E^*| = \delta_{project} + \delta_{RAS\%} + 3.750063 + 0.02932\rho_{200} - 0.001767(\rho_{200})^2 - 0.002841\rho_4 - 0.058097V_a - 0.802208\left(\frac{V_{beff}}{V_{beff}+V_a}\right) + \frac{\alpha_{project} + \alpha_{RAS\%} + 3.871977 - 0.0021\rho_4 + 0.003958\rho_{38} - 0.000017(\rho_{38})^2 + 0.00547\rho_{34}}{1 + e^{(b_{project}+b_{RAS\%}-0.603313+(g_{1\ project}+g_{1\ RAS\%}-0.31335)\log(f)+(g_{2\ project}+g_{2\ RAS\%}-0.393532)\log(\eta))}}$$

Equation 37

Table 30: Project Effect Calibration Parameters for the Modified 1999 Witczak Model

Project	δ	α	b	g1	g2
Indiana	-2.4475	2.41062	-0.8283	-0.0531	0.02603
Iowa	-2.4136	2.45945	-0.4255	-0.0357	0.05663
Minnesota	-0.3767	0.30519	0.10558	-0.1367	-0.0917
Missouri	-2.1956	2.14614	-0.7409	-0.0674	-0.0144

Table 31: RAS Content Calibration Parameters for the Modified 1999 Witczak Model

RAS%	δ	α	b	g1	g2
0	0	0	0	0	0
3	-1.6934	1.7359	-0.0558	0.02851	0.0244
4	2.33881	-2.5261	0.63665	-0.0927	-0.2008
5	1.29883	-1.2563	0.48735	0.0227	0.01138
6	2.37178	-2.3721	0.91856	0.01253	-0.0229

The Modified 2006 Witczak Model

The calibrated modified 2006 Witczak Model is presented in Equation 38. The values of the introduced parameters are listed in Table 32 and Table 33. The R^2 value of the model is improved from 0.75 to 0.99 on a logarithm scale by the calibration.

$$\log_{10}\mathbf{E}^{*} = \delta_{\text{project}} + \delta_{\text{RAS\%}} - \mathbf{0.349} + \mathbf{0.754}\left(|\mathbf{G_b}^{*}|^{-\mathbf{0.0052}}\right) \times \left(\mathbf{6.65} - \mathbf{0.032}\boldsymbol{\rho}_{\mathbf{200}} + \mathbf{0.0027}\boldsymbol{\rho}_{\mathbf{200}}^{\mathbf{2}} + \mathbf{0.011}\boldsymbol{\rho}_{\mathbf{4}} - \mathbf{0.0001}\boldsymbol{\rho}_{\mathbf{4}}^{\mathbf{2}} + \mathbf{0.006}\boldsymbol{\rho}_{\mathbf{38}} - \mathbf{0.00014}\boldsymbol{\rho}_{\mathbf{38}}^{\mathbf{2}} - \mathbf{0.08}\mathbf{V_a} - \mathbf{1.06}\left(\frac{\mathbf{V_{beff}}}{\mathbf{V_a} + \mathbf{V_{beff}}}\right)\right) + \frac{\alpha_{\text{project}} + \alpha_{\text{RAS\%}} + \mathbf{2.56} + \mathbf{0.03}\mathbf{V_a} + \mathbf{0.71}\left(\frac{\mathbf{V_{beff}}}{\mathbf{V_a}+\mathbf{V_{beff}}}\right) + \mathbf{0.012}\boldsymbol{\rho}_{\mathbf{38}} - \mathbf{0.0001}\boldsymbol{\rho}_{\mathbf{38}}^{\mathbf{2}} - \mathbf{0.01}\boldsymbol{\rho}_{\mathbf{34}}}{\mathbf{1} + \mathbf{e}^{(b_{\text{project}}+b_{\text{RAS\%}}-\mathbf{0.7814}+(g_{1\ \text{project}}+g_{1\ \text{RAS\%}}-\mathbf{0.5785})\mathbf{log}|\mathbf{G_b}^{*}|+(g_{2\ \text{project}}+g_{2\ \text{RAS\%}}+\mathbf{0.8834})\mathbf{log}\boldsymbol{\delta}_{\mathbf{b}})}}$$

Equation 38

Table 32: Project Effect Calibration Parameters for the Modified 2006 Witczak Model

Project	δ	α	b	g1	g2
Indiana	-2.084	2.32134	0.09357	0.16969	-0.4511
Iowa	-4.4766	3.92956	-6.6804	0.3434	2.86933
Minnesota	-0.8869	0.52512	-3.5158	0.04846	2.00793
Missouri	-1.4828	1.87323	1.72603	0.08525	-1.012

Table 33: RAS Content Calibration Parameters for the Modified 2006 Witczak Model

RAS%	δ	α	b	g1	g2
0	0	0	0	0	0
3	1.56497	-1.9566	-0.5286	-0.1767	0.84867
4	0.60657	-0.6305	-1.8186	-0.0077	1.1913
5	0.83865	-0.8366	0.57433	-0.0617	-0.0112
6	2.18273	-0.8281	5.8667	-0.0725	-2.5251

The Modified Hirsch Model

The finalized modified Hirsch Model is presented in Equation 39 and Equation 40. The values of the introduced parameters are listed in Table 34 and Table 35. The calibration of the model improves the R^2 value from 0.90 to 0.97. The improvement of the R^2 value is primarily from calibrations addressing the project effects.

$$|\mathbf{E^*}|_{\mathbf{mix}} = \mathbf{Pc} \times \left[(\mathbf{4200000} + \mathbf{Ea_{project}} + \mathbf{Ea_{RAS\%}}) \times \left(\mathbf{1} - \frac{\mathbf{VMA}}{\mathbf{100}} \right) + \mathbf{3} \times |\mathbf{G^*}|_{\mathbf{binder}} \left(\frac{\mathbf{VFA} \times \mathbf{VMA}}{\mathbf{10000}} \right) \right] + (\mathbf{1} - \mathbf{Pc}) \times \left[\frac{\mathbf{1} - \frac{\mathbf{VMA}}{\mathbf{100}}}{(\mathbf{4200000} + \mathbf{Ea_{project}} + \mathbf{Ea_{RAS\%}})} + \frac{\mathbf{VMA}}{\mathbf{3} \times \mathbf{VFA} \times |\mathbf{G^*}|_{\mathbf{binder}}} \right]^{-1}$$

Equation 39

$$\mathbf{Pc} = \frac{(\mathbf{20} + \mathbf{p0_{project}} + \mathbf{p0_{RAS\%}} + \frac{\mathbf{VFA} \times \mathbf{3} \times |\mathbf{G^*}|_{\mathbf{binder}}}{\mathbf{VMA}})^{(\mathbf{0.58} + \mathbf{p1_{project}} + \mathbf{p1_{RAS\%}})}}{\mathbf{650} + \mathbf{P2_{project}} + \mathbf{p2_{RAS\%}} + (\frac{\mathbf{VFA} \times \mathbf{3} \times |\mathbf{G^*}|_{\mathbf{binder}}}{\mathbf{VMA}})^{(\mathbf{0.58} + \mathbf{p1_{project}} + \mathbf{p2_{RAS\%}})}}$$

Equation 40

Table 34: Project Effect Calibration Parameters for the Modified Hirsch Model

Project	Ea	p0	p1	p2
Indiana	0.09072	249.033	0.01266	69.1419
Iowa	-0.0565	-23.347	0.10017	2063.32
Minnesota	-0.1036	-3.9149	0.13319	3078.15
Missouri	0.19421	139.286	0.07432	755.129

Table 35: RAS Content Calibration Parameters for the Modified Hirsch Model

RAS%	Ea	p0	p1	p2
0	0	0	0	0
3	0.85233	-53.876	0.1109	2324.44
4	0.29819	0.73575	0.02706	910.952
5	0	659.784	0.12435	5513.72
6	0.40058	22.6821	0.01392	0.85233

Influences of RAS on Parameters of the E* Predictive Models

Adding Shingles to asphalt mixtures requires an increase in δ and b values and a decrease in the α value in the 1999 and 2006 Witczak models for improved prediction of E* values. Strong linear correlations exist in parameter δ, α and b. There are no rational relationships between the RAS content and the parameters g1 and g2. Shingles do not have significant effects on the parameter Ea, p0, p1, and p2 in the Hirsch Model.

Recommendations

- A low RAS content of less than three percent does not require modification of the 1999 Witczak Model. When a RAS content of four percent or higher is used, it is recommended to use the modified 1999 Witczak Model.
- The modified 2006 Witczak Model is recommended to use when a mix contains six percent RAS or more.
- The δ term in the Witczak models should be increased and α term should be decreased correspondently when RAS is used in asphalt mixture.
- The b constant in the Witczak models should be increased for RAS.
- The g1 and g2 constants in the Witczak models do not need to be modified for RAS.

- The Hirsch Model does not need to be modified for shingles' effects.
- Different projects affect the calibration coefficients and need to be developed if the modified models are used for other projects.
- The modified models were developed from a limited database containing 13 different mixes. The experiments were not specifically designed for the purposes of this research. Mixes containing certain percentages of RAS such as three percent, four percent, and six percent can be only found in one project. The mutual variability of the project and the certain RAS contents cannot be determined. Future research should be conducted to verify the effects of RAS on the 1999 and 2006 Witczak models as well as other E* predictive models that are not included in this research. In addition, comprehensive research should be conducted to investigate the accuracies of the E* predictive models when different methods are used to obtain values of the input parameters such as the binder shear modulus, phase angle, and viscosity. This includes developing a standardized procedure to calibrate the model input parameters.

REFERENCES

[1] New Hampshire Department of Transportation, "Construction cost index,". vol. 2011, 2011.

[2] Pennsylvania Department Of Transportation, "Strategic recycling program fact sheet". vol. 2011, 2006.

[3] D. W. Janisch and C. M. Turgeon, "Minnesota’s Experience Using Shingle Scrap in Bituminous Pavements," *Final Report, Minnesota Department of Transportation, Minnesota,* 1996.

[4] J. D. Brock, *From Roofing Shingles to Roads*: Astec, 1998.

[5] California Department Of Resources Recycling And Recovery, "Asphalt Roofing Shingles Recycling,". vol. 2011, 2006.

[6] Ohio Department Of Transportation, "Revisions to the 2010 Construction & Material Specifications,". vol. 2011, 2011.

[7] Construction Materials Recycling Association and U. S. Environmental Protection Agency, "State Experience in Recycling Asphalt Shingles,". vol. 2011, 2011.

[8] J. Mallela, L. T. Glover, M. I. Darter, H. Von Quintus, A. Gotlif, M. Stanley, and S. Sadasivam, "Guidelines for implementing NCHRP 1-37A ME design procedures in Ohio: volume 1-summary of findings, implementation plan, and next steps," *Columbus: Ohio Department of Transportation,* 2009-01-01 2009.

[9] J. Bari and M. W. Witczak, "Development of a New Revised Version of the Witczak E* Predictive Model for Hot Mix Asphalt Mixtures," *Journal of the Association of Asphalt Paving Technologists,* p. 385, 2006.

[10] D. W. Christensen, T. Pellinen and R. F. Bonaquist, "Hirsch Model for Estimating the Modulus of Asphalt Concrete," *Journal of the Association of Asphalt Paving Technologists,* 2003.

[11] D. E. Newcomb, M. D. O. T. Administration, U. O. M. D. Civil, and M. Engineering, *Influence of Roofing Shingles on Asphalt Concrete Mixture Properties*: Minnesota Dept. of Transportation, Office of Research Administration, 1993.

[12] D. C. Trumbore, "Magnitude and source of air emissions from asphalt blowing operations," *Environmental Progress,* vol. 17, pp. 53-59, 1998.

[13] J. Cory, "Shingle recycling slow to come: few roofing companies have the opportunity to recycle shingles at an affordable price," *Remodeling,* vol. 11, p. 120, 2003.

[14] D. Krivit, "Recycling Tear-Off Asphalt Shingles: Best Practices Guide," Construction Materials Recycling Association (CMRA) 2007.

[15] United States. Environmental Protection Agency. Emission Standards And Engineering Division, *Standards support document, promulgated amendments to the national emission standard for asbestos*. Research Triangle Park, N.C.
Springfield, Va.: U.S. Environmental Protection Agency, Office of Air and Waste Management
National Technical Information Service [distributor, 1978.

[16] D. E. Watson, A. Johnson and H. R. Sharma, "Georgia's experience with recycled roofing shingles in asphaltic concrete," *Transportation Research Record: Journal of the Transportation Research Board,* vol. 1638, pp. 129--133, 1998.

[17] J. W. Button, D. Williams and J. A. Scherocman, "Roofing Shingles and Toner in Asphalt Pavements," 1996.

[18] M. J. Watson, J. McGraw, E. Johnson, D. Linell, and S. Dai, "The effect of recycled asphalt materials on hot mixed asphalt pavement performance," in *Green Streets and Highways 2010: An Interactive Conference on the State of the Art and How to Achieve Sustainable Outcomes - Proceedings of the Green Streets and Highways 2010 Conference* Denver, CO, United states, 2010, pp. 323-336.

[19] A. A. Cascione, R. Christopher Williams, W. G. Buttlar, S. Ahmed, B. Hill, D. S. Haugen, and S. Gillen, "Laboratory Evaluation of Field Produced Hot Mix Asphalt Containing Post-Consumer Recycled Asphalt Shingles and Fractionated Recycled Asphalt Pavement," *Asphalt Paving Technology-Proceedings Association of Asphalt Technologists,* vol. 80, p. 377, 2011.

[20] T. V. Scholz, "Preliminary Investigation of RAP and RAS in HMAC," 2010.

[21] C. W. Schwartz, "Evaluation of the Witcak Dynamic Modulus Prediction Model," in *84th Annual Meeting of the Transportation Research Board* Washington D.C., 2005.

[22] M. W. Witzcak, *Simple performance test for superpave mix design*: Transportation Research Board, 2002.

[23] G. Garcia and M. Thompson, "HMA DYNAMIC MODULUS PREDICTIVE MODELS--AReview," *Urbana,* vol. 51, p. 61801, 2007.

[24] C. E. Dougan, C. D. O. T. Research, Materials, C. T. Institute, and U. O. C. S. Engineering, *E*-dynamic Modulus: Test Protocol: Problems and Solutions*: Connecticut Transportation Institute, School of Engineering, University of Connecticut, 2003.

[25] American Association of State Highway And Transportation Officials, "Standard Method of Test for Determining Dynamic Modulus of Hot Mix Asphalt (HMA)," in *AASHTO TP62-07*, 2009.

[26] D. W. Christen and D. A. Anderson, "Interpretation of Dynamic Mechanical Test Data for Paving Grade Asphalt Cements," *Journal of the Association of Asphalt Paving Technologists,* 1992.

[27] T. K. Pellinen and M. W. Witczak, "Stress Dependent Master Curve Construction for Dynamic (Complex) Modulus," *Journal of the Association of Asphalt Paving Technologists,* p. 287, 2002.

[28] M. W. Mirza and M. W. Witczak, "Development of a Global Aging System for Short and Long Term Aging of Asphalt Cements," *Journal of the Association of Asphalt Paving Technologists,* 1995.

[29] T. R. Clyne, X. Li, M. O. Marasteanu, and E. L. Skok, "Dynamic and Resilient Modulus of MN/DOT Asphalt Mixtures," University of Minnesota, Minneapolis MN/RC – 2003-09, 2003.

[30] Y. R. Kim, M. Momen and M. King, "Typical Dynamic Moduli for North Carolina Asphalt Concrete Mixtures," North Carolina State University, Raleigh FHWA/NC/2005-03, 2005.

[31] B. Birgisson, G. Sholar and R. Roque, "Evaluation of a Predicted Dynamic Modulus for Florida Mixtures," in *84th Annual Meeting of the Transportation Research Board* Washington D.C.: Transportation Research Board, 2005.

[32] F. O. Martinez and S. M. Angelone, "Evaluation of Different Predictive Dynamic Modulus Models of Asphalt Mixtures Used in Argentina," in *88th Annual Meeting of the Transportation Research Board* Washington D.C., 2009.

[33] J. P. Serfass and J. Samanos, "Fiber-Modified Asphalt Concrete Characteristics, Applications and Behavior," *Journal of the Association of Asphalt Paving Technologists,* p. 193, 1996.

[34] S. Wu, Q. Yue, N. Li, and H. Yue, "Effects of Fibers on the Dynamic Properties of Asphalt Mixtures," *Journal of Wuhan University of Technology(Materials Science Edition),* pp. 733-736, 2007.

[35] D. Haugen, "National Pooled Fund Study #1208 Field Notes,", 2010.

[36] Li, X. and R. Christopher Williams, "A Practical Dynamic Modulus Testing Protocol," *Journal of Testing and Evaluation,* vol.40, 2012.

[37] N. Tran and K Hall, "Evaluating the Predictive Equation in Determining Dynamic Moduli of Typical Asphalt Mixtures Used in Arkansas," *Journal of the Association Asphalt Paving Technologists,* vol. 74, pp. 1-17, 2005.

APPENDIX A: DYNAMIC MODULUS RESULTS

Table 36: Dynamic Modulus Test Results for Mix BC-21

		Dynamic Modulus, kPa					
		Mix BC-21, Minnesota Demonstration Project, 5% Mfr. RAS					
Temp., C	Freq., Hz	Sample 1	Sample 2	Sample 3	Sample 4	Sample 5	CV, %
4	25	15763	15688	15505	15636	15745	0.66
4	20	15299	15365	15089	15291	15320	0.70
4	10	14228	14260	13929	14180	14304	1.04
4	5	13165	13172	12786	13075	13259	1.40
4	2	11760	11688	11342	11703	11929	1.83
4	1	10728	10734	10223	10672	10936	2.47
4	0.5	9727	9702	9188	9732	10005	3.07
4	0.2	8470	8528	7884	8549	8784	3.96
4	0.1	7600	7662	6984	7745	7907	4.65
21	25	7192	7118	7708	6544	6938	5.95
21	20	6828	6795	7301	6146	6656	6.14
21	10	5851	5784	6280	5230	5741	6.47
21	5	4985	4960	5345	4407	4886	6.83
21	2	3982	3991	4291	3479	3889	7.45
21	1	3355	3361	3590	2864	3214	8.16
21	0.5	2724	2767	3021	2386	2678	8.36
21	0.2	2210	2164	2347	1813	2033	9.56
21	0.1	1771	1767	1972	1508	1646	9.91
37	25	2412	2409	2514	2460	2246	4.16
37	20	2302	2277	2320	2235	2109	3.75
37	10	1847	1845	1816	1718	1652	4.88
37	5	1407	1413	1476	1374	1337	3.68
37	2	1042	1049	1069	974	947	5.18
37	1	833	842	778	689	680	10.04
37	0.5	632	622	651	576	574	5.63
37	0.2	519	493	461	404	399	11.70
37	0.1	382	451	350	303	298	17.69

Table 37: Dynamic Modulus Test Results for Mix BC-22

		Dynamic Modulus, kPa					
		Mix BC-22, Minnesota Demonstration Project, 5% Tear-off					
Temp., C	Freq., Hz	Sample 1	Sample 2	Sample 3	Sample 4	Sample 5	CV, %
4	25	16508	16642	16825	15743	16480	2.51
4	20	16040	16195	16390	15322	16050	2.53
4	10	14833	14682	15126	14278	14831	2.10
4	5	13569	13655	13692	13053	13523	1.91
4	2	11914	12004	11967	11557	11938	1.53
4	1	10704	10772	10679	10423	10768	1.34
4	0.5	9533	9521	9498	9371	9550	0.75
4	0.2	8009	8110	7965	7970	8137	1.00
4	0.1	6928	7000	6959	7050	7055	0.80
21	25	7280	6288	7217	8057	7211	8.70
21	20	6884	5751	7486	7390	6892	10.02
21	10	5949	4807	6360	6315	5931	10.69
21	5	5040	4222	5269	5282	5068	8.76
21	2	3985	3313	4150	4215	4035	9.19
21	1	3335	2744	3404	3496	3294	9.08
21	0.5	2598	2336	2816	2936	2791	8.69
21	0.2	2054	2048	1985	2124	2160	3.31
21	0.1	1636	1760	1594	1698	1785	4.76
37	25	2485	2137	2744	2482	2478	8.76
37	20	2345	2010	2558	2374	2335	8.51
37	10	1875	1477	1960	1840	1847	10.36
37	5	1410	1059	1530	1397	1461	13.28
37	2	954	687	1069	1034	965	15.95
37	1	651	449	726	728	745	18.65
37	0.5	488	337	604	540	547	20.14
37	0.2	351	253	427	356	357	17.85
37	0.1	197	136	266	341	342	35.16

Table 38: Dynamic Modulus Test Results for Mix BC-23

		Dynamic Modulus, kPa					
		Mix BC-23, Minnesota Demonstration Project, 30% RAP					
Temp., C	Freq., Hz	Sample 1	Sample 2	Sample 3	Sample 4	Sample 5	CV, %
4	25	15865	15771	15857	15846	15862	0.25
4	20	15390	15126	15480	15476	15434	0.96
4	10	14105	13937	14145	14127	14086	0.59
4	5	12807	12596	12811	12876	12825	0.85
4	2	11143	10937	11188	11145	11201	0.96
4	1	9909	9831	9908	9918	9897	0.36
4	0.5	8713	7737	9630	8720	8751	7.69
4	0.2	7325	5935	7694	7303	7951	10.76
4	0.1	6269	5072	6609	6244	6816	10.89
21	25	6421	5339	7141	6397	6386	10.15
21	20	6486	5070	6480	6137	6131	9.59
21	10	5551	4101	5459	5114	5087	11.36
21	5	4611	3434	4408	4217	4175	10.70
21	2	3524	2456	3354	3184	3230	12.99
21	1	2789	1866	2691	2547	2563	14.58
21	0.5	2064	1499	2226	2005	2012	13.94
21	0.2	1563	1146	1438	1506	1445	11.34
21	0.1	1215	891	1122	1173	1106	11.36
37	25	1711	1792	1812	1890	1870	3.90
37	20	1651	1654	1662	1781	1718	3.31
37	10	1274	1222	1264	1269	1316	2.63
37	5	912	828	958	952	1019	7.52
37	2	592	510	670	723	638	12.87
37	1	372	305	441	475	493	18.63
37	0.5	249	206	366	415	367	27.71
37	0.2	190	151	269	261	254	23.01
37	0.1	150	121	214	169	187	20.93

Table 39: Dynamic Modulus Test Results for Mix BC-24

		Dynamic Modulus, kPa					
		Mix BC-24, Iowa Demonstration Project, 0% RAS					
Temp., C	**Freq., Hz**	**Sample 1**	**Sample 2**	**Sample 3**	**Sample 4**	**Sample 5**	**CV, %**
4	25	15407	15309	15380	15385	15412	0.27
4	20	14990	14978	14997	14998	14990	0.05
4	10	13741	13961	13861	13865	13870	0.56
4	5	12853	12608	12724	12723	12692	0.69
4	2	11261	11157	11235	11242	11269	0.40
4	1	10158	10042	10131	10130	10166	0.49
4	0.5	9061	8987	9044	9047	9065	0.35
4	0.2	7674	7674	7685	7684	7673	0.08
4	0.1	6708	6709	6706	6709	6681	0.18
21	25	6426	7088	6687	7096	6091	6.49
21	20	6047	6689	6318	6715	5788	6.38
21	10	5097	5703	5348	5708	4872	6.91
21	5	4251	4826	4493	4819	4054	7.62
21	2	3280	3806	3502	3792	3111	8.80
21	1	2640	3131	2851	3123	2496	9.98
21	0.5	2110	2538	2306	2546	1991	10.85
21	0.2	1543	1931	1712	1919	1447	12.73
21	0.1	1203	1545	1355	1537	1122	14.15
37	25	2237	2782	2567	2814	2416	9.53
37	20	2098	2611	2340	2619	1995	12.29
37	10	1613	2040	1802	2042	1504	13.57
37	5	1218	1575	1382	1575	1132	14.71
37	2	820	1099	952	1093	776	15.83
37	1	576	793	680	786	537	17.37
37	0.5	435	596	512	588	413	16.52
37	0.2	295	407	359	403	282	16.81
37	0.1	219	297	262	294	212	15.67

Table 40: Dynamic Modulus Test Results for Mix BC-25

		Dynamic Modulus, kPa					
		Mix BC-25, Iowa Demonstration Project, 4% RAS					
Temp., C	**Freq., Hz**	**Sample 1**	**Sample 2**	**Sample 3**	**Sample 4**	**Sample 5**	**CV, %**
4	25	15336	15378	14973	15501	15570	1.51
4	20	15018	15082	14548	15084	15198	1.69
4	10	13813	13948	13393	14048	14318	2.45
4	5	13007	12921	12173	12959	13124	2.95
4	2	11521	11558	10721	11656	11849	3.78
4	1	10492	10452	9543	10577	11149	5.52
4	0.5	9480	9462	8716	9404	10236	5.69
4	0.2	8249	8275	7560	8710	8225	5.02
4	0.1	7387	7340	6549	7983	7323	6.97
21	25	7113	7027	7209	6477	6974	4.09
21	20	6948	6635	6689	6094	6633	4.72
21	10	5967	5704	5718	5129	5667	5.46
21	5	5175	4871	4783	4293	4812	6.63
21	2	4164	3883	3817	3327	3817	7.94
21	1	3532	3161	3210	2731	3162	9.03
21	0.5	2716	2627	2489	2506	2694	4.03
21	0.2	1992	2052	1833	2000	2059	4.59
21	0.1	1625	1639	1494	1694	1655	4.67
37	25	2161	2083	2100	1822	2161	6.80
37	20	1984	2001	2019	1734	1946	6.01
37	10	1539	1593	1515	1289	1587	8.30
37	5	1188	1184	1164	1046	1218	5.74
37	2	830	854	780	753	849	5.50
37	1	601	670	511	540	607	10.64
37	0.5	462	486	406	453	470	6.63
37	0.2	327	399	268	301	331	14.85
37	0.1	221	284	230	249	249	9.81

Table 41: Dynamic Modulus Test Results for Mix BC-26

		Dynamic Modulus, kPa					
		Mix BC-26, Iowa Demonstration Project, 5% RAS					
Temp., C	**Freq., Hz**	**Sample 1**	**Sample 2**	**Sample 3**	**Sample 4**	**Sample 5**	**CV, %**
4	25	12702	14036	12711	13034	12360	4.95
4	20	12391	13579	12348	12669	11917	4.93
4	10	11326	12446	11353	11675	11086	4.57
4	5	10766	11813	10009	10620	9653	7.83
4	2	9652	10391	8787	9303	8380	8.37
4	1	8723	9246	7643	8456	7787	7.94
4	0.5	7961	7805	7126	7562	7008	5.55
4	0.2	6757	6164	6131	6413	6379	3.94
4	0.1	5932	5294	5328	5573	5674	4.73
21	25	6276	5692	6891	6341	6258	6.76
21	20	6290	5347	6322	6063	5886	6.63
21	10	5128	4518	5582	5190	5182	7.47
21	5	4376	4032	4797	4427	4190	6.61
21	2	3502	3362	3577	3516	3521	2.29
21	1	2921	2769	2996	2938	2981	3.09
21	0.5	2396	2190	2355	2433	2781	8.90
21	0.2	2194	1836	1629	1947	1843	10.86
21	0.1	1823	1515	1292	1605	1542	12.23
37	25	2146	2181	2496	2297	2333	6.05
37	20	2158	2035	2332	2146	2008	6.00
37	10	1704	1604	1776	1785	1597	5.32
37	5	1341	1194	1403	1342	1420	6.64
37	2	969	811	981	1052	1051	10.09
37	1	748	592	681	818	814	13.07
37	0.5	544	416	609	588	732	19.71
37	0.2	430	330	417	446	509	15.11
37	0.1	290	248	380	401	353	19.08

Table 42: Dynamic Modulus Test Results for Mix BC-27

		Dynamic Modulus, kPa					
		Mix BC-27, Iowa Demonstration Project, 6% RAS					
Temp., C	**Freq., Hz**	**Sample 1**	**Sample 2**	**Sample 3**	**Sample 4**	**Sample 5**	**CV, %**
4	25	12559	13694	13249	13307	13248	3.10
4	20	12254	13312	12849	12930	12826	2.95
4	10	11141	12251	11824	11832	11848	3.39
4	5	10478	11439	10823	10758	10250	4.17
4	2	9310	10104	9552	9522	8774	5.07
4	1	8358	9042	8541	8503	8067	4.17
4	0.5	7746	7801	7467	7609	7342	2.51
4	0.2	6586	6279	6388	6489	6641	2.27
4	0.1	5805	5502	5540	5775	5873	2.93
21	25	5404	5597	5654	5655	5651	1.93
21	20	5142	5402	5352	5323	5319	1.85
21	10	3926	4506	4503	4588	4972	8.32
21	5	3425	3809	3872	3874	4027	5.92
21	2	2489	3021	3053	3052	3466	11.51
21	1	1984	2501	2510	2585	2891	13.10
21	0.5	1437	2070	2068	2072	2644	20.74
21	0.2	1437	1777	1346	1699	1740	12.16
21	0.1	1245	1316	1113	1383	1520	11.55
37	25	1708	2266	2277	2285	2489	13.27
37	20	1872	1894	2196	2127	2063	7.03
37	10	1582	1549	1706	1658	1730	4.73
37	5	1277	1208	1382	1370	1362	5.67
37	2	885	884	993	1054	1053	8.76
37	1	755	721	757	783	786	3.48
37	0.5	544	522	658	699	650	12.60
37	0.2	445	426	467	516	503	8.02
37	0.1	320	347	433	402	422	12.71

Table 43: Dynamic Modulus Test Results for Mix BC-28

		Dynamic Modulus, kPa					
		Mix BC-28, Missouri Demonstration Project, 15% RAP					
Temp., C	**Freq., Hz**	**Sample 1**	**Sample 2**	**Sample 3**	**Sample 4**	**Sample 5**	**CV, %**
4	25	18977	18985	19308	18392	18813	1.76
4	20	18550	18611	18962	18062	18482	1.74
4	10	17611	17598	17883	17100	17635	1.62
4	5	16667	16673	16713	16427	16447	0.82
4	2	15296	15336	15446	15205	15062	0.95
4	1	14296	14279	14254	14137	14307	0.48
4	0.5	13279	13302	13239	12852	13509	1.80
4	0.2	11935	12013	11691	11723	12256	1.94
4	0.1	11011	11038	10734	10817	11334	2.12
21	25	11121	10608	11851	11160	11270	3.96
21	20	10901	10278	11157	10762	10821	2.97
21	10	9420	9182	10151	9774	9746	3.83
21	5	8420	8314	8964	8651	8642	2.91
21	2	7019	7377	7465	7337	7388	2.36
21	1	6152	6504	6599	6472	6441	2.61
21	0.5	5248	5715	5757	5638	5640	3.62
21	0.2	4774	4667	4362	4666	4678	3.37
21	0.1	4149	4014	3750	4002	4043	3.68
37	25	5043	5033	5073	5016	4968	0.77
37	20	4845	4725	4873	4813	4791	1.17
37	10	4011	3964	3990	4011	3895	1.22
37	5	3278	3135	3333	3281	3189	2.45
37	2	2478	2376	2498	2469	2379	2.38
37	1	1894	1879	1934	1901	1791	2.84
37	0.5	1480	1430	1513	1486	1479	2.03
37	0.2	1169	1055	1095	1091	1012	5.35
37	0.1	914	809	934	847	712	10.55

Table 44: Dynamic Modulus Test Results for Mix BC-29

		Dynamic Modulus, kPa					
		Missouri Demonstration Project, 5% Fine RAS/10% RAP					
Temp., C	Freq., Hz	Sample 1	Sample 2	Sample 3	Sample 4	Sample 5	CV, %
4	25	17163	17080	16865	17084	17131	0.68
4	20	16765	16774	16384	16755	16747	1.01
4	10	15961	15923	15723	15955	15943	0.63
4	5	15140	15152	14959	15151	15142	0.56
4	2	14163	14132	13858	14097	14108	0.87
4	1	13339	13341	13094	13289	13323	0.79
4	0.5	12501	12537	11550	13250	12541	4.85
4	0.2	11511	11459	10320	12331	11505	6.27
4	0.1	10666	10636	9622	11580	10635	6.52
21	25	9988	9986	9784	10042	10038	1.06
21	20	9626	9615	9460	9670	9626	0.84
21	10	8785	8785	8425	8761	8690	1.76
21	5	7895	7915	7557	7912	7917	2.02
21	2	6815	6852	6623	6888	6860	1.56
21	1	6153	6102	5873	6163	6110	1.95
21	0.5	5435	5491	5166	5481	5396	2.46
21	0.2	4681	4679	4260	4675	4659	4.03
21	0.1	4091	4140	3781	4128	4103	3.73
37	25	4817	5058	5014	5043	5063	2.08
37	20	4828	4607	4729	4858	4791	2.08
37	10	4210	3969	3939	4155	4143	2.96
37	5	3613	3299	3415	3556	3595	3.85
37	2	2916	2723	2793	2888	2852	2.73
37	1	2456	2291	2288	2431	2450	3.61
37	0.5	2013	1906	2005	2050	2112	3.73
37	0.2	1646	1544	1590	1638	1630	2.63
37	0.1	1308	1239	1373	1365	1403	4.85

Table 45: Dynamic Modulus Test Results for Mix BC-30

		Dynamic Modulus, kPa					
		Missouri Demonstration Project, 5% Coarse RAS/10% RAP					
Temp., C	Freq., Hz	Sample 1	Sample 2	Sample 3	Sample 4	Sample 5	CV, %
4	25	15651	15919	15953	16073	15933	0.97
4	20	15318	15629	15601	15679	15588	0.91
4	10	14365	14721	14685	14748	14804	1.18
4	5	13800	13817	13864	13869	13484	1.17
4	2	12691	12657	12669	12746	12268	1.52
4	1	11744	11766	11746	11734	11628	0.47
4	0.5	10900	10986	10954	10369	11291	3.06
4	0.2	9810	9864	9822	9356	10167	2.96
4	0.1	9134	9156	9158	8514	9343	3.50
21	25	9935	9827	10019	10077	10014	0.97
21	20	9773	9508	9725	9581	9727	1.17
21	10	8617	8708	8717	8806	8736	0.78
21	5	7735	7926	7918	7730	7904	1.29
21	2	6539	7179	6825	6527	6773	3.92
21	1	5775	6403	6084	5772	6025	4.34
21	0.5	4878	5613	5383	5293	5397	5.08
21	0.2	4421	4578	4555	4353	4512	2.11
21	0.1	3831	3971	4010	3813	3997	2.41
37	25	3958	5002	4629	4548	4628	8.27
37	20	3966	4592	4429	4499	4428	5.53
37	10	3340	3906	3728	3764	3772	5.77
37	5	2801	3232	3225	3246	3129	6.00
37	2	2224	2472	2532	2628	2490	6.06
37	1	1807	2035	2063	2123	2100	6.27
37	0.5	1503	1701	1699	1836	1697	7.03
37	0.2	1171	1336	1400	1329	1346	6.54
37	0.1	911	1106	1138	1086	1121	8.59

Table 46: Dynamic Modulus Test Results for Mix BC-31

		Dynamic Modulus, kPa			
		Indiana Demonstration Project, 15%			
Temp., C	Freq., Hz	Sample 1	Sample 2	Sample 3	CV, %
4	25	18757	19174	18262	2.44
4	20	18453	18775	17958	2.24
4	10	17317	17568	16913	1.91
4	5	16163	16395	15669	2.31
4	2	14513	14772	14217	1.92
4	1	13390	13405	13104	1.28
4	0.5	12182	12125	12058	0.51
4	0.2	10692	10500	10755	1.25
4	0.1	9733	9437	9735	1.78
21	25	11111	10925	11085	0.91
21	20	10562	10308	10527	1.31
21	10	9245	9123	9298	0.97
21	5	8396	8243	8330	0.92
21	2	7135	7150	6973	1.39
21	1	6179	6231	6084	1.21
21	0.5	5345	5322	5257	0.85
21	0.2	4381	4207	4380	2.31
21	0.1	3758	3512	3760	3.89
37	25	5002	4869	4964	1.38
37	20	4762	4610	4878	2.84
37	10	3977	3801	3937	2.36
37	5	3210	3031	3296	4.26
37	2	2452	2251	2485	5.27
37	1	1872	1793	1950	4.18
37	0.5	1493	1361	1610	8.38
37	0.2	1179	975	1141	9.91
37	0.1	945	690	917	16.42

Table 47: Dynamic Modulus Test Results for Mix BC-32

		Dynamic Modulus, kPa					
		Indiana Demonstration Project, 3% RAS/HMA					
Temp., C	**Freq., Hz**	**Sample 1**	**Sample 2**	**Sample 3**	**Sample 4**	**Sample 5**	**CV, %**
4	25	17301	16961	16421	16994	16946	1.87
4	20	16764	16419	15978	16473	16435	1.72
4	10	15458	15271	14876	15299	15291	1.42
4	5	14371	14095	13576	14176	14166	2.12
4	2	12675	12453	11849	12413	12528	2.54
4	1	11526	11281	10839	11198	11074	2.27
4	0.5	10621	10113	9541	10101	9965	3.84
4	0.2	9342	8735	8262	8708	8492	4.62
4	0.1	8399	7827	7421	7818	7521	4.89
21	25	9152	9141	8644	9190	9390	3.03
21	20	8827	8793	8400	8785	9047	2.66
21	10	7770	7721	7443	7958	7688	2.39
21	5	6782	6841	6592	6891	6619	1.98
21	2	5668	5658	5396	5495	5629	2.14
21	1	4855	4849	4637	4706	4797	1.99
21	0.5	4104	4116	3817	4082	4178	3.45
21	0.2	3335	3273	3167	3242	3201	2.01
21	0.1	2771	2720	2667	2715	2705	1.37
37	25	3776	3803	3545	3850	3815	3.24
37	20	3627	3619	3475	3639	3608	1.87
37	10	2933	3015	2688	2962	3004	4.59
37	5	2444	2419	2083	2387	2416	6.41
37	2	1800	1769	1529	1749	1755	6.32
37	1	1370	1328	1168	1339	1337	6.12
37	0.5	1069	1022	926	1027	1025	5.20
37	0.2	760	723	587	819	724	11.82
37	0.1	588	481	570	624	465	12.67

Table 48: Dynamic Modulus Test Results for Mix BC-33

		Dynamic Modulus, kPa					
		Indiana Demonstration Project, 3% RAS/WMA					
Temp., C	**Freq., Hz**	**Sample 1**	**Sample 2**	**Sample 3**	**Sample 4**	**Sample 5**	**CV, %**
4	25	18962	19192	19175	19209	19145	0.52
4	20	18604	18766	18786	18738	18751	0.39
4	10	17460	17626	17633	17639	17613	0.43
4	5	16286	16460	16541	16467	16469	0.58
4	2	14710	14986	14993	15022	14940	0.85
4	1	13580	13766	13804	13843	13842	0.80
4	0.5	12689	12424	12631	12677	12615	0.85
4	0.2	11455	10675	11131	11174	11143	2.52
4	0.1	10383	9542	10017	10096	10033	3.02
21	25	9329	9796	10026	9866	9868	2.70
21	20	9024	9497	9614	9460	9482	2.41
21	10	8163	8292	8326	8296	8342	0.85
21	5	6999	7293	7307	7333	7291	1.91
21	2	5747	6081	6072	6031	6022	2.31
21	1	4975	5181	5226	5144	5156	1.86
21	0.5	4251	4373	4361	4435	4371	1.53
21	0.2	3227	3554	3580	3488	3562	4.22
21	0.1	2659	2955	3000	2951	2979	4.85
37	25	3382	4233	4015	4091	4235	8.85
37	20	3581	3923	3938	3926	3887	3.96
37	10	2962	3208	3192	3148	3161	3.17
37	5	2428	2502	2560	2565	2540	2.25
37	2	1804	1817	1867	1871	1851	1.63
37	1	1313	1303	1496	1457	1415	6.16
37	0.5	1035	928	1161	1154	1093	8.97
37	0.2	721	674	828	842	782	9.28
37	0.1	609	487	617	579	588	9.04

APPENDIX B: DSR TEST RESULTS

Table 49: DSR Test Results

		Temperature, C									
		58		64		70		76		82	
Mix	Test	δ, °	G*, Pa	δ, °	G*, Pa	δ, °	G*, Pa	δ, °	G*, Pa	δ, °	G*, Pa
	1	72.44	12510	75.31	5654	78.11	2624	80.54	1302		
BC21	2	72.62	11980	75.50	5468	78.19	2619	80.68	1266		
	3	72.91	11715	75.68	5374	78.39	2531	80.80	1248		
	1	74.95	12460	78.00	5399	80.78	2436	83.15	1157		
BC22	2	74.11	14170	77.22	6223	80.07	2858	82.58	1349		
	3	74.26	13350	77.30	5914	80.15	2693	82.61	1275		
	1	78.54	9254	81.41	4001	83.87	1795				
BC23	2	78.73	8641	81.60	3724	84.00	1683				
	3	78.71	9429	81.59	4044	84.00	1835				
	1	75.72	18190	78.98	7790	81.90	3391	84.29	1563		
BC24	2	75.84	17800	79.15	7505	82.00	3340	84.40	1527		
	3	76.06	18340	79.34	7680	82.17	3377	84.51	1554		
	1	70.07	21240	73.48	9534	76.80	4396	79.78	2095		
BC25	2	69.95	21400	73.29	9722	76.59	4515	79.57	2160		
	3	69.90	21220	73.16	9733	76.47	4489	79.51	2106		
	1	64.50	35160	67.71	16510	71.20	7800	74.60	3790	77.73	1846
BC26	2	64.30	36700	67.50	17340	71.02	8194	74.51	3921	77.65	1950
	3	64.22	37660	67.38	18060	70.86	8586	74.31	4130	77.54	2018
	1	60.80	51000	63.50	25230	66.74	12420	70.22	6085	73.65	3054
BC27	2	60.77	48100	63.60	23440	66.80	11525	70.24	5660		
	3	60.19	59140	62.92	29180	66.13	14295	69.54	7052	73.02	3489
	1	72.62	30580	75.76	13120	78.83	5736	81.50	2632	83.76	1261
BC28	2	72.57	30460	75.74	13045	78.82	5685	81.52	2587	83.79	1230
	3	72.51	31060	75.63	13320	78.69	2616	81.42	2616	83.70	1242
	1			61.83	52200	64.52	25720	67.65	12590	71.03	6160
BC29	2			62.72	39360	65.30	20620	68.38	10150	71.70	4930
	3			62.92	44720	65.45	22170	68.38	11060	71.47	5567
	1			64.76	35600	67.63	17295	70.96	8326	74.29	4100
BC30	2			64.67	36600	67.53	17840	70.98	8470	74.01	4265
	3			64.72	36300	67.07	18790	70.51	8942	72.85	4755
	1	75.23	24370	78.21	10795	81.20	4608	83.63	2090		
BC31	2	75.03	23100	78.30	9720	81.27	4185	83.67	1936		
	3	74.90	25450	78.22	10595	81.20	4580	83.65	2110		
	1	70.33	33500	73.61	14945	76.95	6718	80.01	3082	82.54	1462
BC32	2	70.32	34140	73.68	15060	77.07	6683	80.05	3130	82.64	1461
	3	70.45	31900	73.85	13910	77.18	6238	80.19	2874	82.75	1375
	1	71.19	29220	74.59	12785	77.95	5677	80.79	2652	83.22	1239
BC33	2	71.02	30870	74.50	13300	77.84	5992	80.75	2780	83.16	1317
	3	70.81	32380	74.31	14045	77.72	6205	80.75	2804	83.04	1386

APPENDIX C: DSR FREQUENCY SWEEP TEST RESULTS

Table 50: DSR Frequency Sweep Test Results for Mixes BC-21, 23, 24, and 25

Temp.	Freq.	Mix							
		BC-21		BC-23		BC-24		BC-25	
C	Hz	G*, Pa	Φ	G*, Pa	Φ	G*, Pa	Φ	G*, Pa	Φ
9	0.100			7336000	46.4	12250000	42.0	8991000	40.5
9	0.126			8288000	45.6	13610000	41.2	9933000	39.9
9	0.158			9327000	44.9	15150000	40.5	11070000	39.3
9	0.200			10530000	44.1	16830000	39.8	12220000	38.8
9	0.251			11800000	43.5	18720000	39.1	13370000	38.3
9	0.316			13210000	42.8	20690000	38.4	14740000	37.8
9	0.398			14730000	42.1	22710000	37.8	16160000	37.3
9	0.501			16310000	41.5	25000000	37.1	17850000	36.8
9	0.631			18160000	40.9	27530000	36.5	19760000	36.3
9	0.794			20170000	40.2	30160000	35.9	21720000	35.8
9	1.000			22300000	39.6	33020000	35.2	23580000	35.4
9	1.259			24710000	39.0	36080000	34.6	25780000	34.9
9	1.585			27210000	38.4	39450000	34.0	28210000	34.4
9	1.995			29940000	37.8	42990000	33.4	30680000	34.0
9	2.512			32890000	37.2	46870000	32.9	33460000	33.5
9	3.162			36190000	36.6	50860000	32.3	36510000	33.0
9	3.981			39720000	36.0	55220000	31.8	39720000	32.6
9	5.012			43480000	35.4	59810000	31.2	43100000	32.1
9	6.310			47440000	34.9	64710000	30.7	46790000	31.7
9	7.943			51770000	34.3	70050000	30.1	50760000	31.2
9	10.000			56520000	33.6	75760000	29.7	54970000	30.8
9	12.590			61590000	32.9	81150000	29.0	59340000	30.3
9	15.849			67090000	32.6	87560000	28.4	64070000	29.9
9	19.953			72850000	31.9	94160000	28.0	69070000	29.5
9	25.121			79150000	31.3	10090000	27.5	74450000	29.2
9	31.623			85730000	30.7	10830000	27.0	80060000	28.7
9	39.809			92550000	30.1	11600000	26.3	86220000	28.1
9	50.000			99780000	29.5	12390000	25.7	92680000	27.7
13	0.100	3495000	47.5	3767000	50.4	6696000	45.8	4899000	44.2
13	0.158	4420000	46.2	4934000	48.9	8541000	44.3	6194000	43.0
13	0.251	5622000	45.0	6251000	47.7	10640000	42.9	7633000	41.9
13	0.398	7048000	43.8	7926000	46.3	13140000	41.6	9397000	40.9
13	0.631	8827000	42.7	10030000	45.0	16230000	40.3	11530000	39.8
13	1.000	10970000	41.6	12600000	43.7	19890000	39.0	14100000	38.8
13	1.585	13510000	40.5	15750000	42.4	24220000	37.7	17170000	37.8
13	2.512	16580000	39.3	19480000	41.2	29220000	36.6	20770000	36.8
13	3.981	20210000	38.2	24000000	39.9	35180000	35.4	24970000	35.9
13	6.310	24630000	37.1	29350000	38.7	41890000	34.3	30000000	34.9
13	10.000	29680000	36.1	35550000	37.4	49690000	33.0	35730000	34.0

Table 50: DSR Frequency Sweep Test Results for Mixes BC-21, 23, 24, and 25 (Continued)

Temp. C	Freq. Hz	Mix							
		BC-21		BC-23		BC-24		BC-25	
		G*, Pa	Φ	G*, Pa	Φ	G*, Pa	Φ	G*, Pa	Φ
13	15.849	35510000	35.1	42970000	36.3	58730000	32.1	42460000	32.9
13	25.121	42360000	34.1	51690000	35.2	69200000	31.0	50100000	32.1
13	39.809	50300000	33.1	61750000	33.8	80790000	29.7	59200000	31.2
13	50.000	54710000	32.6	67230000	33.1	86980000	29.2	63950000	30.7
21	0.100	900600	54.0	896400	58.1	1732000	54.1	1364000	50.9
21	0.158	1184000	53.0	1193000	56.9	2287000	52.6	1766000	49.7
21	0.251	1555000	51.9	1602000	55.6	2989000	51.2	2273000	48.6
21	0.398	2023000	50.8	2126000	54.3	3859000	49.8	2914000	47.6
21	0.631	2621000	49.7	2798000	53.1	4967000	48.4	3708000	46.5
21	1.000	3377000	48.6	3650000	51.8	6349000	47.0	4691000	45.5
21	1.585	4332000	47.5	4736000	50.6	8041000	45.7	5901000	44.4
21	2.512	5504000	46.4	6118000	49.4	10120000	44.5	7385000	43.4
21	3.981	6956000	45.3	7859000	48.0	12630000	43.2	9209000	42.4
21	6.310	8746000	44.3	9963000	46.7	15650000	41.9	11440000	41.4
21	10.000	10970000	43.5	12670000	45.5	19350000	40.5	14090000	40.6
21	15.849	13600000	42.2	15950000	44.2	23810000	39.6	17290000	39.3
21	25.121	16830000	41.0	19950000	42.9	29070000	38.1	21050000	38.5
21	39.809	20770000	40.0	24810000	41.5	35290000	37.0	25640000	37.6
21	50.000	22960000	39.5	27580000	40.8	38760000	36.3	28160000	37.0
29	0.100	222100	59.4	200100	64.7	417000	61.1	373200	56.4
29	0.158	299800	58.5	281000	63.4	570400	59.8	498700	55.3
29	0.251	404800	57.7	386000	62.3	774400	58.5	662300	54.2
29	0.398	544200	56.8	528200	61.3	1041000	57.2	870800	53.2
29	0.631	728000	55.8	720500	60.2	1393000	56.0	1137000	52.2
29	1.000	969300	54.8	976200	59.1	1852000	54.7	1483000	51.2
29	1.585	1284000	53.8	1315000	58.0	2444000	53.4	1924000	50.3
29	2.512	1688000	52.9	1759000	56.9	3199000	52.2	2481000	49.4
29	3.981	2207000	52.0	2343000	55.7	4160000	50.9	3189000	48.4
29	6.310	2865000	51.0	3097000	54.3	5366000	49.5	4049000	47.4
29	10.000	3715000	50.0	4111000	53.2	6903000	48.1	5180000	46.6
29	15.849	4784000	49.1	5389000	51.9	8824000	47.0	6564000	45.6
29	25.121	6162000	48.0	7038000	50.6	11200000	45.7	8281000	44.6
29	39.809	7850000	47.0	9086000	49.3	14110000	44.5	10400000	43.6
29	50.000	8842000	46.6	10340000	48.7	15830000	43.8	11630000	43.3
37	0.100	57080	64.6	44810	70.9	98940	67.1	101800	61.7
37	0.158	79240	63.3	64880	69.5	139400	65.8	139100	60.5
37	0.251	110500	62.2	91900	68.3	195100	64.6	189000	59.4
37	0.398	149700	61.3	128600	67.1	269600	63.5	255000	58.4
37	0.631	204400	60.7	179700	66.2	373100	62.3	343100	57.5
37	1.000	280300	59.8	252600	65.2	511200	61.2	460100	56.5
37	1.585	379800	59.0	355700	64.1	695300	60.1	613600	55.6

Table 50: DSR Frequency Sweep Test Results for Mixes BC-21, 23, 24, and 25 (Continued)

Temp. C	Freq. Hz	Mix							
		BC-21		BC-23		BC-24		BC-25	
		G*, Pa	Φ	G*, Pa	Φ	G*, Pa	Φ	G*, Pa	Φ
37	2.512	509400	58.24	493800	63.19	941500	59.00	811400	54.82
37	3.981	685100	57.44	678100	62.18	1265000	57.85	1071000	53.98
37	6.310	916400	56.63	927400	60.96	1699000	56.60	1408000	53.06
37	10.000	1223000	55.65	1271000	60.13	2269000	55.41	1847000	52.23
37	15.849	1623000	54.86	1718000	59.11	2999000	54.27	2409000	51.39
37	25.121	2153000	54.02	2321000	58.21	3951000	53.00	3136000	50.53
37	39.809	2840000	53.24	3113000	57.38	5181000	51.90	4050000	49.89
37	50.000	3261000	52.89	3591000	56.92	5926000	51.27	4584000	49.55

Table 51: DSR Frequency Sweep Test Results for Mixes BC-27, 28, 29, and 30

Temp. C	Freq. Hz	Mix							
		BC-27		BC-28		BC-29		BC-30	
		G*, Pa	Φ	G*, Pa	Φ	G*, Pa	Φ	G*, Pa	Φ
9	0.100								
9	0.126			22950000	33.58	26650000	28.45	26540000	28.34
9	0.158					28720000	28.02	28770000	27.90
9	0.200			26950000	32.52	30950000	27.60	30870000	27.52
9	0.251					33200000	27.22	33020000	27.17
9	0.316			31750000	31.48	35310000	26.89	35570000	26.80
9	0.398					37900000	26.53	37950000	26.47
9	0.501			37230000	30.49	40790000	26.17	40720000	26.14
9	0.631					43580000	25.84	43470000	25.83
9	0.794			43320000	29.57	46640000	25.53	46410000	25.53
9	1.000					49890000	25.22	49400000	25.25
9	1.259			50300000	28.68	53250000	24.92	52610000	24.98
9	1.585					56630000	24.64	56180000	24.70
9	1.995			58140000	27.82	60510000	24.37	59860000	24.44
9	2.512					64330000	24.10	63630000	24.17
9	3.162			66840000	27.01	68480000	23.84	67650000	23.92
9	3.981					72680000	23.61	71960000	23.75
9	5.012			76530000	26.20	77110000	23.41	76530000	23.51
9	6.310					81800000	23.16	81110000	23.29
9	7.943			87530000	25.43	86540000	22.91	86000000	23.05
9	10.000					91540000	22.50	90930000	22.65
9	12.590			99470000	24.49	97250000	22.27	96760000	22.56
9	15.849					102900000	22.22	102500000	22.28
9	19.953			112200000	24.17	109200000	21.90	108300000	22.06
9	25.121					115300000	21.69	114900000	21.89
9	31.623			127400000	22.90	122100000	21.27	121800000	21.57
9	39.809					128900000	21.05	128500000	21.18

Table 51: DSR Frequency Sweep Test Results for Mixes BC-27, 28, 29, and 30 (Continued)

Temp. C	Freq. Hz	Mix							
		BC-27		BC-28		BC-29		BC-30	
		G*, Pa	Φ	G*, Pa	Φ	G*, Pa	Φ	G*, Pa	Φ
9	50.000			134200	22.65	135800	20.78	135300	20.91
13	0.100	5389000	38.64	11470000	38.40	16110000	31.34	16250000	31.06
13	0.158	6545000	37.70	14100000	37.04	19080000	30.37	19240000	30.15
13	0.251	7912000	36.81	16860000	35.89	22110000	29.56	22220000	29.41
13	0.398	9542000	35.97	20110000	34.78	25540000	28.80	25800000	28.68
13	0.631	11450000	35.19	23860000	33.73	29510000	28.10	29850000	27.99
13	1.000	13710000	34.46	28340000	32.69	34060000	27.42	34340000	27.36
13	1.585	16260000	33.77	33270000	31.73	39130000	26.80	39470000	26.75
13	2.512	19280000	33.09	38990000	30.79	44790000	26.22	45090000	26.22
13	3.981	22830000	32.41	45520000	29.88	51140000	25.72	51600000	25.67
13	6.310	26860000	31.77	52840000	29.01	58160000	25.23	58730000	25.23
13	10.000	31510000	31.22	61270000	28.22	65890000	24.55	66630000	24.75
13	15.849	36750000	30.53	70590000	27.31	74910000	24.19	75520000	24.33
13	25.121	42930000	29.99	81160000	26.45	84800000	23.69	85390000	23.74
13	39.809	50080000	29.29	92660000	25.60	95710000	23.09	96450000	23.07
13	50.000	53910000	28.99	98710000	25.15	101400	22.81	102100	22.84
21	0.100	1802000	44.18	3316000	47.12	5934000	37.41	5956000	36.99
21	0.158	2258000	43.18	4220000	45.62	7161000	36.28	7159000	36.01
21	0.251	2826000	42.21	5314000	44.19	8617000	35.23	8612000	35.07
21	0.398	3488000	41.35	6625000	42.86	10280000	34.30	10260000	34.22
21	0.631	4299000	40.50	8219000	41.57	12220000	33.42	12160000	33.43
21	1.000	5274000	39.70	10130000	40.35	14460000	32.63	14390000	32.68
21	1.585	6447000	38.93	12410000	39.18	17050000	31.87	16970000	31.96
21	2.512	7843000	38.19	15090000	38.03	20010000	31.16	19920000	31.28
21	3.981	9510000	37.48	18260000	36.90	23400000	30.55	23300000	30.63
21	6.310	11500000	36.80	21990000	35.83	27230000	29.94	27190000	30.00
21	10.000	13880000	36.22	26320000	34.85	31610000	29.19	31610000	29.41
21	15.849	16630000	35.40	31330000	33.79	36750000	28.78	36690000	28.80
21	25.121	19890000	34.72	37070000	32.92	42500000	28.21	42470000	28.35
21	39.809	23830000	34.12	43970000	31.93	49090000	27.59	49020000	27.64
21	50.000	25970000	33.80	47570000	31.34	52640000	27.30	52590000	27.42
29	0.100	580900	49.25	836800	55.58	1990000	43.55	1971000	43.37
29	0.158	749100	48.21	1114000	54.06	2492000	42.26	2455000	42.25
29	0.251	956500	47.26	1466000	52.60	3083000	41.10	3036000	41.21
29	0.398	1217000	46.36	1913000	51.17	3803000	40.00	3739000	40.20
29	0.631	1540000	45.51	2474000	49.79	4661000	38.98	4577000	39.25
29	1.000	1939000	44.69	3174000	48.44	5665000	38.05	5569000	38.35
29	1.585	2432000	43.90	4047000	47.13	6861000	37.18	6754000	37.50
29	2.512	3038000	43.14	5129000	45.86	8283000	36.44	8157000	36.70
29	3.981	3777000	42.41	6459000	44.60	9968000	35.70	9809000	35.96
29	6.310	4676000	41.70	8060000	43.40	11840000	35.05	11750000	35.24

Table 51: DSR Frequency Sweep Test Results for Mixes BC-27, 28, 29, and 30 (Continued)

Temp. C	Freq. Hz	Mix							
		BC-27		BC-28		BC-29		BC-30	
		G*, Pa	Φ	G*, Pa	Φ	G*, Pa	Φ	G*, Pa	Φ
29	10.000	5768000	40.94	10040000	42.09	14140000	34.21	14040000	34.52
29	15.849	7111000	40.29	12430000	41.14	16880000	33.66	16710000	33.88
29	25.121	8724000	39.57	15330000	39.82	20000000	33.06	19880000	33.22
29	39.809	10710000	38.96	18770000	38.81	23660000	32.45	23510000	32.54
29	50.000	11810000	38.64	20760000	38.28	25650000	32.16	25570000	32.25
37	0.100	189600	53.75	199300	62.80	629000	49.70	605200	49.60
37	0.158	251000	52.62	278400	61.45	811600	48.38	779700	48.43
37	0.251	328400	51.64	372500	60.31	1033000	47.21	991800	47.33
37	0.398	426400	50.73	504700	58.87	1313000	46.09	1259000	46.28
37	0.631	552400	49.89	679200	57.52	1655000	45.03	1593000	45.25
37	1.000	710800	49.11	907700	56.20	2073000	44.02	2004000	44.26
37	1.585	909300	48.35	1207000	54.90	2587000	43.06	2506000	43.33
37	2.512	1163000	47.61	1591000	53.60	3208000	42.12	3118000	42.46
37	3.981	1479000	46.92	2096000	52.27	3982000	41.02	3854000	41.66
37	6.310	1879000	46.24	2717000	51.02	4909000	40.18	4746000	40.85
37	10.000	2369000	45.40	3506000	49.65	5993000	39.38	5820000	39.96
37	15.849	2989000	44.87	4524000	48.39	7325000	38.61	7137000	39.23
37	25.121	3763000	44.24	5788000	47.05	8915000	37.87	8727000	38.49
37	39.809	4713000	43.57	7377000	45.73	10810000	37.19	10620000	37.84
37	50.000	5282000	43.29	8326000	45.19	11910000	36.88	11690000	37.56

Table 52: DSR Frequency Sweep Test Results for Mixes BC-31, 32, and 33

Temp. C	Freq. Hz	Mix					
		BC-31		BC-32		BC-33	
		G*, Pa	Φ	G*, Pa	Φ	G*, Pa	Φ
9	0.100						
9	0.126	15000000	39.38	21390000	36.47	16400000	37.53
9	0.158	16630000	38.67	23510000	35.87	18190000	36.87
9	0.200	18300000	38.01	25810000	35.28	19890000	36.32
9	0.251	20200000	37.35	28100000	34.76	21840000	35.74
9	0.316	22210000	36.70	30710000	34.22	23940000	35.17
9	0.398	24300000	36.09	33470000	33.71	26150000	34.63
9	0.501	26700000	35.46	36410000	33.21	28570000	34.09
9	0.631	29200000	34.86	39670000	32.70	31220000	33.55
9	0.794	32000000	34.25	43200000	32.21	33940000	33.04
9	1.000	34840000	33.68	46900000	31.73	36920000	32.53
9	1.259	38030000	33.10	50740000	31.28	40180000	32.02
9	1.585	41210000	32.57	55030000	30.81	43600000	31.53
9	1.995	44840000	32.00	59480000	30.35	47180000	31.07
9	2.512	48610000	31.47	64180000	29.91	50970000	30.64

Table 52: DSR Frequency Sweep Test Results for Mixes BC-31, 32, and 33 (Continued)

Temp. C	Freq. Hz	Mix					
		BC-31		BC-32		BC-33	
		G*, Pa	Φ	G*, Pa	Φ	G*, Pa	Φ
9	3.162	52580000	30.94	69170000	29.46	55290000	30.20
9	3.981	56870000	30.41	74620000	29.01	59600000	29.77
9	5.012	61440000	29.88	80330000	28.57	64260000	29.39
9	6.310	66100000	29.38	86370000	28.14	69170000	28.94
9	7.943	71090000	28.87	92630000	27.72	74340000	28.51
9	10.000	76730000	28.35	99330000	27.29	79780000	28.09
9	12.590	82220000	27.78	106400000	26.86	85710000	27.69
9	15.849	88180000	27.28	113900000	26.47	91780000	27.23
9	19.953	94450000	26.86	121600000	26.05	98660000	26.66
9	25.121	101000000	26.34	130000000	25.60	105800000	26.30
9	31.623	108100000	25.77	139000000	25.11	113100000	25.75
9	39.809	115600000	25.24	148200000	24.57	120800000	25.38
9	50.000	122900000	24.63	157200000	24.05	128000000	24.82
13	0.100	7531000	44.11	11320000	40.51	8534000	41.61
13	0.158	9462000	42.65	13890000	39.31	10660000	40.31
13	0.251	11700000	41.30	16900000	38.18	12980000	39.16
13	0.398	14410000	39.99	20420000	37.08	15790000	38.03
13	0.631	17610000	38.72	24620000	36.01	19100000	36.93
13	1.000	21280000	37.51	29550000	34.98	22990000	35.86
13	1.585	25710000	36.30	35240000	33.98	27570000	34.82
13	2.512	30820000	35.13	41690000	33.03	32840000	33.88
13	3.981	36660000	34.02	49150000	32.08	38950000	33.00
13	6.310	43560000	32.89	57810000	31.16	45860000	32.09
13	10.000	51370000	31.78	67700000	30.35	53720000	30.93
13	15.849	60330000	30.73	78570000	29.41	63070000	30.25
13	25.121	70420000	29.59	90850000	28.44	73620000	29.33
13	39.809	81800000	28.49	105100000	27.49	85260000	28.33
13	50.000	87840000	27.92	112700000	27.03	91580000	27.83
21	0.100	2039000	52.57	3296000	48.16	2433000	49.17
21	0.158	2646000	51.16	4186000	46.91	3133000	47.88
21	0.251	3437000	49.73	5303000	45.68	3993000	46.65
21	0.398	4414000	48.34	6686000	44.47	5046000	45.46
21	0.631	5635000	46.97	8348000	43.33	6346000	44.32
21	1.000	7139000	45.62	10390000	42.20	7928000	43.20
21	1.585	8965000	44.30	12850000	41.09	9850000	42.13
21	2.512	11210000	42.99	15810000	39.99	12170000	41.04
21	3.981	13920000	41.69	19300000	38.91	14970000	39.95
21	6.310	17150000	40.43	23500000	37.84	18310000	38.92
21	10.000	20990000	39.19	28380000	36.78	22230000	37.66
21	15.849	25610000	37.86	34210000	35.72	26930000	36.66
21	25.121	31030000	36.72	40890000	34.75	32450000	35.70

Table 52: DSR Frequency Sweep Test Results for Mixes BC-31, 32, and 33 (Continued)

Temp. C	Freq. Hz	Mix					
		BC-31		BC-32		BC-33	
		G*, Pa	Φ	G*, Pa	Φ	G*, Pa	Φ
21	39.809	37350000	35.54	48960000	33.83	38960000	34.75
21	50.000	40810000	34.90	53260000	33.33	42540000	34.24
29	0.100	489800	60.08	901400	54.80	622600	56.56
29	0.158	664500	58.82	1189000	53.59	833700	55.36
29	0.251	897500	57.54	1567000	52.39	1108000	54.05
29	0.398	1197000	56.27	2041000	51.24	1461000	52.78
29	0.631	1594000	54.97	2643000	50.11	1909000	51.57
29	1.000	2113000	53.64	3404000	48.98	2477000	50.44
29	1.585	2773000	52.32	4360000	47.85	3185000	49.37
29	2.512	3616000	50.96	5549000	46.74	4083000	48.28
29	3.981	4681000	49.63	7032000	45.62	5203000	47.18
29	6.310	6009000	48.31	8851000	44.54	6595000	46.00
29	10.000	7657000	47.08	11060000	43.30	8309000	44.63
29	15.849	9714000	45.52	13800000	42.26	10460000	43.77
29	25.121	12220000	44.32	17080000	41.21	13100000	42.63
29	39.809	15310000	43.02	21130000	40.21	16250000	41.55
29	50.000	17060000	42.38	23370000	39.64	18070000	41.06
37	0.100	114000	66.38	240500	60.65	157600	62.64
37	0.158	158000	65.26	330000	59.35	215600	61.44
37	0.251	219900	64.12	447300	58.26	298300	60.17
37	0.398	305200	62.97	602500	57.23	401300	59.22
37	0.631	421600	61.80	801500	56.20	538500	58.17
37	1.000	578000	60.65	1064000	55.16	723700	57.23
37	1.585	782300	59.51	1411000	54.10	975200	56.11
37	2.512	1060000	58.32	1855000	53.08	1296000	55.02
37	3.981	1424000	57.12	2423000	52.06	1716000	53.94
37	6.310	1901000	55.92	3151000	51.00	2246000	52.89
37	10.000	2517000	54.59	4080000	50.03	2937000	51.62
37	15.849	3327000	53.22	5257000	48.77	3823000	50.66
37	25.121	4361000	51.95	6741000	47.82	4927000	49.46
37	39.809	5680000	50.55	8582000	46.69	6353000	48.53
37	50.000	6484000	49.88	9648000	46.20	7184000	48.11